Renewable and Sustainable Energy Reviews 16 (2012) 5021–5058

Contents lists available at SciVerse ScienceDirect

Renewable and Sustainable Energy Reviews

journal homepage: www.elsevier.com/locate/rser

An overview of fundamental studies and applications of phase change material slurries to secondary loop refrigeration and air conditioning systems

P. Zhang*, Z.W. Ma

Institute of Refrigeration and Cryogenics, Shanghai Jiao Tong University, Shanghai 200240, China

A R T I C L E   I N F O

Article history:
Received 29 May 2011
Received in revised form
24 March 2012
Accepted 31 March 2012
Available online 27 June 2012

Keywords:
Phase change material slurries
Secondary refrigerant
Ice slurry
MPCS
CHS

A B S T R A C T

Phase change material slurries (PCS) can be employed in the refrigeration and air conditioning systems as both secondary refrigerant and cold energy storage media simultaneously, which benefits not only the system efficiency improvement by the high cold carry capacity but also the reduction of the environment-negative-impact gas emission. This paper reviews the previous researches and developments on the applications of PCS, including ice slurry, microencapsulated phase change material slurry (MPCS) as well as clathrate hydrate slurry (CHS), to the secondary loop refrigeration and air conditioning systems. The paper mainly focuses on the generation approaches and storage strategies of these slurries which are considered as the most important issues relevant to the application of PCS, while the flow and heat transfer characteristics of PCS in both tubes and heat exchangers are also summarized. Moreover, several application cases of PCS and the corresponding operation performances are presented.

Contents

* Corresponding author. Tel.: +86 21 34205505; fax: +86 21 34206814.
E-mail address: zhangp@sjtu.edu.cn (P. Zhang).

1364-0321/$ - see front matter © 2012 Elsevier Ltd. All rights reserved.
http://dx.doi.org/10.1016/j.rser.2012.03.059

1. Introduction

The application of the secondary refrigerant to the refrigeration and air conditioning systems can reduce the charging amount of the environment-negative-impact refrigerant, like CFCs and HCFCs, etc., consequently the emission of these refrigerants to the atmosphere is reduced. Meanwhile, the cold energy storage is often employed in the refrigeration and air conditioning systems to shift the peak-load to the off-peak time, and thus many merits can be achieved: reducing the system scale, minimizing the partial load compressor operation to improve its efficiency, improving the system COP by the extended night time operation at lower environment temperature, reducing the financial cost by producing and storing the cold energy during night time when the electricity is cheaper and releasing the cold energy during day time when the electricity is more expensive. The inspiring aspect is that both the roles of the secondary refrigerant and cold energy storage medium can be undertaken by phase change material slurries (PCS) simultaneously, such as ice slurry, microencapsulated phase change material slurry (MPCS) and clathrate hydrate slurry (CHS). The latent heat of the fusion of the solid particles containing in PCS makes it possible to preserve cold energy with high cold storage density, therefore the volumes or sizes of the utilized storage tank, piping, pump and the refrigerator are relatively small; the easily pumpable performance of PCS through tubes as well as heat exchangers without clogging provides the qualification for PCS being a good secondary refrigerant with high cold carry capacity, then the pumping power is significantly reduced since the required flow rate is low. Therefore, PCS was considered promising as "functional thermal fluids" [1].

The utilization of ice slurry has been widely investigated over the world from the fundamental thermal properties to the practical applications [2–4]. Ice slurry is a homogeneous mixture of very small ice crystals, usually 0.1–2 mm in characteristic size, and the base liquid can be either pure water or binary solution of water and freezing point depressing agent, e.g. ethanol, glycol or salt, etc. The latent heat of ice crystals is about 333.55 kJ kg^{-1}, which results in a high cold carry capacity. Compared to single-phase water or glycol solution, ice slurry with 30 wt% ice fraction offers an 80% reduction of flow rate and therefore the pumping power while maintaining the same cooling load [5]. Due to its excellent cooling and transporting features, ice slurry can be employed in many fields, such as the building cooling, supermarket display, food industry, brewery, mine cooling, fish processing, as well as medical cooling. However, the practical application is still limited by the following disadvantages: the evaporation temperature is low for air conditioning using; heavy mechanical power is required to generate small and smooth ice crystals and to maintain the ice slurry in homogeneous state; the pressure drop and pumping power of ice slurry with high ice fraction are very high. Therefore, the utilization of ice slurry is not common except in Japan, and only few projects exist in USA and Europe up to date.

MPCS is a kind of solid–liquid suspension consisting of the carrier liquid and small particles of phase change material (PCM) with a thin shell. The diameter of the microcapsules is in the range of 1–1000 μm, the core PCM can be solid, liquid, or even mixture. Paraffin waxes are often used as the core materials due to its extended melting temperature range. The shell material is usually natural or synthesized polymer, such as polyester and polyethylene, which has high strength and flexibility. The carrier liquid is usually water. Compared to non-encapsulated PCM slurry, MPCS owns several advantages: the agglomeration of PCM particles and the in turn clogging in piping are avoided; the PCM does not contact with environment directly, which avoids disadvantageous changes of PCM composition and property; the microencapsulation offers a protective structure element which improves the mechanical stability, thus permits the frequent changes in volume of the core material as phase change occurs; large heat transfer area is achieved by the surface of the microencapsulation. So far, however, the investigations about MPCS are mostly on its fabrication methods and thermal properties [6–8] and the flow and heat transfer characteristics through tubes [9–15]. Due to the high cost of MPCS preparation, only few laboratorial applications of MPCS to chilled ceiling panels [16,17] and an industrial cooling project at Narita Airport in Japan [18] are reported in the open literature.

Clathrate hydrate can be formed in some aqueous solution of tetraalkylammonium salts with simple anions (such as halides, sulfate, formate, etc.) [19] at the atmospheric condition, in which the water molecules form structure lattices as host and molecules of another substance fill the lattices as guest; also, gases, like CO_2, N_2, CFCs and so on, can form hydrate in water under the higher pressure and low temperature conditions; however, such type of gas hydrate slurry would not be discussed in the present paper because its application require more rigorous conditions. Researchers in Japan [20] applied CHS to the air conditioning system as cold storage and transportation medium, and found that tetrabutylammonium bromide (TBAB) CHS was quite suitable to the air conditioning application due to its following merits: TBAB CHS can be easily generated at atmospheric pressure and room temperature by cooling down the aqueous solution; TBAB CHS has a freezing point between 0 and 12 °C depending on TBAB concentration in the aqueous solution, which fits quite well with the necessary coolant temperature in the air conditioning system; the cooling capacity of TBAB CHS is about 2–4 times as large as that of chilled water within the temperature range of 5–12 °C; the fluidity of TBAB CHS is also good. Researchers in JFE Engineering Corporation also successfully applied TBAB CHS to a 4000 m^2 office building [21] for cooling and the operational results showed 47% reduction of the pumping power. Except the application projects conducted by JFE Engineering Corporation [21,22]; however, other studies of TBAB CHS still focused on the fundamental

Nomenclature

C_p	specific heat (kJ kg^{-1} K^{-1})
D	diameter (m)
d_p	particle size (m)
f	friction factor (dimensionless)
f_F	Fanning friction factor (dimensionless)
Gz	Graetz number (dimensionless), $Gz=RePrD_h/x$
h	heat transfer coefficient (W m^{-2} K^{-1})
ΔH	enthalpy change (kJ kg^{-1})
H	height (m)
K'	fluid consistency coefficient (dimensionless)
L	length (m)
n	flow behavior index (dimensionless)
Nu	Nusselt number (dimensionless)
Pr	Prandtl number (dimensionless)
ΔP	pressure drop (Pa)
q_w	wall heat flux (W)
Re	Reynolds number (dimensionless)
Re_{MR}	modified Reynolds number (dimensionless)
Ste	Stefan number (dimensionless)
T	temperature (°C)
ΔT	temperature difference (°C)
v	flow velocity (m s^{-1})
x_s	particle fraction (wt%)
Δx_s	particle fraction difference (wt%)
x	distance from inlet (m)

Greeks symbols

μ	viscosity (mPa s)
λ	thermal conductivity (W m^{-1} K^{-1})
φ, Φ	volume fraction (dimensionless)

Subscripts

a	average value
B	Bingham
BT	Bingham parameters in Tomita equation
cf	carrier fluid
f	fluid
h	hydraulic
i	inner
is	ice slurry
local	local value
m	mean value
overall	overall value
s	slurry
w	wall

properties [23], the flow and heat transfer characteristics of TBAB CHS flowing through tubes [24–31] as well as in heat exchangers [32,33]. In addition, other CHS materials, such as trimethylolethane (TME) hydrate slurry [34–37] and tetrabutylammonium fluoride (TBAF) hydrate slurry [38], have also been studied as the thermal energy storage medium.

This paper presents a review of the current main applications of PCS, including the aforementioned ice slurry, MPCS and TBAB CHS, to the refrigeration and air conditioning systems as both the cold storage medium and secondary refrigerant. The generation methods and storage strategies which are very important to PCS application are summarized, and the flow and heat transfer characteristics of PCS in tubes and heat exchangers are also discussed. Some application cases of the practical projects or laboratorial studies are displayed, and the corresponding operation results are also discussed.

2. Generation approaches and storage strategies

2.1. Generation approaches of ice slurry and TBAB CHS

The generation processes of ice crystals in water or aqueous solution and that of TBAB clathrate hydrate are similar in that the crystals initiate and grow up in the solution. The generation process generally include the following steps: supercooling of the base liquid, nucleation and growth of the crystals. The base liquid is first cooled down to the temperature lower than its phase change temperature but without phase change, the state of which is named as the supercooled state. Then the nucleation occurs, which is usually heterogeneous since the alien dust particles as well as the rough container wall provide nuclei for the nucleation. And then it is followed by the growth of crystals. After these three steps, size and shape of the crystals are affected by the processes of attrition, agglomeration and ripening [39]. If the generated slurry is agitated or collides with other materials, attrition will happen due to shear stress on the crystals, and large crystals will break off during the attrition. Agglomeration may occur during the slurry generation or storage without stirring, and small crystals collide and stick to each other to form the large size crystals. If the slurry is stored for long time, small crystals may dissolve slowly and then the size distribution changes, which is called Ostwald ripening.

Usually, small and globular crystals are expected for easy pumping through tubes as well as heat exchangers, therefore the attrition process is commonly utilized for crystal size reduction and edge smoothing. On the other side, it was reported that the ice crystals produced in pure water were dendritic and had very rough surface, which resulted in the poor fluidity and easy agglomeration and clogging even though the crystal size was small [4]. The improvement on this dendritic structure can be achieved by smoothing the crystals in chemical way through adding the freezing point depressing agents to water, such as ethanol, glycol, propylene glycol and sodium chloride and so on. Hayashi and Kasza [40] produced ice slurry in glycol solution, and found that even very small amount of glycol could improve the fluidity of the generated ice slurry significantly, and the higher concentration the better fluidity.

The generation approaches are the pivotal technology for the applications of both ice slurry and CHS, since not only the crystal properties, i.e., size, shape and roughness, are determined by the generation process, but also the system energy efficiency and reliability mainly lie in the generator performance. The generation of ice slurry has been widely investigated in the alternative ways, which can be mainly categorized to the methods using moving parts and the methods without moving parts. Therefore, the following contexts are mainly focused on the research results of ice slurry, and these approaches can also be applied to CHS because of the similar generation mechanism as aforementioned.

2.1.1. Scraped surface generator

Scraped surface ice slurry generator has been widely investigated and developed over the world, and it has been applied in large-scale systems [5]. The scraped surface generator commonly

utilizes a shell-and-tube heat exchanger in which the evaporating refrigerant flows through the shell side while the crystals are generated in the tube side. Driven by a motor, a rotatable scraper is mounted on the center of the inner tube to prevent the crystals from sticking to the cold heat transfer surface, as shown in Fig. 1(a) [39]. Stamatiou [41] and Stamatiou and Kawaji [42] developed a compact heat exchanger with scraper inside the channel to generate ice slurry, as shown in Fig. 1(b). The scraper moves up and down to eliminate the ice crystals on the tube wall. The authors obtained 30% power saving by using compact heat exchanger instead of tubular one, since four times lower agitation speed was required to maintain the ice-free heat transfer surface.

The blades of the scraper may be plastic or brush type so that they can have good contact with the tube wall to detach the crystal layer, since it is believed that the nucleation took place on the coldest area inside the tube, i.e., the inner tube wall, and then the crystals layer grows on the wall forming a thermal resistance layer which reduces the heat transfer coefficient between the refrigerant and fluid inside the tube. However, other researchers thought that the crystals were formed in the bulk of the supercooled liquid but had a tendency to adhere to the cold wall by the cohesion force, and this was why the blades were needed. Moreover, the scraper movement also contributes to the great enlargement of the fluid turbulent degree, therefore the heat transfer performance of the heat exchanger is promoted. Rodriguez Pascual et al. [43] investigated the influences of the plastic blade geometries on crystal layer removal efficiency and the slurry mixing effect by visualization and simulation. The authors found that the mixing of scraped ice crystals with the bulk solution by the streamlined blade was inadequate, while the vertical blade promoted the mixing but accumulated the crystals in front of it.

Alternatively, Lakhdar et al. [44] employed stainless steel blades rather than the plastic ones. The authors permitted a small gap between the blade and the tube wall, and found the permanent ice layer only existed when the gap was large enough, about 1 mm according to their study. This fact may indicate that the ice crystals nucleate inside the solution. Helical-blade auger can also be utilized as the scraper for ice slurry generation [45–47], as shown in Fig. 1(c). In addition to the effect of scraping the heat transfer surface, the rotating auger also provides a negative pumping pressure to suck the water (or solution) flowing through the generator, hence it can provide the function of the pump.

The generation of ice slurry using scraped surface is considered as very reliable, even in the case of little freezing point depressing agent being added to water. During the generation, the increase of ice fraction is usually implemented by adjusting the liquid flow rate. Using a Sunwell scraped surface ice slurry generator, Wang and Kusumoto [5] produced 0–35 wt% ice slurry with about 100 μm ice crystals, and the used base liquid is an aqueous solution with 6–10% ethylene glycol. However, drawbacks exist in this generator: the tight contact of the plastic scraper blade on the tube wall causes strong friction, and then the blades need to be replaced after a certain time interval of utilization; since the generator employs additional mechanical components, the initial investment and the energy consumption are high.

The scraped surface generator is also suitable to TBAB CHS generation. Douzet et al. [48] successfully applied a scraped surface heat exchanger (about 200 L, supplied by HeatCraft Ltd., France) to TBAB CHS air conditioning system. Daitoku and Utaka [49] investigated the scrape effect of different scraper shapes on the detachment of TBAB clathrate hydrate from heat transfer surface. The authors found that type B TBAB clathrate hydrate cohered to the surface more tightly and needed stronger force to detach, and a relief angle of the scraper was required to avoid the accumulation of crystals on the clearance between the scraper and the heat transfer surface when detaching type B hydrate.

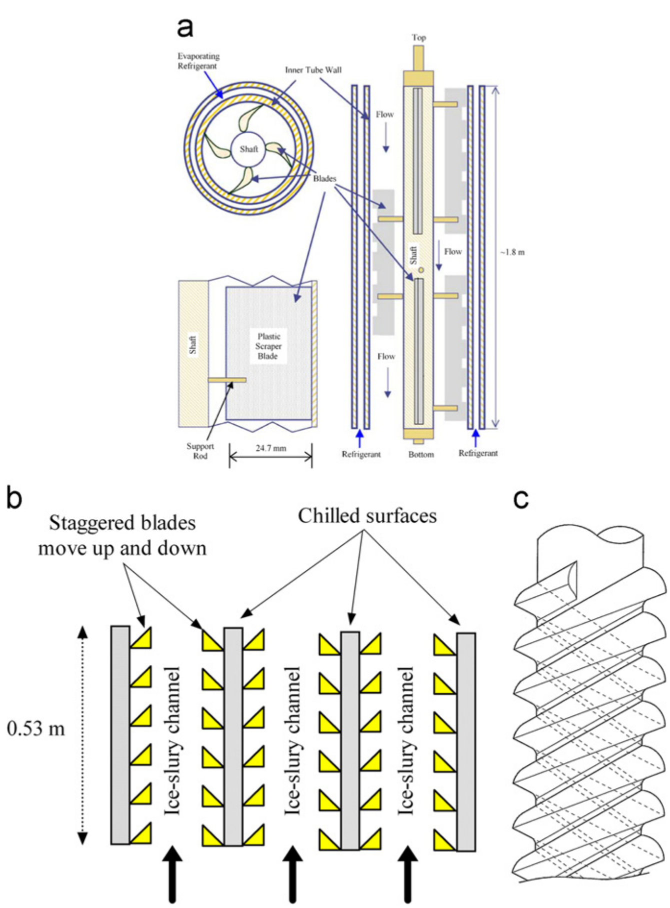


Fig. 1. Schematic diagram of the scraped surface ice slurry generators, (a) shell-and-tube type [39]; (b) compact heat exchanger type [41] and (c) auger type scraper [47].

2.1.2. Orbital rod ice slurry generator

Another type of ice slurry generator using moving parts is the orbital rod generator, as shown in Fig. 2 [50]. This generator is usually a vertical shell-and-tube heat exchanger with evaporating refrigerant flowing from bottom to top in the shell side, while inside the shell is a tube bundle consisted many thin tubes. As shown in the figure, each of tube has a rotatable whip rod inside, which does not rotate in the tube center but around the tube circumference. The rotating rods undertake several roles: pushing part of the upper income liquid flowing around the tube circumference to form a falling film; enhancing the film coefficient and the flow turbulence and therefore the heat transfer coefficient between the film and the refrigerant; preventing the generated ice crystals from sticking to the heat transfer surface, just like the function of scraper in the scraped surface ice slurry generator. The rotation of the whip rod is much faster (e.g., 850 rpm) than that of the scraper (e.g., 450 rpm), however, it is believed that the falling film acts as the lubricant which minimizes the drive power of the motor.

Orbital rod ice slurry generator is also widely used, e.g., Paul Mueller Company [51] developed ice slurry units using this generator which has the standard production sizes from 3 to 520 t (about 10.55–1828.68 kW). They utilized the generator in many fields, including refrigeration, HVAC and process cooling and so on. Stamatiou et al. [39] compared the performances of the orbital rod and the scraped surface ice slurry generators. It is believed that both the two kinds of generators are stable, and the generated ice crystals are homogeneous due to influence of the

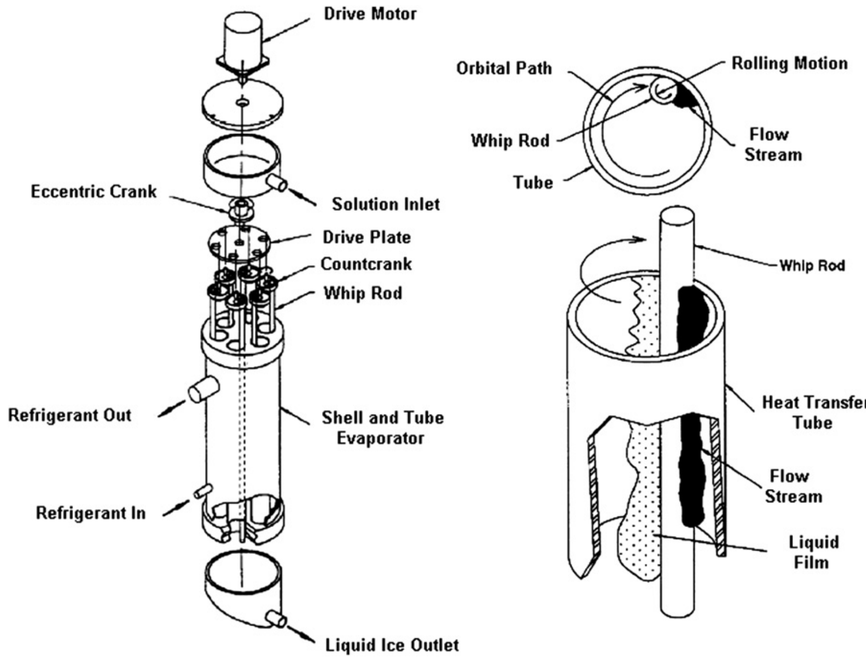


Fig. 2. Schematic diagram of the orbital rod ice slurry generator [50].

rapid rotated scraper or rods. The scraped surface ice slurry generator has a slight higher cooling capacity, however, the drive power for the scraper rotation is also larger; the overall heat transfer coefficient of the orbital rod ice slurry generator is higher due to the falling film heat exchange. The whip rod is metallic and has no direct contact with the tube, therefore it survives longer time than that of the plastic scraper blade which attaches to the tube tightly as aforementioned. However, the drive mechanism of whip rods is complicated and there are many associated problems.

2.1.3. Fluidized bed generator

The fluidized bed heat exchanger was proposed in 1970s for sea water desalination [52]. Small solid particles are inserted into the tubes in a shell-and-tube heat exchanger to detach the adherence on the tube wall. The insert particles are usually cylindrically shaped stainless steel made by wire, or globular glass balls. As the fluid flowing upward in the tube, the solid particles are fluidized and continuously impact on the heat transfer wall, therefore the deposits on the wall are broken off and fall into the fluid, as shown in Fig. 3 [53]. Meanwhile, the heat transfer coefficient is also improved by the following three mechanisms [53]: the laminar boundary layer that acts as heat transfer resistance layer is broken up by the fluidized particles; the solid particles transport the heat from the heat transfer wall to the fluid by conduction as the particles contacting the wall and then the fluid; the deposit layer on the wall is broken off. Therefore, the heat transfer coefficient is determined by the flow velocity of the fluid and also the bed voidage (the ratio of the space that not occupied by the solid particles to the entire space).

Klaren and van der Meer [54] first applied the fluidized bed heat exchanger to produce ice slurry in 1991, then Meewisse and Infante Ferreira [55,56] and Pronk et al. [53,57–59] conducted a lot of works on producing ice slurry by the fluidized bed. Schematic diagrams of the typical fluidized bed ice slurry generators are shown in Fig. 4. The generator shown in Fig. 4(a) is the stationary fluidized bed, in which the insert solid particles are kept inside the tube during the operation. Shown in Fig. 4(b) is the so-called circulating fluidized bed, where the solid particles will

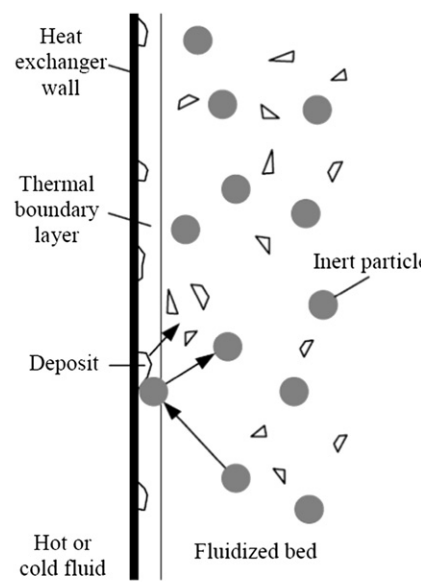


Fig. 3. Schematic diagram of the effect of fluidized solid particles [53].

flow out of the tube together with the generated ice slurry, and then are separated from the slurry and return to the bottom via a downcomer. Measurement results by Meewisse and Infante Ferreira [56] showed that the heat transfer coefficients of the fluidized bed during ice slurry generation was in the range of 2500–4000 $W\,m^{-2}\,K^{-1}$, which was about 2–4 times as large as that of single-phase flow and was not influenced by the ice slurry generation. They also proposed the empirical heat transfer correlations which predicted the heat transfer accurately. Compared to the stationary mode, the use of the circulating fluidized bed is more flexible since the solid particle can flow at a high velocity range, and the advantages include the improvement of the ice crystals breaking off from the tube wall by increasing flow velocity and also the heat transfer coefficient is increased by 1–25% [58].

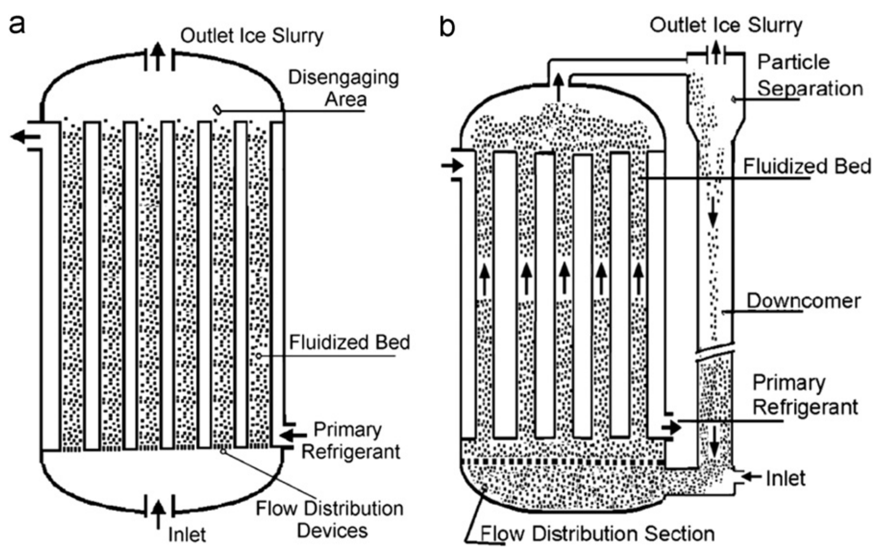


Fig. 4. Schematic diagram of the fluidized bed ice slurry generator, (a) stationary type and (b) circulating type [57].

The shell-and-tube design of the fluidized bed is simple and results in an inexpensive and low operation cost for ice generation. Due to the violent impacts of solid particles on the tube wall, the generated ice particles can be homogeneous, which is usually in the shape of cylindrical or ellipsoidal with the size of about 300 μm [57]. The main disadvantage of the fluidized bed ice slurry generator is the existence of a maximum allowable temperature difference between the fluid inside the tube and the refrigerant (or the tube wall), below which ice slurry can be generated stably with nearly constant heat transfer coefficient. The higher temperature difference enlarges the amount of ice crystals sticking on the tube wall, which are hard to be removed efficiently by the impact of solid particles. The gradually thickening crystal layer deteriorates the heat transfer between the slurry and the refrigerant, thereafter ice slurry generation becomes unstable. Meewisse and Infante Ferreira [55] measured this temperature difference limit in a circulating fluidized bed, as shown in Fig. 5. It was found that the temperature difference limit varied linearly with the freezing temperature of the aqueous solution. Lower freezing temperature (or higher additive concentration) caused a higher temperature difference limit. The other disadvantage of this ice slurry generator is the requirement of higher fluid velocity, so that the momentums of the solid particles are sufficient to impact the wall for ice crystal layer detachment.

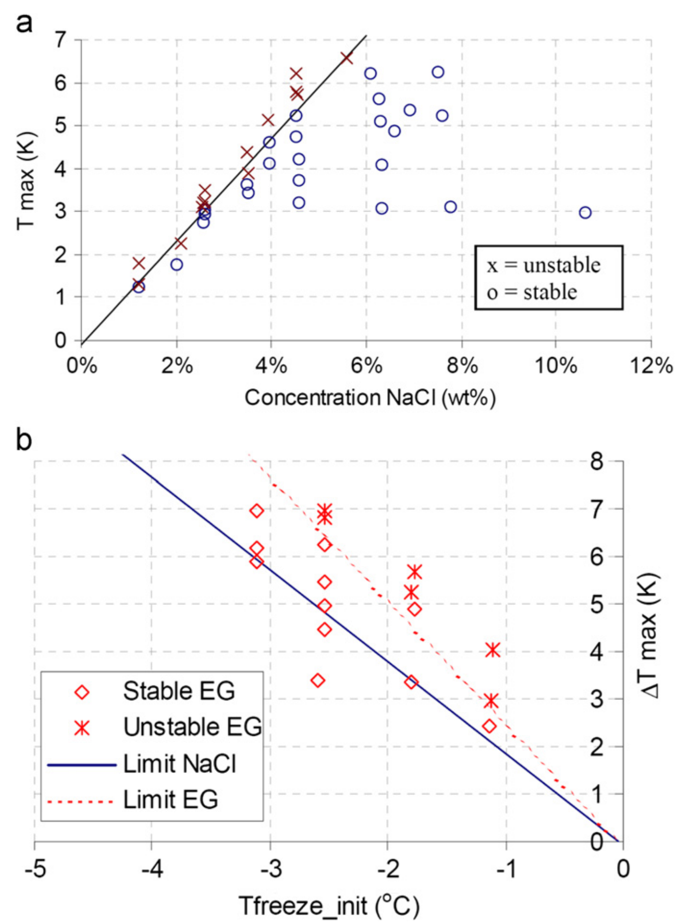


Fig. 5. Range of stable ice slurry production using circulating fluidized bed, (a) range of NaCl and (b) comparison of the operating ranges of NaCl and ethylene glycol (EG). (ΔT_{max} is the temperature difference between the slurry and the refrigerant, the bed voidage is 0.8) [55].

2.1.4. Supercooling method

Ice slurry generation using supercooling concept employs the following steps: water or aqueous solution is cooled in an evaporator to a few degrees below its freezing temperature without crystallization; the supercooled liquid is forced to flow through a special device, i.e., supercooling releaser, to release the supercooling state; then ice crystals are generated in the liquid and the liquid turns to solid–liquid ice slurry. This method is considered as simple and having low operation cost since there is no other complex apparatus. However, the evaporator for supercooling and the supercooling releaser must be carefully designed to achieve stable ice slurry generation.

The heat exchanger for supercooling must ensure that there is no crystallization happened inside, otherwise the slurry generation may stop due to the blockage by the accumulatively generated ice crystals. Bédécarrats et al. [60] regarded that the stochastic character of crystallization resulted in a hard control of ice generation within heat exchanger and it was necessary to control the evaporation temperature accurately. They studied the influences of the supercooling degree, refrigerant temperature and fluid flow rate on the ice generation. By developing models for predicting the fluid temperature variation, they tried to avoid the ice generation inside supercooling heat exchanger.

Several requirements for the supercooling heat exchanger are given as follows:

(1) The heat transfer surface should be smooth, since the rough surface enhances the crystallization. Through the observations of crystallization within tubes with different roughness (between 0.63 and 13.3 μm), Faucheux et al. [61] found strong influence of surface roughness on supercooling degree and concluded that larger roughness caused lower supercooling degree.
(2) The flow channel for the water or solution should be regular, since the sudden change of the channel, e.g. bend, contraction or expansion, results in strong collision between liquid and solid surface, which accelerates the nucleation.
(3) The heat exchange inside the evaporator should be uniform everywhere of the heat exchanger; otherwise crystallization may occur locally where the temperature of the fluid is low.

The supercooling releaser is also important to the effective crystal generation, and several releasing approaches are investigated and utilized as follows:

(1) The collision of the supercooled fluid with a solid surface, or free liquid surface or liquid bulk in the tank, or with itself, as shown in Fig. 6 [62–65]. The collision provides the momentum increase to release the supercooling state. The probability of freezing mainly depends on the collision force [66]. Moreover, the system requires special device to avoid ice crystals agglomeration near the impact place.
(2) *Ultrasonic vibration*: Researchers [67,68] reported that the ultrasonic vibration can strongly promote the transition of supercooled water to ice slurry, and this method is reliable for ice generation but it is only limited to laboratorial investigation.
(3) *Partial low temperature*: Partial liquid being cooled to the temperature much lower than its freezing temperature can be helpful to the nucleation. This process can be achieved by a small electronic refrigerator.
(4) *Electric charge*: Though scientists have tried to investigate the mechanism of the nucleation by electric charge, the basic mechanism is still controversial [69]. However, some experimental results have been identified to shown the influential factors. Okawa and Saito [66] disclosed supercooling released by the utilization of electric charge with the voltage less than DC 100 V, and found that the influential factors were the voltage, the size of electrode and the distance between the two electrodes.

Okawa and Saito [66] also treated the reciprocally rubbing of glass against glass as one of the effective supercooling release approach, which was depended upon the frequency and amplitude of the rubbing. On the other hand, the authors believed the convection, vibration, and non-contacting shock had no effect on supercooling release.

Tanino and Kozawa [70] and Kozawa et al. [71] applied a pipe type releaser for large-scale ice slurry generation, which generated 2.5 wt% ice slurry for one circulation, and they finally obtained 35 wt% ice slurry. While Ise et al. [72] used this kind of releaser to generate about 23 wt% ice slurry for a building usage.

Nearly the same approach can be employed for CHS generation, e.g., JFE Engineering Corporation [73] successfully applied TBAB CHS air conditioning to several large-scale buildings [21,22,74]. Ogishi et al. [75] employed a tube type heat exchanger (such as shell-and-tube heat exchanger) as the supercooling evaporator for TBAB CHS generation. The heat exchanger also took the role of supercooling releaser, therefore there was at least one of the tubes had irregularity for supercooling release. Hydrates would be generated inside the heat exchanger. The authors reported the deposition of hydrate crystals on the tube inner wall and treated them to be useful nuclei for stable hydrate generation, while the other hydrates were removed by the shear force of the flowing aqueous solution or slurry. The thickness of

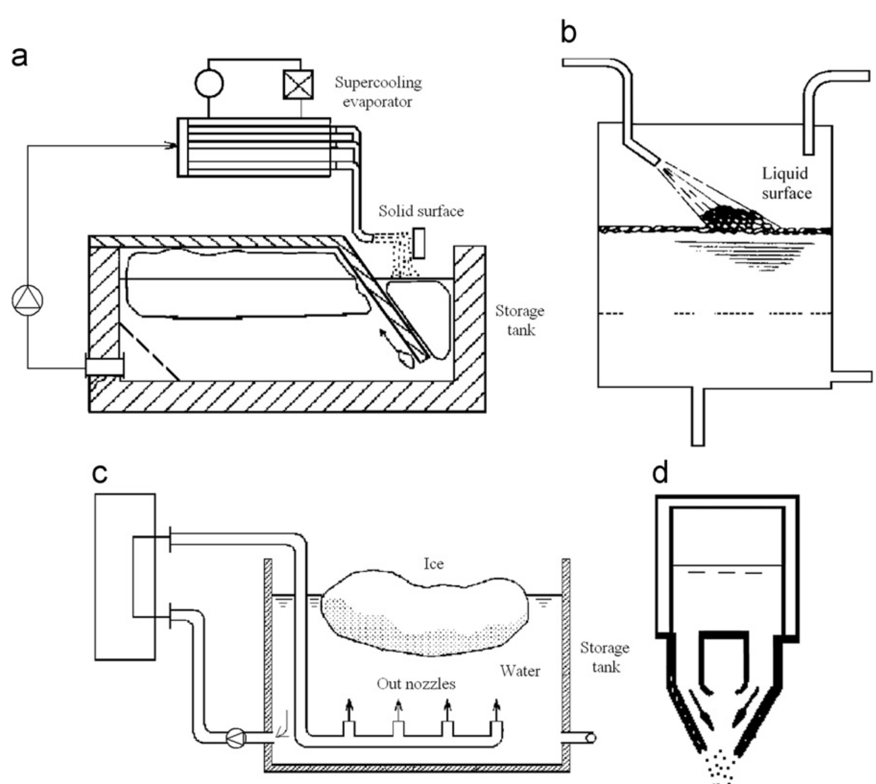


Fig. 6. Collision modes for supercooling release, (a) supercooled liquid and solid surface [63]; (b) supercooled liquid and liquid surface in the tank [64]; (c) supercooled liquid and bulk liquid in the tank [65] and (d) supercooled liquid and itself [62].

the deposition layer was further controlled by adjusting the slurry flow rate and regulating the refrigerant temperature. Moreover, Song et al. [76] validated the effect of ultrasonic vibration on TBAB CHS generation in 25 wt% TBAB solution, and the nucleation was observed to be generated in a very short time under the ultrasonic vibration and the crystallization process also finished in several seconds. The authors found that the crystals may be cracked under the force of ultrasonic vibration, and the obtained TBAB hydrate crystals were fine, smooth and uniform without agglomeration.

2.1.5. Direct contact heat exchanger

Using the direct contact heat transfer between water or aqueous solution with immiscible cool refrigerant, including primary and other secondary refrigerants, ice slurry can be generated directly inside the storage tank [77–83]. Fig. 7(a) shows the utilization of primary refrigerant. During the evaporation of the two-phase primary refrigerant, dispersed ice particles are generated while the refrigerant can be easily separated since it turns to vapor. However, the heat exchanger needs to work under high pressure. Fig. 7(b) shows the application of secondary refrigerant which has lower freezing temperature and usually larger density than water, the refrigerant sinks to bottom of the tank after heat exchange and then returns to the pump and chiller for another cycle.

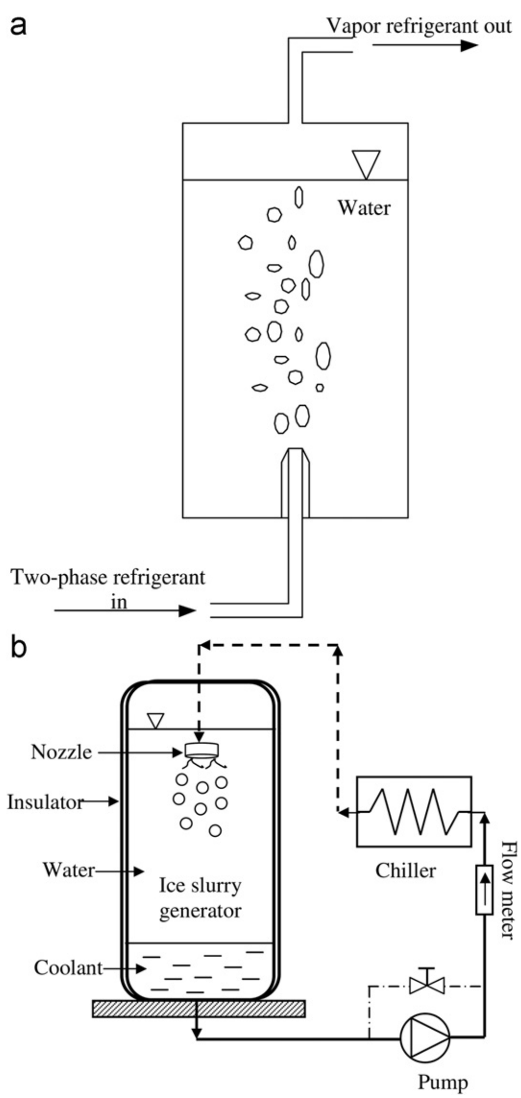


Fig. 7. Schematic diagrams of the direct contact heat exchanger for ice slurry generation, (a) using primary refrigerant [78] and (b) using secondary refrigerant [83].

Within a storage tank of 0.3 m in diameter and 1.1 m in height, Kiatsiriroat et al. [78] utilized the primary refrigerant, including R22 and R12 in the temperature range of -8 to -15 °C, as the coolant for direct contact heat exchange with water. The flow rates of the two refrigerants were 0.02–0.08 kg s^{-1} (about 0.28–1.13 kg m^{-2} s^{-1}) while water was stagnant and kept inside the tank. They found that the volumetric heat transfer coefficients in the cases of R12 and R22 were around 2–16 kW m^{-3} K^{-1} and 2–52 kW m^{-3} K^{-1}, respectively. The promoted heat transfer performance by R22 was attributed to its higher water solubility. Thitipatanapong et al. [79] investigated ice generation using R12 and R134a in direct contact heat exchange while both the refrigerant and water were forced flowing into the heat exchanger. It was noticed that higher water flow rate resulted in higher volumetric heat transfer coefficient. The volumetric heat transfer coefficients obtained by the authors was about 91.62 kW m^{-3} K^{-1} and 209.7 kW m^{-3} K^{-1} in the cases of R12 and R134a with water flow rates of about 16.35 kg m^{-2} s^{-1} and 16.20 kg m^{-2} s^{-1}, respectively, which was higher than those obtained by Kiatsiriroat et al. [78]. Due to the saturation pressure of refrigerant, the ice slurry forming temperature increased to 4.0 °C and 8.8 °C in the case of R12 and R134a, respectively, therefore the storage temperature at about 4.5 °C and 10.0 °C can be achieved, which was considered suitable to air conditioning system application. Thongwik et al. [80] injected low temperature CO_2 (-15 to -60 °C) to water at a flow rate of 0.003–0.017 kg s^{-1}, and the corresponding volumetric heat transfer coefficient was ranged from 1 to 25 kW m^{-3} K^{-1}. After the direct contact with the primary refrigerant, the base liquid is inevitably contaminated by the compressor oil, therefore the authors added the compressor oil and surfactant Tween 60 (polyoxyethylene sorbitan monostearate, which was used to merge water and oil) to water to investigate its influence on slurry generation. It was found lower oil concentration increased the risk of blockage around injector since the non-merging water formed plain ice and blocked the injector, and the optimum composition of water/oil/surfactant was 100/6/1.

Researchers in Singapore [81–83] proposed a special coolant, named Fluroinert (FC-84), as the suitable secondary refrigerant used in direct contact ice slurry generation. FC-84 is heavier than water, the density of which is about 1730 kg m^{-3}, while the freezing temperature is -95 °C. As shown in Fig. 7(b), FC-84 was sprayed by a nozzle at the top of the storage tank. The coolant was at about -10 to -15 °C while the flow rate was 8–12 L min^{-1}. Through modeling and calculation, the overall heat transfer coefficient of the heat exchange between water and FC-84 was in the range of 3.0–6.5 kW m^{-2} K^{-1}. The generated ice crystals were in the shape of thin and long flake with the length of about 1–4 mm, which was quite large compared to those obtained by other methods.

Compared to other ice slurry generators, the utilization of direct heat exchange avoids the sticking of ice crystals on the heat transfer surface and strongly enhances the heat transfer performance. Therefore the COP of the refrigerator increases, for example, about 3.4–3.6, higher than that of the conventional system [77]. The disadvantages of this method are as follows: the nozzle used in the system must be well designed, otherwise blockage may occur; small amount of primary refrigerant trapped in the ice crystals will be released to the environment.

2.1.6. Vacuum ice slurry generator

Ice slurry can be generated in a deep vacuum freezer. Water inside the freezer is kept at deep vacuum close to the triple-point of water, hence part of the water becomes vapor, which absorbs the latent heat of vaporization from the left water, and it is then frozen and converted to ice particles or ice-water mixture.

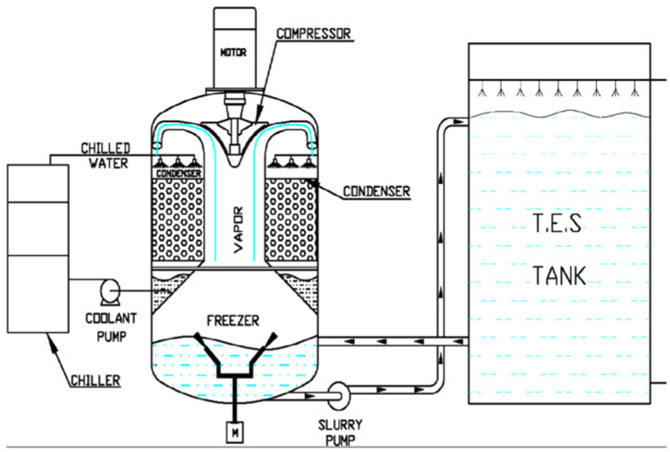


Fig. 8. Vacuum ice slurry generator used in thermal energy storage system [85].

IDE Technologies Ltd. [84–86] developed a vacuum ice slurry generator, and the schematic diagram is shown in Fig. 8. A high speed centrifugal compressor driven by a motor was utilized to generate deep vacuum condition. The generated ice slurry inside the freezer, containing 0.5–1.0 mm ice crystals, was then pumped to the storage tank, and the slurry fraction could reach 50%. To generate ice slurry continuously, water vapor was compressed and then forced flowing through a condenser, where the vapor was cooled by chilled water (e.g., 5 °C) and converted to liquid phase. The cooling capacity of this generator can achieve 3500 kW. The generator has been applied to district cooling and heating, thermal energy storage, mine cooling and snow making, and hundreds units have been installed worldwide [86]. However, due to large specific volume of water vapor under deep vacuum condition, the size of the generator is quite large. On the other side, Bapat and Kulkarni [87] employed a lithium bromide vapor absorption machine to generate the vacuum condition for ice slurry generation, which is compact in size and less electric energy consumption.

Researchers in Korea [88,89] sprayed water droplets with initial temperature at 20 °C and 50 μm in size by nozzles in a vacuum chamber to generate ice slurry. The pressure in the chamber was kept lower than the pressure of triple point, and spherical ice crystals with size below 300 μm were then formed. To avoid the generation of ice crystals around nozzles, the authors added 7% ethylene glycol to water. Different from the vacuum generator shown in Fig. 8, the formed vapor was then removed from the chamber. The feeding of water was maintained at low rate to obtain water droplets, therefore the cooling capacity was only 0.23 kW (theoretical value), which could be improved by increasing the nozzle number.

2.2. Storage strategy of ice slurry and TBAB CHS

The storage of ice slurry and TBAB CHS in tanks is mainly conducted in two modes, homogeneous storage and heterogeneous storage [90], as shown in Fig. 9.

As shown in Fig. 9(a), the homogeneous storage required agitation to maintain the slurry fluidizing inside the storage tank and to avoid the agglomeration of particles. The agitation is usually provided by propeller, pumps, paddles and so on. Since the absence of agglomeration in homogeneous slurry storage, it is very easy to extract the slurry with very fine crystals and the pumping is also quite reliable. It was reported [91] that the maximum ice fraction in homogeneous storage could be up to 30–35 wt%, beyond which the power consumed by the agitator increased significantly, e.g., the power consumed by Danish Technological Institute to agitate 52 wt% ice slurry was 10 times larger than that of 30 wt%.

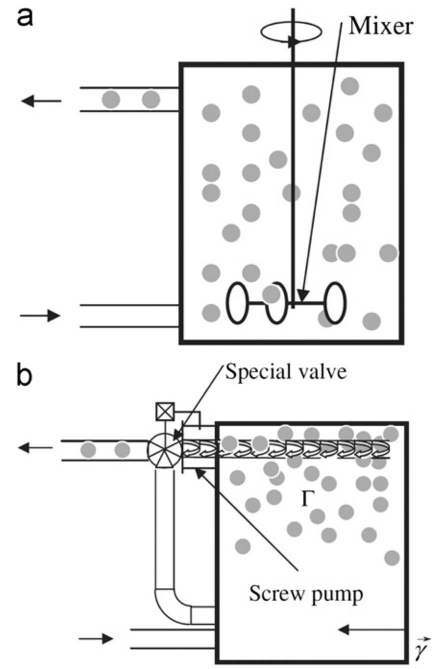


Fig. 9. Storage strategies of ice slurry, (a) homogeneous storage and (b) heterogeneous storage [90].

Since the agitation is significant energy consuming, Meili et al. [92] reported that the mixing of the slurry could be stopped for about 12 h, and then homogeneous ice slurry could be still obtained after restarting the agitation. Moreover, adding freezing point depressing agents to water can smooth the generated ice particles and prevent the agglomeration. However, Grandum and Nakagomi [93] and Inaba et al. [94] believed the additions of freezing point depressing agents resulted in a low refrigerator COP because of the depressed freezing temperature. Therefore, the authors utilized other additives, for example, antifreeze proteins (AFPs), antifreeze glycoproteins (AFPs), silane coupling agents, surfactants and so on and considered them as suitable since the low additive concentration (less than 1 wt%) led to relative high freezing temperature.

Fig. 9(b) shows the method of heterogeneous storage. Due to the different density of the solid crystals from that of the carrier liquid, such as ice is lighter than water and TBAB hydrate is heavier than the solution, crystals in heterogeneous storage tank tend to accumulate at the top or deposit at the bottom of the tank. Compared to homogeneous storage, the ice fraction in heterogeneous storage tank can reach about 50–60 wt% [91], and the necessary volume of the storage tank is then reduced. The difficult thing in this storage mode is that the extraction of ice from the tank. Eglof et al. [90] considered using a screw pump to extract the high fraction ice slurry from the top of the tank and then mixed it with the low fraction ice slurry pumped from the bottom region through a special valve. This proposal has not been experimentally validated yet and needs further investigation. Douzet et al. [48] employed this approach for TBAB CHS storage, they pumped the high fraction TBAB CHS (about 40–50% in volume) from the bottom of the tank using a lobes pump and mixed it with the liquid sucked through the top of the tank using another pump, then they obtained TBAB CHS with about 20% volume fraction for air conditioning application. Actually, pure ice particles can be obtained by a harvester [91], though the shaved ice particles (e.g., 1–2 mm) were larger than the original

generated ones (e.g., 0.1 mm), the particles are mixed with the cold water extracted from the bottom of the tank to form ice slurries with different fractions.

2.3. Fabrication of MPCS

MPCS requires the technology that coating the PCM with suitable shell material to envelop the core PCM. Gibbs et al. [95] reported several forms of the microcapsules, as shown in Fig. 10. Generally three steps are required for microcapsules preparation: forming the shell around the PCM, ensuring there is no leakage, and ensuring the undesired materials are not included in the capsule. Though the microencapsulation technology was discovered and developed in the 1940s and 1950s [96] and then many approaches were developed for food industrial [97], only coacervation, polymerization, spray drying were found being employed in PCM encapsulation. These processes are simply introduced in the following contexts, the detailed information about the fabrication and the further properties of the formed microencapsulated PCMs can refer to the review articles [7,8].

2.3.1. Coacervation

There are two types of coacervations: simple coacervation and complex coacervation. The complex one is commonly used for PCM microencapsulation. First, polymer in water as the coating material, e.g. gelatine in water, is prepared. Then the core material is dispersed to the gelatine solution at a temperature range of 40–60 °C, at which the coating material is liquid. The simple coacervation employs only one kind of colloid, while another colloid, such as gum Arabic, is added to the solution for complex coacervation at this step. The step is followed by coacervation. Simple coacervation is induced by change of condition, such as the temperature, the addition of nonsolvent or microions, which causes the dehydration of macromolecules. Complex coacervation is usually induced by increasing the polymer concentration or reducing the solution pH (usually 4–4.5). The system is then cooled to room temperature. Finally, the microcapsules are hardened and isolated. Hardening is conducted by cross-linking agent, such as formaldehyde, the increasing of pH to 9–11 (by NaOH solution, e.g.) and temperature to 50 °C can hasten this process. The temperature should be reduced and maintained at about 5–10 °C for 2–4 h, then the capsules are filtered and dried in a vacuum oven.

Using the complex coacervation, Hawlader et al. [98] obtained around 1 μm spherical and smooth microcapsules of paraffin wax. The latent heat was about 234.05 $J\,g^{-1}$, 224.31 $J\,g^{-1}$ and 196.38 $J\,g^{-1}$ when the core-to-coating ratio was 2:1, 1:1 and 1:2, respectively. The encapsulation efficiency was in the range of 80–95%, and it decreased as increasing the ratio of core-to-coating since incomplete coating on core material might occur when the coating material was deficient. Özonur et al. [99] applied the same method to encapsulate the natural coco fatty mixture for thermal energy storage (melting temperature of the PCM was in the range of 22–24 °C). The size of the obtained microcapsules varied from 1 μm to 1 mm depending on the stirring speed and time. After encapsulation, there was an increment of about 7 °C on the melting temperature.

2.3.2. Polymerization

Polymerization are used widely for fabricating microencapsulated PCM, and there are several different type polymerization approaches. Yang et al. [100] and Brown et al. [101] employed the so-called "in-situ" polymerization to encapsulate tetradecane and dicyclopentadiene, respectively. The former study utilized several types of polymers, e.g., polyvinyl acetate (PVAc), polystyrene (PS), polymethylmethacrylate (PMMA), polyethyl methacrylate (PEMA). The authors mixed the PCM and polymer with surfactants, initiator and deionized water in a flask accompanying with agitation, and then heated the mixture to and maintained it at a certain temperature. The mixture was then cooled down naturally by continuous stirring for 4–5 h. It was found that the coating material strongly influenced the thermal properties of the formed MPCM. After encapsulation, the melting temperature decreased from 6.7 °C (pure tetradecane) to 5.97 °C as the coating material was PMMA and to 5.68 °C as the coating material was PEMA, while the freezing temperature increased from 1.98 °C to 2.95 °C and to 3.19 °C, respectively. The obtained microcapsules were 5–30 μm in diameter and 66.26 $kJ\,kg^{-1}$ in melting heat with 40% tetradecane. The latter study described their detailed preparation process in Fig. 11. Using this process, 10–1000 μm microcapsules were obtained by adjusting the agitation rate between 200 and

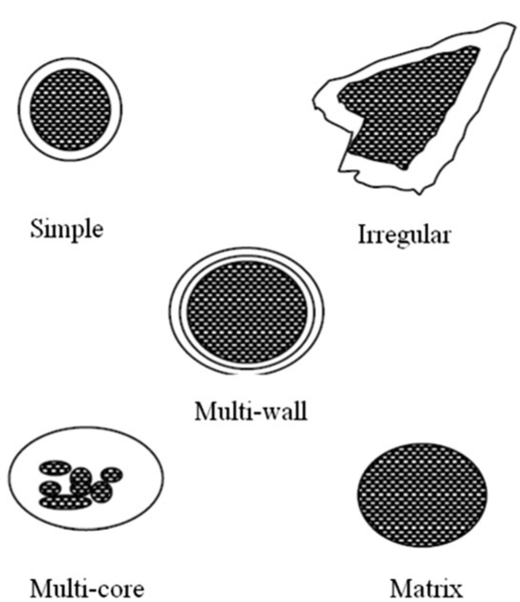


Fig. 10. Several forms of the microcapsules [95].

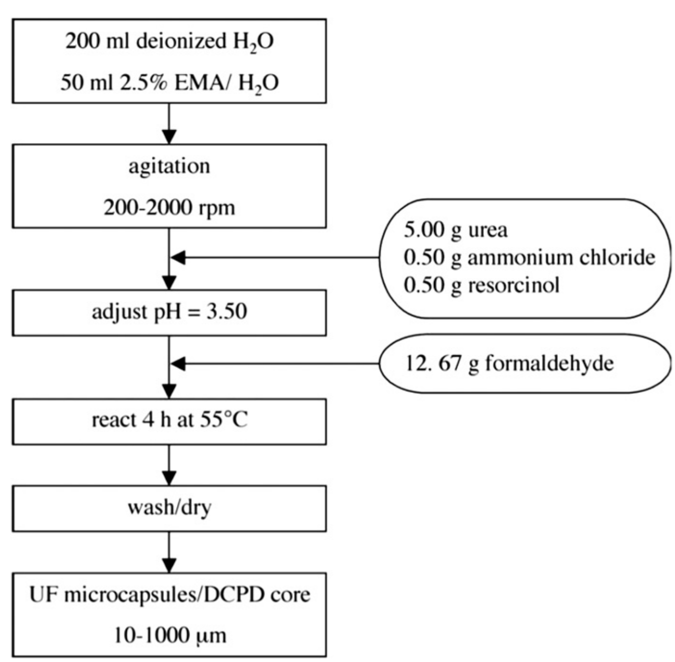


Fig. 11. In-situ polymerization for microencapsulation [101].

2000 rpm, and the wall thickness was in the range of 160–220 nm. It was noticed that the surface roughness reduced as the agitation rate increased. Fill content of the obtained microcapsules was beneficially up to 83–92 wt%. Using in-situ polymerization and the assistance of ultrasonic, Fang et al. [6] coated *n*-octadecane with polystyrene as shell and obtained very fine nanoencapsulated PCM, the particles were regular spheres and diameter was only 50–200 nm. The phase change temperature was found very close to that of pure *n*-octadecane, while the latent heat dropped nearly 50% due to the existence of the coating material.

Alkan et al. [102] prepared the microcapsules using emulsion polymerization. They used docosane as core and PMMA as shell. Docosane was first mixed with deionized water and Triton X-100 (surfactant), and then was heated to the temperature higher than the melting temperature of docosane under nitrogen atmosphere. This process was followed by the addition of methylmethacrylate and allyl methyl acrylate and $FeSO_4 \cdot 7H_2O$ solution, of which the allyl methyl acrylate was used as cross-linking agent to prevent the formation of secondary particles. The mixture was then agitated violently for 30 min. $Na_2S_2O_7$ solution and tertbutylhydroperoxide solution were added and the mixture was heated to 90 °C. Thereafter the polymerization started. After casting water, the precipitate was dried under vacuum at 40 °C for 24 h. The average diameter of the obtained PMMA microcapsules was 0.16 μm. The influences of microencapsulation on the melting and freezing temperature were slight, and only 0.6 °C decrease of the melting temperature and 0.2 °C increase of the freezing temperature were observed after the microencapsulation. The melting and freezing heat were measured, which were 54.6 kJ kg^{-1} and 48.7 kJ kg^{-1}, respectively. Therefore the slurry contained 28 wt% docosane.

Cho et al. [103] and Siddhan et al. [104] applied almost the same interfacial polymerization to encapsulate the PCM (octadecane) using TDI (toluene-2, 4-diisocyanate) and DETA (diethylenetriamine) as coating material. Surfactant NP-10 [poly(ethylene glycol) nonylphenyl ether] was treated as emulsifier by the former study while the latter study used NP-9.5. The NP-10 (or NP-9.5) aqueous solution and organic solution of octadecane, cyclohexane and TDI were prepared and mixed with each other accompanying with violent agitation to form an oil-in-water emulsion. Then the DETA aqueous solution was added to the emulsion drop by drop to start the interfacial polymerization which happened between TDI and DETA at the oil–water interface. The rotation speed of the agitator was slowed down and the mixture was heated to 60 °C. This state was maintained for 45 min (the latter study added more DETA solution for further diffusion and polymerization). Finally, the microcapsules were filtered and washed and dried. Both studies obtained small capsules, 0.1–1 μm in the former study and less than 14 μm in the latter one. By additionally adding DETA solution, Siddhan et al. [104] obtained higher core fill content (about 40–68 wt%) than that obtained by Cho et al. (26.0–46.4 wt%). The encapsulation efficiency was 75.4–87.2% in the former study, while the latter study noticed that the efficiency was largely depended on the core-to-monomer ratio (varied from about 50% to 90% as the ratio increased from about 2 to 6.5) and PCM-to-cyclohexane ratio (varied from about 87% to 97% as the ratio increased from about 1 to 12).

Ai et al. [105] used suspension polymerization for *n*-hexadecane microencapsulation, while polystyrene was used as shell. Considering casein in solution and dispersed form as an excellent emulsifier, the authors utilized casein instead of the necessary surfactants as emulsifier in other polymerization processes to emulsify the mixture of core material, monomers and initiators. The usage of casein provided extra effect of protecting the oil droplets against recoalescence before the microcapsules formation. Thus, the application of casein in polymerization process could simplify the process since no more additives were needed. The size of the obtained microcapsules was 3–15 μm. The latent heat was in the range of 76.01–124.7 kJ kg^{-1} depending on the polymerization time, which was much lower than that of the pure material, 236 kJ kg^{-1}. Sánchez et al. [106] also considered this method as simple, cheap and technically feasible. They coated several kinds of phase change materials, including paraffin wax, tetradecane, nonadecane, etc., by a coating material of styrene. The other necessary materials included benzoyl peroxide as initiator, polyvinylpyrrolodone as stabilizer and water. After the violent agitation, the mixture was heated to 110 °C at one atmosphere for 6 h, then it was washed, filtrated and dried. The capsules size ranged between 20 μm and 700 μm with the average value of 237 μm, which was also dependent on different core materials. The core fill content for paraffin wax, tetradecane and nonadecane was 20.56 wt%, 39.10 wt% and 49.36 wt%, respectively.

2.3.3. Spray drying

Spray drying is a technology that can generate powder instantaneously by atomizing the liquid production in a hot air or nitrogen [107], which is considered as economic for microencapsulation. The spray drying process in microencapsulation involves the following basic steps: mixing the core solution and the coating material solution; heating and agitating the mixture to obtain homogeneous mixture; if needed, adding the emulsifier to the mixture, which depends on the properties of the coating material; ensuring the formed emulsion are stable over a certain period; atomizing the emulsion in the drying chamber where the solvent (usually water) is evaporated; cooling and dehydrating the obtained particles. Hawlader et al. [98] employed a spray dryer to spray dry the emulsions of paraffin wax and the coating material with a feeding rate of 20 mL min^{-1} by a centrifugal atomizer operated at 25,000 rpm. The authors compared the microcapsules produced by spray drying with that by complex coacervation, and it was found the spray drying made much smaller particles (around 0.1 μm compared to around 1 μm), however, the latent heat was also smaller than that produced by the complex coacervation (about 221.5 kJ kg^{-1} compared to 234 kJ kg^{-1}, when the core-to-coating ratio was 2:1).

3. Flow and heat transfer characteristics

Flow and heat transfer characteristics of PCS in tubes and heat exchangers are significant to its application. The rheology, flow and heat transfer behaviors of ice slurry have been previously reviewed by Ayel et al. [108] in 2003, and Zhang et al. [7] also presented the flow and heat transfer characteristics of MPCS and CHS in 2010. However, there are many new researches about the PCS that have been conducted thereafter. Therefore we emphasize the present review on the recent research details of the flow pattern, flow frictions and heat transfer coefficients of PCS in tubes and heat exchangers and also the impact of particle fraction and tube diameter on mentioned behaviors.

3.1. Flow pattern of ice slurries

The usual flow patterns of solid-liquid two-phase flow are homogeneous flow, heterogeneous flow, moving bed and stationary bed. The pressure drop increases with flow velocity at the homogeneous and heterogeneous flows but decreases at moving bed and stationary bed flows. All these flow patterns have ever been observed in ice slurry flow, however, Kitanovski et al. [109]

pointed that the flow pattern classification by simple observation showed quite large uncertainty.

Using the Ultrasonic Doppler Profiler (UVP), Vuarnoz et al. [110] obtained both the vertical and horizontal velocity profiles of 7.5–7.6% ice slurry flowing through a 20 mm × 20 mm rectangular channel, as shown in Fig. 12(a). With the decrease of flow rate, both velocity profiles became bulgy in the axes. The vertical profiles were more sensitive to the flow rate reduction due to the gravity effect, therefore the flow became slower at the top and faster at the bottom since the accumulation of ice particles at the top, as shown in the figure; meanwhile, the horizontal profiles remain symmetrical as decreasing flow rate. Using a hot film anemometer (HFA) and an on-line ice slurry sampling/calorimetry technique, Stamatiou and Kawaji [111,112] obtained the velocity profiles of 0–5.9 vol% ice slurry and 3.1–9.0 vol% ice slurry with heat exchange flowing through a vertical 610 mm × 310 mm × 25.4 mm channel as shown in Fig. 12(b1)–(b4). When ice fraction was low, i.e. 0–0.9 vol% in Fig. 12(b1), the velocity profiles were hardly influenced by the ice particles, therefore the results were similar to that of single-phase fluid; ice particles influence the velocity profiles when the ice fraction is in the range of 0–5.9 vol%, as shown in Fig. 12(b2), larger ice fraction results in blunter profiles; when heat flux was imposed to ice slurry flow, the formation of ice-free layer near the heated wall led to larger fluid

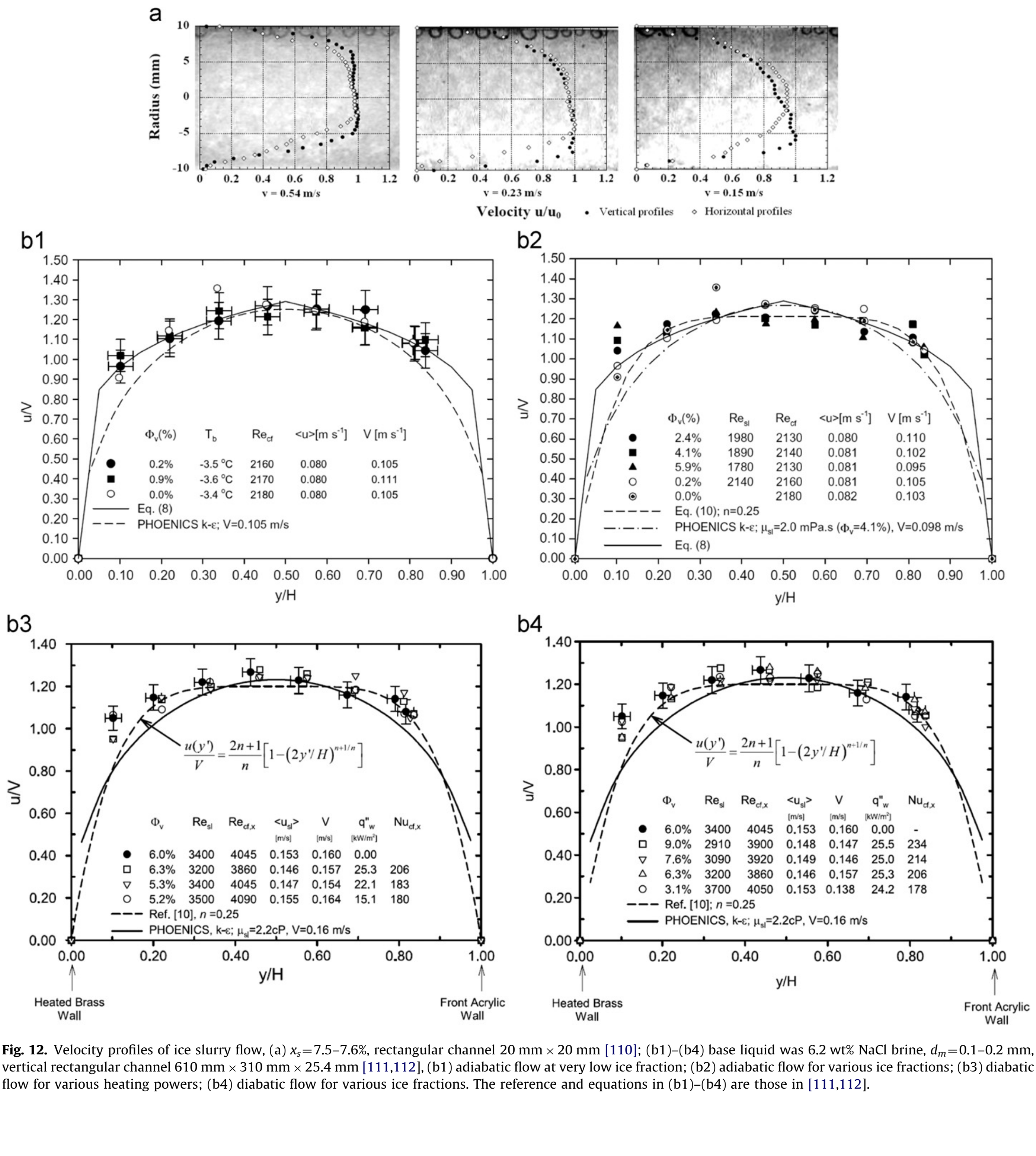


Fig. 12. Velocity profiles of ice slurry flow, (a) x_s = 7.5–7.6%, rectangular channel 20 mm × 20 mm [110]; (b1)–(b4) base liquid was 6.2 wt% NaCl brine, d_m = 0.1–0.2 mm, vertical rectangular channel 610 mm × 310 mm × 25.4 mm [111,112], (b1) adiabatic flow at very low ice fraction; (b2) adiabatic flow for various ice fractions; (b3) diabatic flow for various heating powers; (b4) diabatic flow for various ice fractions. The reference and equations in (b1)–(b4) are those in [111,112].

density in this area than fluid in the flow center, therefore the flow near the heated wall decelerated as shown in Fig. 12(b3) while the flow in the tube center changed little; Fig. 12(b4) shows that there is no clear influence of ice fraction on the velocity profiles of ice slurry under heating.

Ice fraction profile of ice slurry is related to many factors, e.g., density of carrier liquid, density of ice particle, shape and size of ice particle, tube diameter, and the flow velocity [109]. Kitanovski and Poredoš [113] modeled and numerically calculated the concentration profiles of 10 wt% and 25 wt% ice slurry flow though 27.2 mm tube, as shown in Fig. 13. It was believed that the 10 wt% ice slurry flow was homogeneous at υ_s=2.0 m s^{-1} and was heterogeneous at υ_s=0.5–1.5 m s^{-1} and moving bed appeared at υ_s=0.5 m s^{-1}, as shown in Fig. 13(a), and the larger ice faction resulted in earlier transition from homogeneous flow to heterogeneous flow as comparing Fig. 13(a) and (b).

With the reduction of flow velocity, flow of ordinary solid-liquid two-phase slurry will transit from heterogeneous flow to moving bed at a critical velocity, which is named as deposition velocity. On the basis of velocity profiles, Kitanovski [114] evaluated the deposition velocities of ice slurry with different ice particle diameters as well as different tube diameters, as shown in Fig. 14(a). As the ice fraction increasing from 5 wt% to 25 wt%, the deposition velocity of ice slurry had a maximum value at x_s=15 wt%. Both the increase of tube diameter and ice particle diameter caused easier deposition corresponding to the larger deposition velocity as shown in the figure. Rached et al. [115] reported a new method to determine the deposition velocity of ice slurry. They measured the cross-section areas of the moving bed as increasing the flow velocity gradually, and then extrapolated the deposition velocity corresponding to the disappearance of the moving bed which could not been observed directly. Deposition velocities of 10–32 wt% ice slurry flowing through 50 mm and 75 mm tubes were obtained, as shown in Fig. 14(b). As seen from the figure, the deposition velocity reduced with ice fraction but increases with tube diameter.

On the other hand, different from the aforementioned flow patterns, Hirochi et al. [116] observed three types of flow patterns of ice slurry with chipped ice particles. The authors believed that the behavior of ice slurry was different from that of ordinary solid-liquid two-phase slurry due to the cohesive nature of ice particles. The cohesive nature of ice particles dominated ice slurry flow pattern while the gravity dominated that without cohesive nature. Therefore, the states of moving bed and stationary bed were not observed but instead of cluster flow and column flow, where the pressure drop also decreased as the reduction of the flow velocity, as shown in Fig. 15.

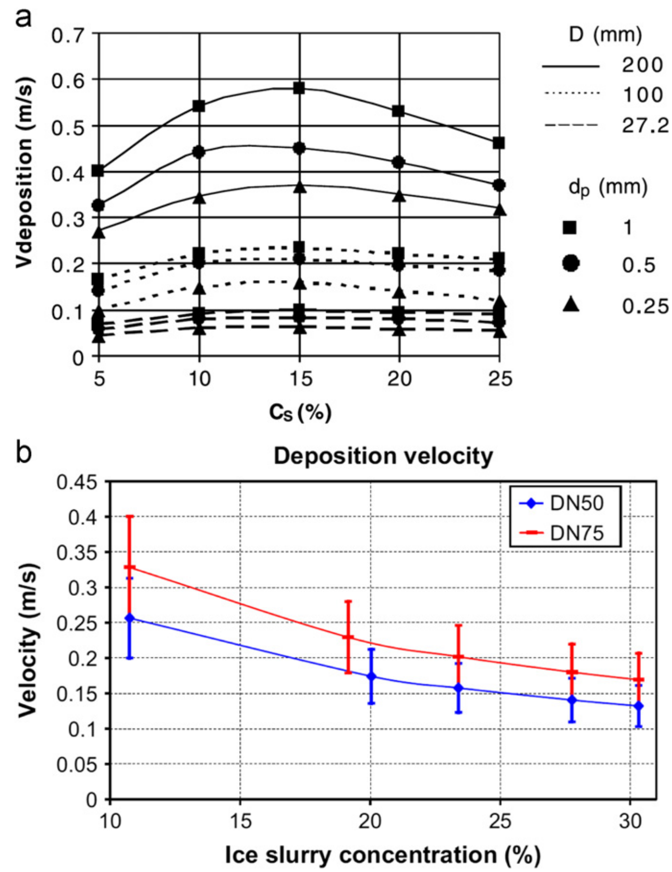


Fig. 14. Deposition velocities of ice slurry flow in tubes, (a) Kitanovski [114] and (b) Rached et al. [115].

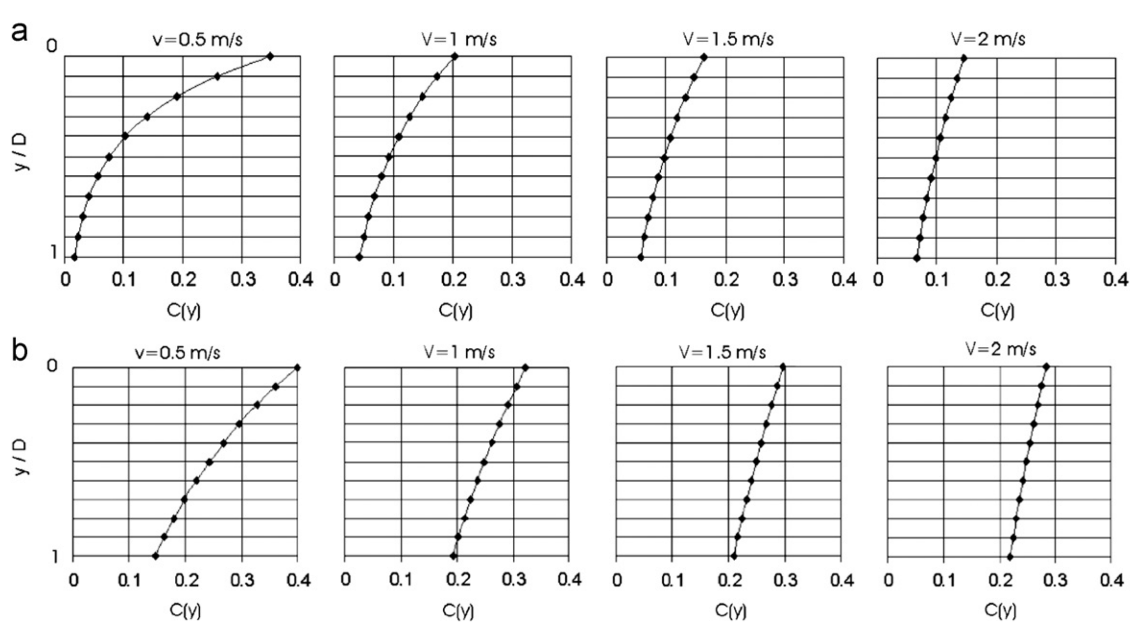


Fig. 13. Ice fraction profiles of ice slurry flow (simulated), base liquid was 10% ethanol/water mixture, d_m=1 mm, D_i=27.2 mm, (a) x_s=10 wt% and (b) x_s=25 wt% [113].

3.2. Rheology of PCS and the friction factor correlations

3.2.1. Ice slurry

It was commonly considered that ice slurry with low ice fraction, i.e. 6–15% [108], behaved as Newtonian fluid. Therefore the flow friction can be easily predicted by empirical correlations while the apparent viscosity was usually calculated by Thomas relation [108,109]

$$\mu = \mu_f(1+2.5\varphi+10.05\varphi^2+0.00273e^{16.6\varphi}) \quad (1)$$

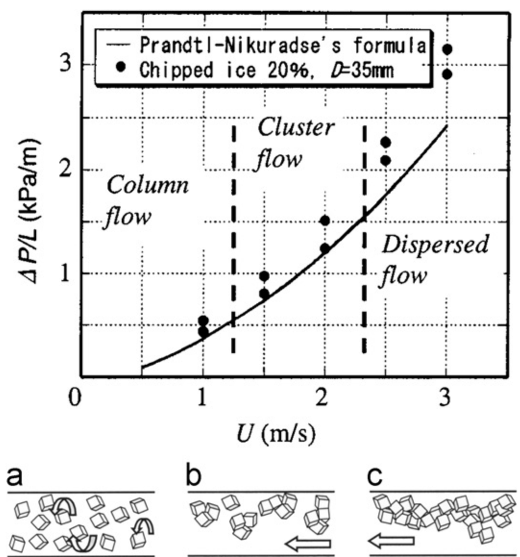


Fig. 15. Flow patterns and pressure drops of ice slurry with chipped ice particles in tube [116]. (a) *Dispersed flow*, *U*=2.5 m/s, (b) *cluster flow*, *U*=1.5 m/s and (c) *column flow*, *U*=1.0 m/s.

Using Poiseuille equation for laminar flow and Blasius correlation for turbulent flow, Grozdek et al. [117] concluded that the calculation discrepancies were smaller than 10% for both the laminar flow of ice slurry with $x_s < 20$ wt% in 9 mm tube and the turbulent flow with $x_s < 15$ wt% in 9 mm and 15 mm tubes. Fernández-Seara et al. [118] also treated the 5–15 wt% ice slurry as Newtonian fluid in a fan-coil unit and predicted the flow friction with relative error of −21.5 to 29 % in laminar region by Poiseuille equation, while with relative errors of −6.3 to 9% and −17 to 1% in turbulent region by Petukhov and Blasius equations, respectively.

However, many other researchers considered ice slurry as non-Newtonian fluid and developed semi-empirical correlations based on rheological properties, e.g., the Bingham model, the Ostwald model (also known as the Power-law model), the Casson model and the Herschel–Bulkley model.

Based on the experimental flow curves of 0–30 wt% ice slurries in 10–20 mm tubes as shown in Fig. 16(a), Niezgoda-Żelasko and Zalewski [119] determined ice slurry as Bingham fluid, which indicated that the ice slurries would behave as Newtonian fluid after conquering the yield stress. The corresponding yield stress and apparent viscosity for ice slurries with different ice fractions were measured, then the friction of laminar flow was estimated by Buckingham–Reiner equation, i.e., Eq. (2), with excellent agreement and the friction factor of turbulent flow was calculated by Tomita equation, i.e., Eq. (3), with the uncertainty better than 10%

$$\frac{1}{Re_B} = \frac{f_F}{16} - \frac{He}{6Re_B^2} + \frac{He^4}{3f_F^3Re_B^8} \quad (2)$$

$$\frac{1}{\sqrt{f_{FBT}}} = 4.0\,\lg(Re_{BT}\sqrt{f_{FBT}}) - 0.4 \quad (3)$$

where Re_{BT} was calculated by the equation given by Tomita [119].

Different from Niezgoda-Żelasko and Zalewski [119], Kumano et al. [120] treated ice slurry as pseudo-plastic fluid based on their

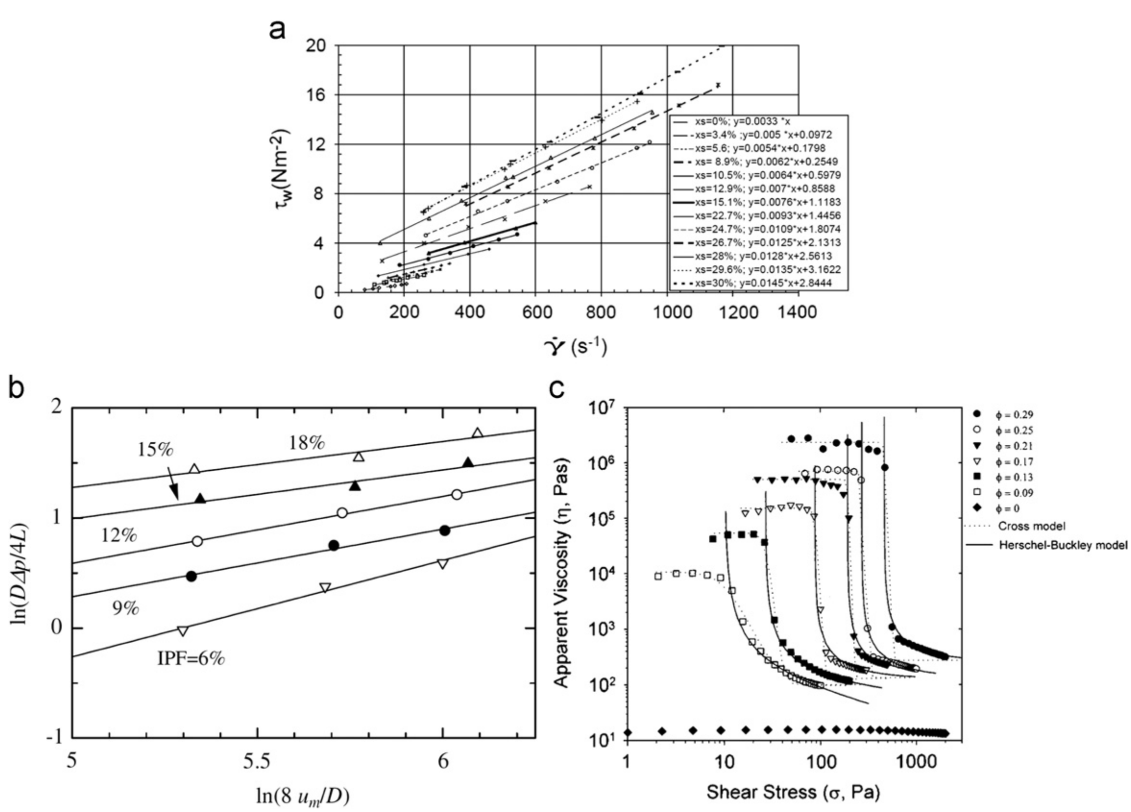


Fig. 16. Rheological feature determination of ice slurry, (a) shear stress and shear rate of ice slurry flowing through 16 mm tube [119]; (b) flow curve of ice slurry flowing through 10.2 mm tube [120] and (c) apparent viscosity of ice slurry measured by rheometer [121].

measured flow curves of 6–24 wt% ice slurries in 4.3–10.2 mm tubes, as shown in Fig. 16(b). The authors utilized the Power-law model to illustrate the flow characteristics of ice slurry, and obtained the corresponding parameters: flow behavior index n and fluid consistency coefficient K', then the modified Reynolds number, Re_{MR}, was used to describe the flow of power-law ice slurries, as given in the following:

$$Re_{MR} = \frac{D\nu\rho}{K}\left(\frac{4n}{3n+1}\right)^n\left(\frac{8\nu}{D}\right)^{1-n} = \frac{D^n\nu^{2-n}\rho}{K'8^{n-1}} \tag{4}$$

It was found that the ice slurry deviated from Newtonian fluid more with higher ice fraction and in larger tube.

Stokes et al. [121] measured the apparent viscosities of 0–29 vol% ice slurries by a rheometer, results are shown in Fig. 16(c). As shown in the figure, there was a large zero-shear viscosity at low applied stress, after which the apparent viscosity dropped drastically as the increasing shear stress. Therefore, the authors suggested that the Herschel–Bulkley model should be applied to ice slurries.

Grozdek et al. [117] tried several types of models and friction correlations on the flow of 0–30 wt% ice slurry in 9–25 mm tubes and revealed that: Buckingham–Reiner equation for laminar flow predicted the experimental results with the relative error within $\pm 15\%$ for only 60% of all results, and the inclusion of stratification effect would extend this error range to 82% of all experimental data; Dodge–Metzner correlation for Power-law fluid, i.e., Eq. (5) and Tomita equation for Bingham fluid showed good agreement with the experimental results in turbulent flow

$$\frac{1}{\sqrt{f_F}} = \frac{4.0}{n^{0.75}}\log(Re_{MR}f_F^{(2-n/2)}) - \frac{0.4}{n^{1.2}} \tag{5}$$

However, Reynolds numbers utilized in the study were not corresponding to each rheological model, but just used Reynolds number defined as Newtonian fluid (apparent viscosity was calculated by Thomas relation).

Niezgoda-Żelasko and Żelasko [122] proposed a general method to estimate the flow friction of ice slurry flowing through passages with arbitrary cross-section. The calculation process was similar to that of Power-law method, however, the geometrical parameters of the flow passage was added to the expressions of flow behavior index and fluid consistency coefficient. Re_{MR} was then obtained, using which Poiseuille equation for laminar flow and Dodge–Metzner correlation as well as Blasius equation for turbulent flow could be employed by non-Newtonian ice slurry flow. The comparison between the calculated and measured friction factors of ice slurry flow through circular tube (16 mm in diameter) and rectangular channel (3 mm × 38.5 mm and 78 mm × 26.5 mm) showed the uncertainties were less than 5% in laminar region and 10% in turbulent region.

On the basis of the experimental results obtained by Bédécarrats et al. [123] and Grozdek et al. [117], Monteiro and Bansal [124] evaluated the mentioned four rheological models. Among these models, the Herschel–Bulkley model was considered as the best one and the only one which predicted the trend of experimental results well due to the consideration of ice particles diameter.

3.2.2. MPCS

It is believed that MPCS can be treated as Newtonian fluid if the slurry is homogeneous due to the very fine particles, and this conclusion has been verified by many measured viscosities using rheometer [9–15,125–128], as given in Table 1, except Zhang et al. [129] who obtained pseudo-plastic feature of 10–40 wt% MPCS using a rotating cylinder type of rheometer.

The results reveal the viscosity of MPCS is related with the particle fraction and temperature. Vand's equation was used by many researchers [9,10,12,125,127] to predicted the viscosity of MPCS, given by the following equation:

$$\mu = \mu_f(1-\varphi-A\varphi^2)^{-2.5} \tag{6}$$

where A is the constant that concerning the particle size, shape and rigidity, which is 1.16 with the assumption that the particles are ideal rigid sphere. Dammel and Stephan [125] found this equation underestimated the viscosity of MPCS, since the particles in MPCS was obviously not rigid sphere; Yamagishi et al. [9] used $A=3.7$ while Wang and Lin [127] determined the value of 4.4 according to their experimental result. Considering as Newtonian fluid, the calculated friction factor using Poiseuille equation and Blasius equation given by Yamagishi et al. [9] showed perfect agreement with the measured result, as shown in Fig. 17(a); the friction factor of MPCS in turbulent flow region measured by Wang et al. [12] was higher than the predicted value by Blasius equation, as shown in Fig. 17(b), and the authors attributed this higher value to the high tube wall roughness; Inaba et al. [10] reported the overestimation of Blasius equation in MPCS turbulent flow, as shown in Fig. 17(c), the authors explained it by the flow drag reduction effect of the fine particles (1.5 μm) and found that the increase of the ratio of larger particles (17 μm) caused the smaller discrepancy between the measured friction and the calculated values by Blasius equation.

3.2.3. CHS

So far, CHS was determined as non-Newtonian fluid in all the open literature [24–33,36,37,131]. Based on the measured flow curves of TBAB CHS in 16 mm tubes, as shown in Fig. 18(a), Darbouret et al. [25] believed that TBAB CHS behaved as Bingham fluid. The authors presented the corresponding yield stress and viscosity which were about 0–14.18 Pa and 0.008–0.17 Pa s, respectively, depending on the volume fraction of CHS, and found good agreement between the measured pressure drop in laminar flow region and the predicted values using Buckingham–Reiner equation. In addition, Song et al. [27] also treated TBAB CHS as Bingham fluid in their study of heat transfer characteristics of the slurry.

Other researchers determined TBAB CHS as pseudo-plastic fluid by the flow test in pipes, including Hayashi et al. [24], Xiao et al. [26], Ma et al. [28], and Kumano et al. [30]. The results of the relation between $\ln(D\Delta P/4L)$ and $\ln(8\nu/D)$ of type B TBAB CHS measured by Ma et al. [28] are shown in Fig. 18(b), which indicated that the Power-law model was appropriate to TBAB CHS. The flow behavior index n and fluid consistency coefficient K' obtained by different authors are summarized and presented in Fig. 19, and it was commonly accepted that larger slurry fraction caused the slurry deviated Newtonian fluid more. Using the modified Reynolds number (Eq. (4)), Ma et al. [28] calculated the slurry pressure drop in straight tubes: Poiseuille equation was used for laminar flow, and the relative error was +10% and +15% in 6 mm and 14 mm tube, respectively; while Dodge–Metzner correlation was used for turbulent flow, and the relative error was −20% to −25% and +8%, respectively.

Based on the tested viscosities using rheometer, Suzuki et al. [36,37] obtained the shearing-thinning pseudo-plastic behavior of TME CHS, and Hashimoto et al. [131] obtained the similar behavior of TBAB CHS and TBAF CHS. The latter study also found that the TBAB and TBAF solution were both Newtonian fluid when the shear rate was low but their apparent viscosity increased when shear rate was larger than 500 s^{-1}.

3.3. Pressure drops and flow friction of PCS

Compared to single-phase fluid, pressure drops of the two-phase PCS are dominated by many other parameters in addition

Table 1
Measured viscosities of MPCS.

Authors	Materials (including PCM material and coating material)	Slurries	Temperature, °C	Viscosity, mPa s	Descriptions
Yamagishi et al. [130]	*n*-Tetradecane; melamine resin	d_p=5 μm; φ_s=20–30 vol%	25	3–1000 with 0.2–100 s^{-1} shear rate	μ decreased with increasing shear rate
	n-Tetradecane; melamine resin; 1 wt% surfactant			1–7	μ was independent of shear rate
Yamagishi et al. [9]	Octadecane; melamine-formaldehyde	d_p=2–10 μm; φ_s=7–30 vol%	25	1.17–10.4	μ increased with particle fraction; nearly independent of temperature
Alvarado et al. [11]	*n*-Tetradecane; gelatin	d_p=2–10 μm; x_s=4.6–17.7 wt%	2–12	The ratio to that of water about 1–3.5	μ increased with particle fraction, and was independent of temperature
Wang et al. [12,13]	1-Bromohexadecane amino plastics	$d_{p,a}$=10.112 μm; x_s=5–27.6 wt%	20	1.57–8.42	μ increased with particle fraction
Inaba et al. [10]	Small particle: *n*-tetradecane Large particle: *n*-docosane	$d_{p,a}$=1.5 μm; x_s=20 wt%; $d_{p,a}$=17 μm; x_s=0–50 wt% (compared to small particles)	4–67	0.5–5	μ increased with particle fraction and decreased with temperature
Chen et al. [14]	Urea-formaldehyde	d_p=1–20 μm; x_s=5–15.8 wt%	10, 20	1.5–4.5	
Dammel and Stephan [125]	*n*-Eicosane; polymethylmethacrylate	d_p=1.5–12 μm; x_s=10–20 wt%	30–60	0.5–4	
Ho et al. [126]	*n*-Eicosane; urea-formaldehyde	d_p=4–10 μm; x_s=2–10 wt%	10–50	0.5–2.1	
Wang and Lin [127]	*n*-Octadecane; melamine-formaldehyde	d_p=0.3–3 μm; x_s=5–20 wt%	20–40	1.5–6	
Zeng et al. [128]	1-Bromohexadecane ($C_{16}H_{33}Br$); amino plastics	d_p=1–20 μm (8.2 μm average); x_s=5.0 wt%, 10.0 wt%, 15.8 wt%	14.3	10 °C: 5.0 wt% slurry: 2.05,10.0 wt% slurry: 2.23, 15.8 wt% slurry: 4.18	μ decreased with the temperature rising
Zhang et al. [129]	Nonadecane melamine resin	d_p=0–4.5 μm; x_s=10–40 wt%	10–50	10–30 wt% slurry: 2–12; 40 wt% slurry: 12–35	μ increased with particle fraction and decreased with temperature; however, the shear stress did not vary linearly with shear rate, therefore the fluid was considered as pseudo-plastic fluid
Tumuluri et al. [15]	Octadecane gelatin	d_p=2–10 μm; x_s=7, 11 wt%	17–32	7 wt% slurry: 1.8–2.2 times as large as that of water; 11 wt% slurry: 2.5–3.0 times as large as that of water	μ was almost constant with respect to temperature; μ increased with particle fraction; MPCS was Newtonian fluid up to 18 wt% fraction
	MPCS with multi-walled carbon nanotubes	11 wt% MPCM; 1.1 wt% MWCNT	25–35	10–1000 with 0.2–100 s^{-1} shear rate	μ increased with temperature; fluid exhibited non-Newtonian behavior, and Herschel–Buckley model was used

to the flow velocity and tube diameter, including particle fraction, particle diameter and shape and so on. Therefore, the former measured results of PCS pressure drops exhibit irregularities. The recent experimental results of PCS pressure drops are summarized in Tables 2–4.

3.3.1. Laminarizing effect

Most of the experimental results showed that the pressure drops of ice slurry were higher than that of the carrier fluid at the same flow velocity in tubes [108]. However, Knodel et al. [132] found that the flow friction of ice slurry with 2–3 mm ice crystals in a 24 mm stainless steel tube reduced with increasing ice fraction in a nonlinear manner. The friction factor was close to the value of water when the ice fraction was low, and a sudden decline occurred as the ice fraction increasing from 2 to 4 wt%, thereafter the friction factor changed to another constant value. The authors characterized the decline as re-laminarization phenomenon by considering the flow turned from turbulent state to laminar state as ice fraction increasing. This phenomenon can be explained by

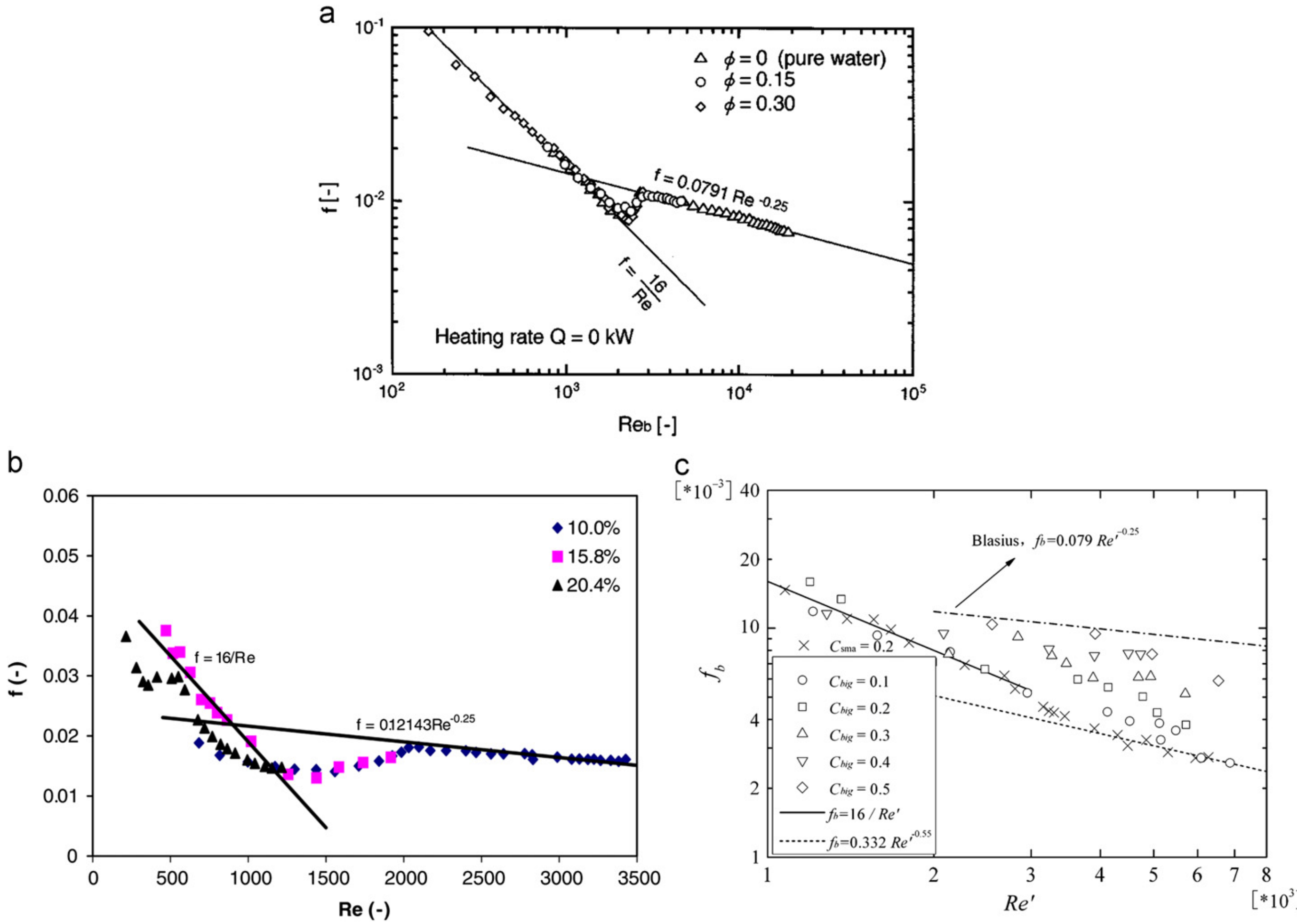


Fig. 17. Friction factor prediction of MPCS, (a) Yamagishi et al. [9], 10.1 mm tube; (b) Wang et al. [12], 4 mm tube and (c) Inaba et al. [10], 15 mm tube.

the laminarizing effect of the ice crystals: the interactions of ice crystals and the carrier fluid reduce the fluid turbulence level. By comparing the results with their former experiments of ice slurry in larger tube diameter (48 and 100 mm tube diameter, 8 wt% transition ice fraction), they believed that the interactions between ice crystals and tube wall were enhanced when the tube diameter was small, and the transitional ice fraction was low.

The re-laminarization phenomenon was also observed when ice slurry flowing through 10–20 mm copper tubes by Niezgoda-Żelasko and Zalewski [119] and in 22 mm inner tube of double-tube heat exchanger with smooth and corrugated surfaces by Bédécarrats et al. [123]. As shown in Fig. 20, ice slurry flowing at a certain velocity is gradually damped from fully turbulent to laminar state as the ice fraction increasing. In the fully turbulent region, the pressure drop is nearly constant when the ice fraction is low, and then gradually increases with ice fraction. Bédécarrats et al. [123] believed that the liquid phase dominated the flow pressure drop when the ice fraction was low, therefore the pressure drop did not change significantly in the turbulent region. The pressure drop increases more rapidly in the laminar region than that in turbulent region, which was attributed by Bédécarrats et al. [123] to the increasing friction of ice particles on the tube wall. Moreover, pressure drop reduces with ice fraction when ice slurry flows in the transitional region, and the transitional ice fraction moves towards the high ice fraction with increasing flow velocity as clearly shown in the Fig. 20(a).

Similar phenomena were observed in the flows of MPCS and TBAB CHS. Yamagishi et al. [9] noticed the lower pressure drop of 30 vol% MPCS at the flow velocity of 2.0–2.5 m s^{-1} compared to that of water, and attributed the laminarizing effect to the depression of longitudinal eddy diffusivity of slurry since the particle size was smaller than the turbulence length. The authors also pointed the laminarization was beneficial for pumping power reduction. Xiao et al. [142] and Ma et al. [28] reported the laminarization during the flowing of TBAB CHS in tubes, the variations of pressure drop with particle fraction at the certain flow velocity were quite similar to that of ice slurry, as shown in Fig. 21(a) and (b), the reduction of pressure drop were both noticed occurred at the slurry fraction range of 12–16 vol%. Ma et al. [28] also noticed that the laminarizing effect was particle fraction and flow velocity dependent, which indicated the laminarizing effect would disappear when the particle fraction and flow velocity were both high. This was caused by the enlarged particle interactions and therefore the mechanical friction was larger.

3.3.2. Influence of flow passage geometry on flow friction

Different from that of the single phase fluid, the flow friction of solid–liquid two-phase slurry is composed of viscous friction caused by the fluid viscosity and the mechanical friction which is resulted from the interactions between solid particle and the flow boundary [144]. Therefore, the flow friction of PCS is largely related to both the slurry fraction and flow passage geometry, such as passage diameter, roughness and pattern.

Relationships between the flow friction and Reynolds number of ice slurry in tubes with different diameters were obtained by

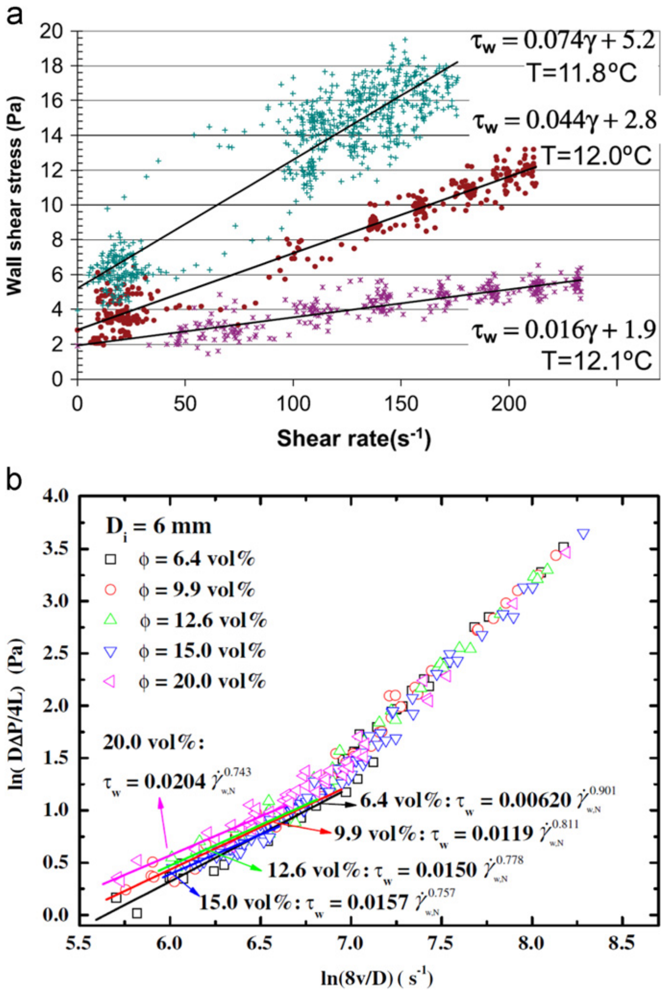


Fig. 18. Rheological feature determination of TBAB CHS, (a) wall shear stress and shear rate of TBAB CHS flowing through 16 mm tube [25] and (b) flow curve of TBAB CHS flowing through 6 mm tube [28].

Gozdek et al. [117], Niezgoda-Żelasko and Zalewski [119] and Illán and Viedma [133]. As shown in Fig. 22(a)–(c), the experimental results obtained by these studies show similar friction factor–Reynolds numbers relationships though the used Reynolds numbers were defined in different ways: Grozdek et al. [117] determined the Reynolds number using the viscosity calculated by Thomas relation (Re_{is}), Niezgoda-Żelasko and Zalewski [119] used the Reynolds number based on the Bingham model (Re_B), while Illán and Viedma [133] employed the referenced Reynolds number (Re_{cf}) corresponding to the carrier fluid at 0 °C. In the laminar flow region, it was noticed that both the higher ice fraction and the larger tube diameter resulted in larger flow friction, and the corresponding deviation from that of the Newtonian fluid also became larger. Grozdek et al. [117] illuminated the influence of the tube diameter on the ice slurry flow: ice slurry flowing through smaller tubes tended to be more homogeneous at larger mean velocity but still in laminar state, while the mean velocity was relatively low in larger tube which resulted in heterogeneous flow with more ice particles at the tube top but less at the bottom, therefore the distorted flow pattern led to higher flow friction. Kumano et al. [120] observed the similar influence of tube diameter on the flow of ice slurry while narrow tubes with the tube diameter of 4.3 mm, 7.5 mm and 10.2 mm.

Ma et al. [28] regarded that the particle-tube wall interactions was enlarged when TBAB CHS flowing through tube with smaller diameter, hence the fluidity of the slurry deviated from Newtonian fluid much more compared to that of the slurry flowing in larger tube, and then the flow friction was higher due to the larger mechanical friction loss in the slurry. In their study, the measured flow friction factor in 6 mm tube was about 20–25% larger than the predicted value by Dodge–Metzner correlation as mentioned before, while the prediction error in the case of 14 mm tube was only +8% larger. They believed this tube wall constraint effect on slurry flow would disappear if the tube diameter was large enough compared to the particle size.

Both Bédécarrats et al. [123] and Illán and Viedma [133] observed reasonably higher pressure drop of ice slurry in corrugated tube compared to that in smooth tube. In the former study, different from the slight increase in smooth tube, the pressure

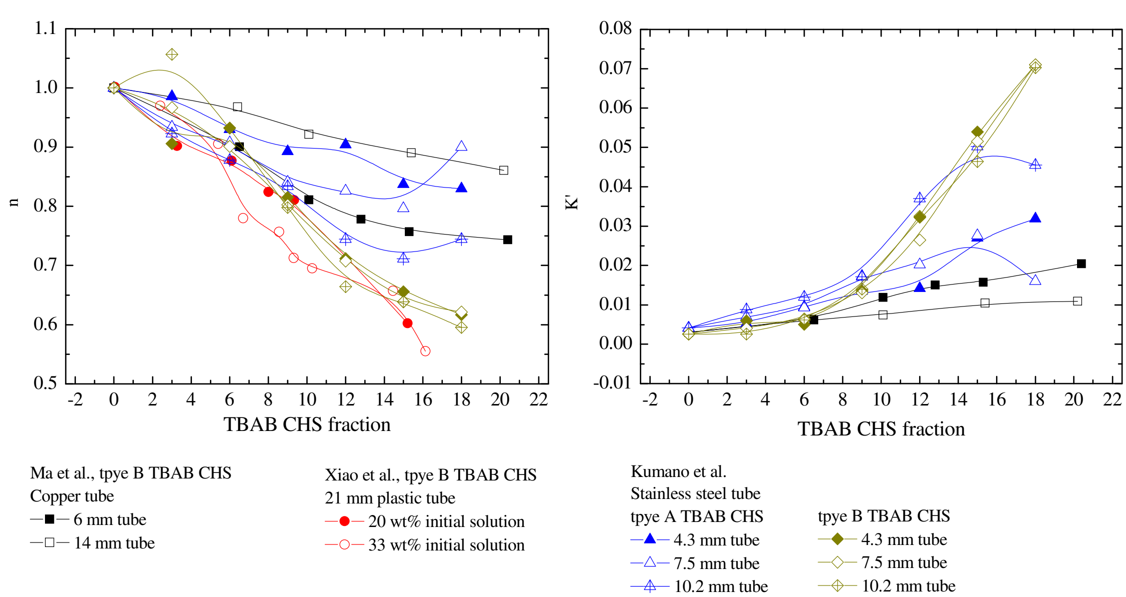


Fig. 19. Summary of the parameters of Power-law model for TBAB CHS, including researches by Xiao et al. [26], Ma et al. [28] and Kumano et al. [31] (the used TBAB CHS fraction in [26] is volume fraction while in [28,31] are mass fraction).

Table 2
Pressure drops of ice slurries.

Authors	Base liquids	Slurries	Geometries	Flow rates	Correlations	Descriptions
Knodel et al. [132]	Water	d_p=2–3 mm; $x_s<12$ wt%	Stainless steel tube, D_i=24 mm, L=4.596 m	2.8–5.0 m s^{-1}	$f=0.946\times0.184Re^{-0.2}$, $38{,}000<Re<74{,}000$	$\Delta P/L$ was nearly constant when $x_s<2$ wt% and $x_s>5$ wt%; $\Delta P/L$ reduced when $2<x_s<5$ wt% due to the laminarizing effect
Meewisse and infante Ferreira [134]	5–39% Various water–brine	d_p=0.1–1 mm; $x_s<30$ wt%	Circular tube, D_i=20 mm	3 m s^{-1}		$\Delta P/L$ increased with ice fraction; $\Delta P/L$ depended on the added freezing point depressant. Slurry with methanol, NaCl and potassium formate had lowest pressure drop
Bellas et al. [135]	5% Propylene solution	d_p=0.17–0.6 mm; $x_s\leq20$ wt%	Plate heat exchanger, 24 plates, D_h=4 mm, W=112 mm, H=310 mm	1.0–3.7 m^3 h^{-1}		ΔP increased with v_s and x_s; only a 3–8% increment in ΔP was observed as x_s varying from 5.0 to 20.0 wt%
Nørgaard et al. [136]	16% Propylene glycol solution	$x_s\leq30$ wt%	Plate heat exchanger, 10 plates, D_h=4 mm, W=70 mm, H=300 mm	50–300 L h^{-1}		ΔP of ice slurry in heat exchange generally increased with v_s and x_s; slight reduction was observed when flow rate increased from 100 to 150 L h^{-1} with inlet 30 wt% ice fraction
Hägg [137]	33.2 wt% HYCOOL solution and 35 wt% ethanol solution	$x_s\leq30$ wt%	Stainless steel tube, D_i=9, 15, 25 mm, L=1.2 m	0.5–2 m s^{-1}		$\Delta P/L$ increased with v_s and x_s and with reduced pipe dimensions
Niezgoda-Żelasko and Zalewski [119]	10.6% Ethyl alcohol solution	d_p=0.05–0.35 mm, $x_s\leq30$ wt%	Copper tubes, D_i=10, 16, 20 mm, L=4.6 m	0.1–4.5 m s^{-1}	Buckingham–Reiner equation for laminar flow, excellent agreement; Tomita method for turbulent flow, uncertainty was better than 10%	$\Delta P/L$ increased at the fully turbulent and more rapidly at the laminar flow regions with x_s at a certain v_s, but decreased at the transitional region, while the x_{tra} increased with v_s; Re_{tra} increased with x_s
Shire et al. [138]	4.76 wt% NaCl brine	0.02–0.05 mm in width, 0.1–0.2 mm in length, $41\leq x_s\leq67$ wt%	Borosilicate glassware, D_i=25 mm, L=1 m	0.5–2 m s^{-1}		$\Delta P/L$ increased with v_s and x_s; $\Delta P/L$ depended largely on a critical yield stress for high x_s
Illán and Viedma [139]	9% NaCl brine	$d_p\approx0.5$ mm, $x_s\leq25$ wt%	Stainless steel corrugated tube, D_i=16 mm, L=1.25 m	700, 1200 kg h^{-1}	$f=6.12\kappa^{0.46}Re_{cf}^{-0.16}$, κ is the severity number of the corrugated tube	ΔP was almost constant with x_s
Shire et al. [140]	5% NaCl brine	0.02–0.05 mm in width, 0.1–0.2 mm in length, $10<x_s\leq60$ vol%	Plate heat exchanger, 12 plates, D_h=7 mm, W=250 m, H=1000 m, tubular heat exchanger, D_h=24 mm, L=3 m	0–2.5 L s^{-1}		ΔP increased with v_s and x_s; ΔP had sharp increase when x_s was higher than 40 vol% in the tubular heat exchanger; required pressure drop was lower than the predicted from models; mixing mitigated the block caused by high ice fraction as well as large ice particles
Bédécarrats et al. [123]	10% Ethanol solution	$d_p\approx0.1$ mm, $x_s\leq30$ wt%	Smooth and corrugated tube, D_i=22 mm, L=2 m	0.3–1.9 m s^{-1}		At a certain v_s, $\Delta P/L$ increased slowly with x_s within smooth tube, but the increment stopped at critical x_s, while $\Delta P/L$ was nearly constant within corrugated tube; then $\Delta P/L$ reduced to a minimum value and then rapid increase; x_{tra} increased with v_s
Grozdek et al. [117]	10.3 wt% Alcohol solution	$d_p\approx0.3$ mm, $x_s\leq30$ wt%	Stainless steel tube, D_i=9, 15, 25 mm, L=1.2 m	0–2.6 m s^{-1}	The authors tried several kinds of correlations, the best ones were the modified Buckingham–Reiner for laminar flow and Dodge–Metzner and Tomita for turbulent flow	Ice slurry flow behaviour was time dependant; $\Delta P/L$ generally increased with x_s at a certain v_s, however, the delayed laminar–turbulent transition with higher x_s resulted in lower $\Delta P/L$ than that of carrier fluid sometimes; when $x_s<10$–15 wt%, the slurry could be treated as Newtonian fluid
	9% NaCl brine	$d_p\approx0.5$ mm, $x_s\leq26$ wt%	Stainless steel tube, d_m/D_i=0.014–0.031	0.2–5 m s^{-1}	Smooth tube (subscript *cf* stands for the carrier liquid at 0 °C): *Laminar flow*: $f=ARe_{cf}^{a}$,	f increased with x_s in laminar region, but was nearly constant in turbulent flow region; f increased with the

Table 2 (*continued*)

Authors	Base liquids	Slurries	Geometries	Flow rates	Correlations	Descriptions
Illán and Viedma [133]					$A=0.00024(1-0.1x_s/100)B^{1.8122} \times \left[3.95\left(\frac{d_p}{D_i}\right)^{0.678}\right]^a \exp((a+1)b)$ $a=(0.1427-0.174\ \ln B)$, $b=(0.22435-0.000308\rho_{cf})x_s/100$ $B=1.295D^2\rho_{cf}e^b 10^{0.05x_s}\mu_{cf}^{-2}\left(\frac{d_p}{D_i}\right)^{1.166}$, *Turbulent flow*: $f=0.316cRe_{cf}^{-0.25d}$, $c=1.4074(1-0.1x_s/100)e^{-0.07185x_s}$ $d=1.1-0.02847x_s$	decrease of d_m/D_i in laminar region, but was nearly constant in turbulent flow region; sharp increase was found when x_s was up to 26 wt% in corrugated tube
Kumano et al. [120]	5 wt% Ethanol solution	d_p=0.1–0.4 mm, $x_s \leq 25$ wt%	D_i=4.3, 7.5, 10.2 mm, L=2.5 m			Homogeneous flow without ice particles accumulated at the tube top; $\Delta P/L$ increased with x_s in the laminar flow region; $\Delta P/L$ was constant or decreased slightly with x_s in the turbulent flow region when x_s was low, but increased with x_s when x_s was high; slurry flowing through larger tube deviated more from the Newtonian fluid and had higher flow friction
Fernández-Seara et al. [118]	10 wt% Ethylene glycol solution	d_p=0.025–0.25 mm, $x_s \leq 20$ wt%	Fan coil heat exchanger, smooth copper tube, D_i=3/8″	0.3–1.1 m s^{-1}	Poiseuille model for laminar flow with relative errors of –21.5% to 29%, Petukhov equation for turbulent flow with relative errors of –6.3% to 9%, Blasius equation for turbulent flow with relative errors of –17% to 1%	$\Delta P/L$ increased with v_s and x_s

Table 3
Pressure drops of MPCS.

Authors	PCM and shell material	Slurries	Geometries	Flow rates	Correlations	Descriptions
Yamagishi et al. [9]	Octadecane; melamine-formaldehyde	d_p=2–10 μm, φ_s=7–30 vol%	Stainless steel pipe, D_i=10.1 mm, L=800 m	0–3.0 m s^{-1}	Poiseuille equation for laminar flow and Blasius equation for turbulent flow with perfect agreement	$\Delta P/L$ increased with v_s; $\Delta P/L$ of 7–20 vol% slurry was higher than that of water and increased with φ_s; laminarization was observed when φ_s=30 vol%, which caused $\Delta P/L$ smaller than that of water at v_s=2.0–2.5 m s^{-1}
Rao et al. [141]	*n*-Octadecane; polymethylmethacrylate	d_p=1–5 μm, x_s=5–20 wt%	Rectangular copper minichannels, 2 mm × 4.2 mm × 150 mm	0.1–1.4 m s^{-1}		ΔP increased with v_s and x_s
Alvarado et al. [11]	*n*-Tetradecane; gelatin	d_p=2–10 μm, x_s=5.9–15.2 wt%	Copper pipe, D_i=10.9 (smooth), 8 (smooth), 8 mm (enhanced), L=12.2 m	0.5–1.5 m s^{-1} in 10.9 mm tube; 1.2–2.5 m s^{-1} in 8 mm tube		$\Delta P/L$ increased with v_s; In 10.9 mm smooth tube, $\Delta P/L$ was slightly higher than that of water (calculated value); In 8 mm tube, $\Delta P/L$ of 5.9 wt% slurry was smaller than that of water (calculated value) due to the turbulence suppress effect by small particles; $\Delta P/L$ in smooth and enhanced tubes were similar
Chen et al. [14]	1-Bromohexadecane; urea-formaldehyde	d_p=1–20 μm, x_s=15.8 wt% at 10 and 20 °C	Stainless steel pipe, D_i=4 mm, L=1.85 m	0.2–1.0 m s^{-1}		ΔP increased with v_s *and* increased slightly with temperature; ΔP was higher than that of water at the same v_s, but the difference reduced with increasing flow velocity
Dammel and Stephan [125]	*n*-Eicosane; polymethylmethacrylate	d_p=1.5–12 μm; x_s=10–20 wt%	Rectangular copper minichannels, 2 mm × 4.2 mm × 390 mm	0.2–0.8 kg min^{-1}		ΔP increased with v_s and x_s

Table 4
Pressure drops of CHS.

Authors	Initial solution concentration	Slurries	Geometries	Flow rates	Correlations	Descriptions
Darbouret et al. [25]	20 wt%, 35 wt%	TBAB CHS, Type A: x_s=4–55 wt%; Type B: x_s=28–43 wt%	D_i=16 mm, L=1 m	0–300 L h^{-1}	Buckingham–Reiner equation for laminar flow	ΔP increased with x_s, and increased linearly with flow rate; Bingham fluid was determined for TBAB CHS
Xiao et al. [26]	22 wt%, 30 wt%	TBAB CHS: φ_s=0–16.24 vol%	PVC pipe, D_i=21 mm, L=2 m	0–5.25 m s^{-1}	*Laminar flow*: Poiseuille equation; *Turbulent flow*: $f_F=0.3226Re_{MR}^{-0.4271}$	ΔP increased with v_s; ΔP sometimes decreased with φ_s; power-law feature was determined for TBAB CHS
Suzuki et al. [36,37]	25 wt%	TME CHS: x_s=0–18.8 wt%; Ethoquad O/12 as surfactant	D_i=5 mm, L=0.5 m	*Re* (calculated based on water viscosity) was in the range of 2000–20,000		Drag reducing by the used surfactants was effective for TME CHS when the flow rate and the slurry fraction were both high
Xiao et al. [142]		Type A TBAB CHS: x_s=0–27 wt%	PVC pipe, D_i=16 mm, L=2.8 m	0–3.5 m s^{-1}		ΔP increased with v_s; as the increase of x_s, the flow of CHS was in the turbulent region first and ΔP increased slightly; when x_s was in the range of 10–15 wt%, laminarization was observed, and ΔP dropped largely; then ΔP increased rapidly in the laminar flow region
Ma et al. [28]	10 wt%	Type B TBAB CHS: φ_s=0–20 vol%	Copper tube, D_i=6, 14 mm, L=1.5 m	0–2.5 m s^{-1} in 6 mm pipe, 0–1.2 m s^{-1} in 14 mm tube	*Laminar flow*: Poiseuille equation; *Turbulent flow*: Dodge–Metzner correlation	In laminar region, ΔP increased slightly with φ_s in 6 mm tube but changed little in 14 mm tube; in the transitional and turbulent regions, the laminarizing effect caused a decrease of ΔP with φ_s, however, the laminarizing effect was volume fraction and flow velocity dependent
Kumano et al. [30]	22.5 wt% 8.5 wt%	Type A TBAB CHS: x_s=0–20 wt% Type B TBAB CHS: x_s=0–20 wt%	Stainless steel pipe, D_i=4.3, 7.5, 10.2 mm, L=1 m			ΔP increased with v_s; ΔP increased with x_s in laminar flow region but slightly decreased in turbulent flow region; In turbulent flow region, the flow characteristics changed at a certain flow velocity while x_s was about 15 wt%, then ΔP dropped a lot
Hashimoto et al. [131]	20 wt% TBAB solution; 18 wt% TBAF solution	TBAB CHS: x_s=0–70 wt%; TBAF CHS: x_s=0–42 wt%; Ethoquad O/12 as surfactant				The addition of surfactant caused the drastically reduction of the viscosities of both TBAB CHS and TBAF CHS
Ma et al. [33]	10 wt%	Type B TBAB CHS: φ_s=0–17.5 vol%	Plate heat exchanger, 10 plates, D_h=4 mm, W=72 mm, H=310 mm	2.5–13 L min^{-1}	$f=51.002Re_{MR}^{-0.3}$, $60<Re_{MR}<400$	ΔP increased with v_s; ΔP was always higher than water; ΔP was almost constant when $5<\varphi_s<13.6$ vol%, but increased a lot when φ_s=17.5 vol%
Ma et al. [29]	15 wt%	Type B TBAB CHS: x_s=0–30 wt%	Copper pipe fittings, 14 mm 90° elbow, 14–6 mm sudden contraction, 6–14 mm sudden expansion, 14 mm tee	1–8 m s^{-1} in 6 mm pipe, 0.4–2.4 m s^{-1} in 14 mm tube		The local loss friction increased slightly with x_s when x_s was low but increased rapidly if x_s was larger than 20 wt%
Suziki et al. [143]	35 wt% ammonium alum	Ammonium alum hydrate slurry: x_s=12 wt%	Copper tube, D_i=13 mm, L=2 m	0.5–1.5 m s^{-1}		ΔP of slurry was slightly larger than that of water at the same *Re*. surfactant was effective, with which ΔP was even lower than that of water

drop of ice slurry flowing in the turbulent region in corrugated tube was nearly constant or only had slight reduction as increasing the ice fraction. In the latter study, pressure drop in the laminar region was noticed a sharp increase when the ice fraction was up to 26 wt%, and the authors also successfully introduced the severity parameter relevant to the corrugated geometrical characteristics to predict the pressure drop. Alvarado et al. [11] compared the pressure drops of 5.9 wt% MPCS in regular and enhanced 8 mm tubes (the tube roughness was considered as 0.1 mm), however, the results showed the similar pressure drop in magnitude.

3.4. Heat transfer characteristics of PCS

Numerous experiments have been performed to investigate the overall and local heat transfer coefficients of PCS flowing through the heated tube and heat exchangers, the relating investigations were summarized in Tables 5–7. It was expected that the latent heat of the solid particles in slurry could improve the heat transfer of ice slurry, and many reported investigations validated this improvement, as shown in Fig. 23 which presented the heat transfer enhancement of ice slurry summarized by Stamatiou and Kawaji [112], however, the comparison may conducted under the

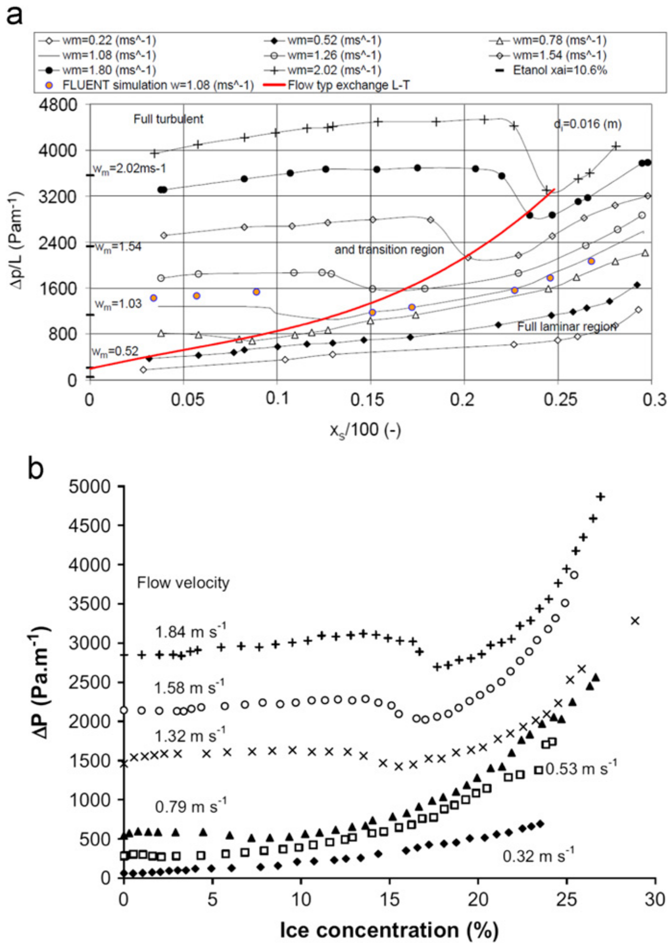


Fig. 20. Pressure drops of ice slurry as the increase of ice fraction, (a) 16 mm copper tubes [119] and (b) 22 mm inner tube of double-tube heat exchanger with smooth surface [123].

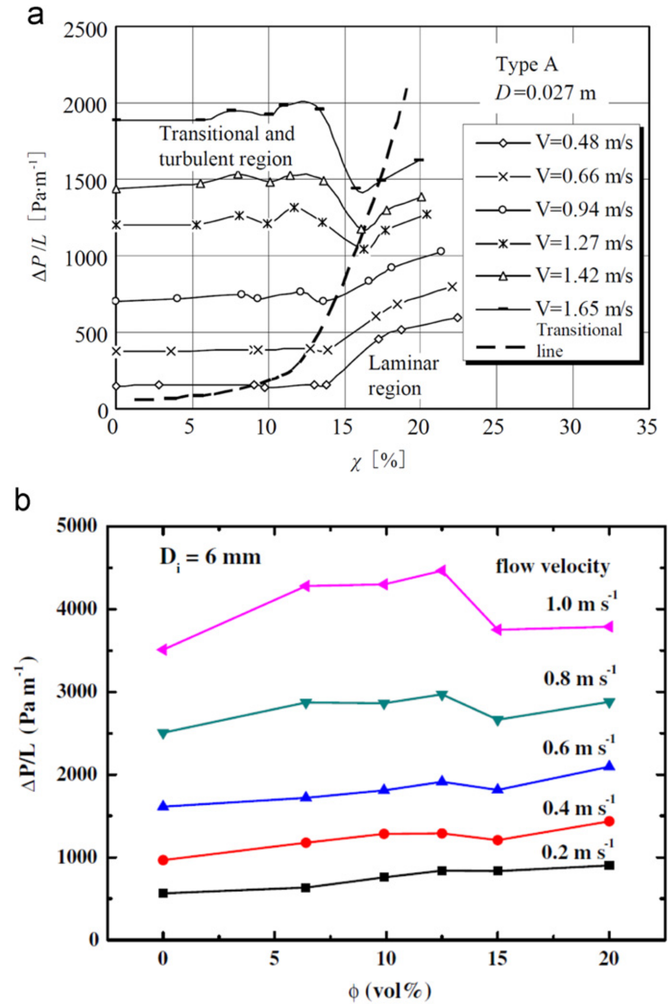


Fig. 21. Pressure drops of TBAB CHS as the increase of particle fraction, (a) type A TBAB CHS in 27 mm PVC tube [142] and (b) type B TBAB CHS in 6 mm copper tube [28].

same Reynolds numbers since the flow turbulence of slurry was damped by the particle flow. Some researchers also attributed this heat transfer coefficient improvement to the turbulence in the near-wall thermal boundary layer due to the movement of solid particles. However, it was believed that particle fraction, flow velocity, heat flux, particle shape and size, pipe shape and dimension, heat exchanger type and size imposed influences on the heat transfer of ice slurry, therefore the combined effect can be complicated.

3.4.1. Local heat transfer along the flow direction

Stamatiou and Kawaji [112] obtained the variations of local Nusselt numbers of ice slurry flowing though heated rectangular channels, as shown in Fig. 24(a). Nu_{local} was large at the channel inlet and decreased slightly towards the exit of the channel. The authors attributed the large Nu_{local} at the inlet to the developing flow and the following decrease to the more developed flow. Hägg [137] reported the similar slight reduction of local heat transfer coefficient of ice slurry along the flow direction in 21 mm stainless steel pipe, as shown in Fig. 24(b). The authors believed that the phase change and turbulence caused by ice particles in the thermal boundary layer led to smaller temperature gradient at the entrance and therefore high h_{local}, and the turbulence reduced as the ice particles melting along the flow direction and therefore h_{local} decreased. Moreover, Ionescu et al. [147] reported h_{local} of ice slurry decreased greatly at the channel inlet, followed by nearly constant values.

Yamagishi et al. [9], Alvarado et al. [11], Wang et al. [12,13] and Tumuluri et al. [15] obtained similar h_{local} variations of turbulent flow of MPCS in heated tubes, typical results were shown in Fig. 25. The local heat transfer coefficient increased at the tube inlet, where the slurry temperature was lower than its phase change temperature (supercooled slurry). The increasing h_{local} was caused by the gradually increasing melted particles near the tube wall; then the slurry temperature reached its phase change temperature, and h_{local} decreased in this region since the number of solid particles decreased gradually and the fully melted layer near the tube wall deteriorated the heat transfer from tube wall to fluid core. After the slurry was finally fully melted, h_{local} increased again due to the rising slurry temperature. Yamagishi et al. [9] and Wang et al. [12,13] also showed the variation of h_{local} in laminar flow region, which generally decreased along the flow direction. The former study pointed that the phase change particles in the laminar flow was possibly not completely melted, leading to generally decreasing solid particle number and then decreasing heat transfer coefficient.

As shown in Fig. 26(a), Kumano et al. [31] reported the generally decreasing h_{local} of TBAB CHS in laminar flow region, and attributed the decrease to the undeveloped boundary layer of the slurry. The authors also found that the variation of h_{local} along the heating tube changed little under the turbulent flow condition, which was caused by the rapidly developed boundary layer.

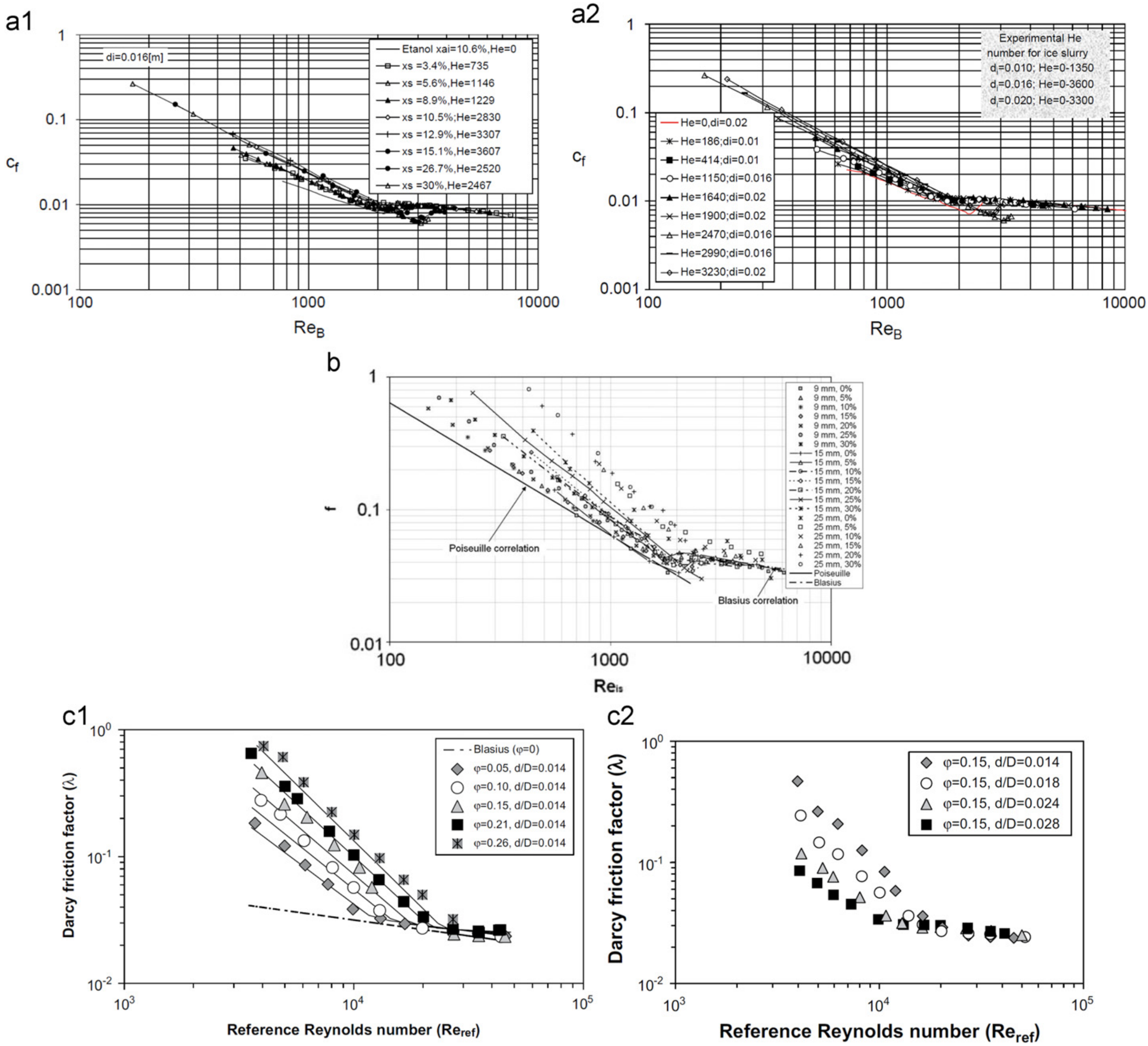


Fig. 22. Relationships between Reynolds number and friction factor of ice slurries, (a1) and (a2) Niezgoda-Żelasko and Zalewski [119] and (b) Grozdek et al. [117]; (c1) and (c2) Illán and Viedma [133].

The results reported by Ma et al. [28] were shown in Fig. 26(b), and it can be seen from the figure that h_{local} decreased along the heating tube but increased after all the solid particles were fully melted. This variation was explained by the similar reason to that of MPCS, except there was no supercooling region for TBAB CHS.

3.4.2. Influence of particle fraction on heat transfer

Heat transfer performances of ice slurry flowing through heated circular tubes have been investigated by many researchers. However, sometimes quite different even opposite characteristics of the heat transfer coefficients with ice fraction were reported, and the same phenomena happened to MPCS and CHS.

Similar to the re-laminarization phenomenon of the ice slurry flow as aforementioned, Knodel et al. [132] also observed the reduction of the Nusselt number of ice slurry in the heated tube, as shown in Fig. 27(a). This reduction was attributed to the damped flow turbulent degree by laminarzing effect. As the reported by Niezgoda-Żelasko [145] and Niezgoda-Żelasko and Żelasko [148], there was a slight increment of the heat transfer coefficients of ice slurry as ice fraction increasing from 5 to 30 wt% in the laminar flow region, while the heat transfer coefficients were nearly constant in the turbulent flow region, as shown in Fig. 27(b). Clearly, there is a sharply decline of the heat transfer coefficients as ice slurry flowing in the transitional region. Moreover, the authors pointed that the influence of ice fraction on heat transfer was more distinct in the laminar flow region while the heat transfer coefficients were more strongly dominated by flow velocity than by ice fraction in the turbulent flow region. The same conclusion was also obtained by Grozdek et al. [149] and Kumano et al. [150] in the case of heated tubes, and Bédécarrats et al. [123] in the case of double-tube heat exchanger. Grozdek et al. [149] observed generally increased heat transfer coefficient with ice fraction as well as flow rate, as shown

Table 5
Heat transfer of ice slurries.

Authors	Base liquids	Slurries	Geometries	Flow rates	Correlations	Comments
Knodel et al. [132]	Water	d_p=2–3 mm, $x_s < 12$ wt%	Stainless steel tube, D_i=24 mm, L=4.596 m	2.8–5.0 m s^{-1}	$Nu_m = 0.885 Nu_{Petukhov}$	Nu_m reduced when $x_s < 6$–8 wt%
Bellas et al. [135]	5% Propylene solution	d_p=0.17–0.6 mm, $x_s < 22$ wt%	Plate heat exchange, 24 plates, D_h=4 mm, W=112 mm, H=310 mm	1.0–3.7 m^3 h^{-1}		$h_{overall}$ remained fairly constant as the increase of x_s; $h_{overall}$ increased with υ_s; 30% increment in heat transfer capacity was observed as the x_s varying from 5.0 to 20.0 wt%
Nørgaard et al. [136]	16% Propylene glycol solution	$x_s \leq 30$ wt%	Plate heat exchange, 10 plates, D_h=4 mm, W=70 mm, H=300 mm	50–300 L h^{-1}		$h_{overall}$ increased with υ_s and x_s; increment with x_s became little at high υ_s
Stamatiou and Kawaji [112]	6.2 wt% NaCl brine	d_p=0.1–0.2 mm, $x_s < 25$ wt%	Rectangular channels, 533 mm × 305 mm × 25 mm, 533 mm × 100 mm × 13 mm		*Laminar flow*: $Nu(x) = 4.0 Gz_{cf}{}^{0.486} x_s^{0.3} (\mu_{cf}/\mu_w)^{0.24}$ *Turbulent flow*: $Nu_m = Nu_{Gn}[1 + 1.85 \times 10^5 x_s^{0.72} Re_{cf}^{-1.3} (\mu_{cf}/\mu_w)^{2.47}]$ Nu_{Gn} was the single-phase Nusselt number calculated by Gnielinski equation	Nu_{local} was high at the inlet and decreased slowly along the flow direction; Nu_{local} and Nu_m increased with x_s and heat flux
Niezgoda-Żelasko [145]	10.6% Ethanol solution	d_p=0.1–0.15 mm, $x_s \leq 30$ wt%	Copper tubes, D_i=10, 16, 20 mm, L=4.6 m	0.1–4.5 m s^{-1}	*Laminar flow*: $Nu = 0.78 (Re\,Pr\,\delta)^{0.72} \left(\frac{\Delta H}{C_p \Delta T}\frac{\Delta x}{100}\right)^{-0.027} \left(\frac{d_p}{D_i}\right)^{-0.29}$ *Turbulent flow*: $Nu = 0.031 (Re\,Pr)^{0.73} \left(\frac{\Delta H}{C_p \Delta T}\frac{\Delta x}{100}\right)^{-0.018} \left(\frac{d_p}{D_i}\right)^{0.21}$ δ was the Bingham term	h changed little with heat flux density; h increased slightly with x_s in laminar region; h decreased with x_s at the transitional region; h was more strongly dependent on υ_s than on x_s in turbulent region; h of 10–20 wt% ice slurry can be lower than that of single-phase carrier fluid; Nu was much larger than that of carrier fluid
Lee et al. [146]	6.5% Ethylene glycol solution	$d_p \approx 0.27$ mm, $x_s < 26$ wt%	Double-tube heat exchanger, inner tube: D_i=13.84 mm, outer tube: D_i=25 mm, L=1.5 m	800–3500 kg m^{-2} s^{-1}		At low flow rate, $h_{overall}$ did not change with x_s when x_s was smaller than about 10%, then increased sharply with x_s; $h_{overall}$ increased gradually with x_s at high flow rate range; hot water temperature had little impact on $h_{overall}$
Ionescu et al. [147]		Composed by ice particles and oil, $d_p \approx 0.1$ mm, x_s=20, 25, 30 wt%	Rectangular channel, 8 mm × 80 mm × 1000 mm		$Nu_m(x)$ indicated $Nu(x)$ integrated from 0 to x *Laminar flow*: *–for a constant wall temperature*: $Nu_m(x) = 0.34 \left(\frac{x}{x+D_h}\right)^{-1.12} Re^{0.42}\,Pr^{0.33} (1+x_s)^{2.3}$ *–for a constant heat flux*: $Nu_m(x) = 0.22 \left(\frac{x}{x+D_h}\right)^{-1.49} Re^{0.51}\,Pr^{0.33} (1+x_s)^{2.7}$ *Transition flow*: $Nu_m(x) = 0.03 \left(\frac{x}{x+D_h}\right)^{-0.35} Re^{0.75}\,Pr^{0.33} (1+x_s)^{2.45}$	h_{local} had a great decrease at the inlet, followed by a nearly constant value; h_{local} increased with υ_s and x_s

					Turbulent flow: –*for a constant wall temperature*: $Nu_m(x) = (1.57 + 26.1x_s^{0.75})$ $Gz^{0.33+1.76x_s^2-1.1x_s}$ –*for a constant heat flux*: $Nu_m(x) = (2.06 + 78.8x_s^{1.85})$ $Gz^{0.33+0.55x_s^2-0.54x_s}$	
Niezgoda-Żelasko and Żelasko [148]	10.6% Ethanol solution	d_p=0.1–0.15 mm, $x_s \leq 30$ wt%	Copper tubes, D_i=10, 16, 20 mm, L=4.6 m, rectangular tube, 0.0078 m × 0.0265 m × 3 m, rectangular (slit) tube, 0.003 m × 0.0358 m × 2 m	0.1–4.5 m s^{-1}	*Laminar flow*: $Nu = A\ Gz^m \left(\frac{\Delta H}{C_{p_B}\Delta T}\frac{\Delta x}{100}\right)^n \left(\frac{d_p}{D_i}\right)^p \left(\frac{K^*(T_f)}{K^*(T_w)}\right)^y$ *Turbulent flow*: $Nu = A(Re\ Pr)^m \left(\frac{d_p}{D_i}\right)^p$ All parameters are seen in [148]	Similar to Niezgoda-Żelasko [145]; smaller hydraulic diameter of channel caused smaller increase in h of ice slurry compared with h of carrier fluid
Gozdek et al. [149]	10.3% Alcohol solution	$d_p \approx 0.3$ mm, $x_s \leq 22$ wt%	Stainless steel tube, D_i=21 mm, L=0.94 m	0–1.25 m s^{-1}	*Laminar flow*: $Nu(x) = 87.3Gz^{0.1}(x_s/100)^{0.67}$ *Turbulent flow*: $\frac{Nu}{Nu_{cf}} = 1 + 0.00103x_s - 2.003$ $Re_{cf}^{-0.192\frac{30-x_s/100}{30}}(x_s/100)^{\frac{0.339Re_{cf}}{10^4}}$	h changed little with heat flux; h generally increased with x_s and v_s; x_s had greater impact on h than v_s; h of 10–15 wt% ice slurry had little increase or no increase in comparison with carrier fluid; heterogeneous flow pattern of ice slurry in laminar region caused higher h
Bédécarrats et al. [123]	10% Ethanol solution	$d_p \approx 0.1$ mm, $x_s < 30$ wt%	Double-tube heat exchanger with smooth and corrugated tubes, inner tube: D_i=22 mm, L=2 m, outer tube: D_i=33 mm, L=1.5 m	0.3–1.9 m s^{-1}		At a certain v_s and as increasing x_s, $h_{overall}$ increased up to a critical x_s within smooth tube, followed by a reduction to a minimum value and then a rapid increase; $h_{overall}$ decreased first within corrugated tube, then increased; $h_{overall}$ depended on heat flux and flow pattern; $h_{overall}$ was more strongly dependent on v_s than x_s in turbulent region
Illán and Viedma [158]	9% NaCl brine	$d_p \approx 0.5$ mm, $x_s < 26$ wt%	Fan-coil heat exchanger, cooper tube, D_i=8.8 mm	1000–4600 kg h^{-1}		Heat transfer rate increased with v_s; frost formation, partial blockage and excessive diameter ratio caused the worse behaviour prediction
Illán and Viedma [133]	9% NaCl brine	$d_p \approx 0.5$ mm, $x_s < 26$ wt%	Stainless steel tube, d_m/D_i=0.014–0.031	0.2–5 m s^{-1}	*Smooth tube*: $Nu = (0.845 - 0.01216x_s)Nu_{cf}$, $Nu_{cf} = 0.0344(Re_{cf} - 1500)^{0.78}Pr_{cf}^{0.37}$ *Corrugated tube (κ was the corrugated parameter)*: $Nu = (0.892 - 0.01824x_s)Nu_{cf}$, $Nu_{cf} = 0.374\kappa^{0.25}(Re_{cf} - 1500)^{0.74}Pr_{cf}^{0.44}$	Nu_m decreased with x_s
Fernández-Seara et al. [118]	10 wt% Ethylene glycol solution	d_p=0.025–0.25 mm, $x_s \leq 20$ wt%	Fan coil heat exchanger, smooth copper tube, D_i=3/8″	400, 600, 800 kg h^{-1}		Heat transfer rate of ice slurry was higher than chilled water by the factor of 3.7–4.6 depending on ice fraction and fan rotation rate; 80–88% of the overall thermal resistance was on the air side
Kumano et al. [150]	5 wt% Ethanol solution	$d_p \approx 0.15$ mm, $x_s \leq 25$ wt%	D_i=4.3, 7.5, 10.2 mm, L=2.5 m		*Laminar flow*: $Nu = 50.1Re_M^{0.0741}\left(\frac{x_s}{100}\right)^{0.822}\left(\frac{D_i}{d_p}\right)^{0.292}$ *Turbulent flow*: $Nu = 0.023{Re_M}^{0.8}Pr^{1/3}$	h increased with x_s and v_s; h depended more strongly on x_s than on v_s in laminar flow region; in turbulent region, h was nearly constant at low x_s but increased largely with v_s; h_{local} changed little with distance

Table 6
Heat transfer of MPCS.

Authors	Materials	Slurries	Geometries	Flow rates	Correlations	Comments
Goel et al. [151]	*n*-Eicosane, urea-formaldehyde	$d_p=100$, 250 μm, $\varphi_s=5$–20 vol%	Copper tube, $D_i=3.14$ mm, $L=0.4$ m	Reynolds number was 200, 1000 (only for 5 vol% slurry)		Stefan number was the most dominant factor on heat transfer; lower Stefan number (or heat flux) caused lower wall temperature; effect of φ_s for a given Stefan number could be expected when φ_s was 5 vol%; larger particle led to lower wall temperature; the effect of homogeneity could be negligible
Yamagishi et al. [9]	Octadecane; melamine-formaldehyde	$d_p=2$–10 μm, $\varphi_s=7$–30 vol%	Stainless steel tube, $D_i=10.1$ mm, $L=800\ D_i$	0–3.1 m s^{-1}		In laminar flow region, *h* decreased along the flow direction; in turbulent flow region, *h* increased in the supercooling region along the flow direction, and then decreased in the melting region, then increased after finishing the melt; higher heating power led to lower *h*; *h* generally increased with x_s and ν_s
Inaba et al. [10]	Small particle: *n*-Tetradecane; large particle: *n*-Docosane	$d_{p,a}=1.5$ μm, $x_s=20$ wt%; $d_p=17$ μm, $x_s=0$–50 wt% (compared to small particles)	Stainless steel tube, $D_i=15$ mm, $L=5.85$ m	$300<Re_{MR}<8000$		Nu_{local} decreased along the flow direction and reached nearly constant when fully melted; Nu_m increased with ν_s and the ratio of large particle
Alvarado et al. [11]	*n*-Tetradecane; gelatin	$d_p=2$–10 μm, $x_s=5.9$–15.2 wt%	Copper tube, $D_i=10.9$ (smooth), 8 (smooth), 8 mm (enhanced)$L=12.2$ m			The variation of *h* along the flow direction was similar to the result in [6]; *h* increased significantly with ν_s; increase of x_s caused lower flow turbulence and then lower *h*, and *h* was lower than that of water at the same flow velocity; the enhanced tube did improve the heat transfer, however, the enhancement effect was weak in the case of high x_s
Wang et al. [12,13]	1-Bromohexadecane, amino plastics	$d_{p,a}=10.112$ μm, $x_s=5$–27.6 wt%	Stainless steel tube, $D_i=4$ mm, $L=1.46$ m	$400<Re_m<3500$	*Laminar flow*: $Nu_{local}=cNu_{Shan\ and\ London}$, *c* was 1.336–1.418 in the case of 5–15.8 wt% MPCS, ±15% relative error $Nu_m=0.8148Re_m^{0.4593}\ Pr_m^{0.4836}\ Ste^{-0.1277}[(L_1+L_2)/D]^{0.3059}$ L_1+L_2 was the phase change region, ±10% relative error for 5–27.6 wt% MPCS *Turbulent flow*: $Nu_m=4.8527\times10^{-4}Re_m^{0.7733}\ Pr_m^{2.7941}\ Ste^{0.3159}[(L_1+L_2)/D]^{-0.333}(\mu_m/\mu_w)^{-2.4349}$ ±10% relative error for 5–10 wt% MPCS	In laminar flow region, *h* decreased along the flow direction and reached a nearly constant value in the fully melted region; Nu_{local} increased with x_s and was almost independent of heating power; In turbulent flow region, *h* decreased along the flow direction in the supercooling region, and then decreased in the melting region, then increased in the fully melted region; higher heating power caused higher *h* in the last region; Nu_m of 5 wt% was higher than that of 10 wt% MPCS at same *Re*
Rao et al. [152]	*n*-Octadecane, polymethylmethacrylate	$d_{p,a}=4.97$ μm, $x_s=5$–20 wt%;	Rectangular copper minichannels, 2 mm × 4.2 mm × 150 mm	0.05–0.35 kg min^{-1}		h_m increased with ν_s; h_m increased with x_s when ν_s was 0.05 kg min^{-1}, but decreased with x_s when ν_s was high
Diaconu et al. [153,154]	Rubitherm RT6, polycyclic cell	$d_{p,a}=2.24$ μm	Helically coiled copper tube in tank, $D_i=10$ mm, 140 mm helix diameter; Water flowed inside tube while MPCS was contained in tank		Nature convection correlation, $Nu_m=0.802Ra^{0.278}$, $10^{11}<Ra<10^{13}$	
Wang and Lin [127]	*n*-Octadecane, melamine-formaldehyde	$d_p=0.3$–3 μm, $x_s=5$–20 wt%	Aluminum rectangular tube, 12.8 mm × 1.8 mm × 900.2 mm	4.17–10.0 g s^{-1}		Based on the dimensionless wall temperature, MPCS had better heat transfer performance than that of water except at very small dimensionless axial distance
Wang et al. [155]		$d_p=0.5$–5 μm, $x_s=5$–20 wt%, with 0.5 wt% TiO_2 nanoparticles	Copper tube, $D_i=3.97$ mm, $L=1.834$ m			Nu_{local} decreased along the flow direction; Nu_{local} was close to that of water; the heat transfer was enhanced by TiO_2 nanoparticles, and the enhancement ratio increased with x_s

Delgado et al. [156]	Paraffin, polymer	d_p=1–20 μm, x_s=10 wt%	Copper tube, D_i=10 mm, L=1.82 m	20–50 kg h^{-1}	h decreased significantly at the entrance of the heating tube, thereafter decreased smoothly; h was approximately 25% higher than that of water at the same v_s
Dammel and Stephan [125]	n-Eicosane; polymethylmethacrylate	d_p=1.5–12 μm, x_s=10–20 wt%	Nine parallel minichannels, 2 mm × 4.2 mm × 350 mm	0.1–0.4 kg min^{-1}	Compared to water, MPCS was beneficial since which could achieve lower wall temperature
Tumuluri et al. [15]	Octadecane, gelatin	d_p=2–10 μm, x_s=7, 11 wt%	Copper tube, D_i=10.5 mm, L=10 m	0.8–1.1 m s^{-1}	h increased in the melting region, and then decreased in the fully melted region; h increased with Re; h increased slightly with x_s at the same Re, but decreased distinctly with x_s at the same v_s
	MPCS with multi-walled carbon nanotubes	11 wt% MPCM; 1.1 wt% MWCNT, d_p=10–100 nm, L_p=0.5–40 nm			h of the blend was always higher than that of MPCS

in Fig. 27(c). There were ice fraction thresholds at about 10–15 wt%, after which the heat transfer coefficient increased drastically. The authors believed that the transition of ice slurry flow pattern from homogeneous to heterogeneous caused the accumulating of ice particles near the top tube wall and the direct contact of ice particles with tube wall enhanced the heat transfer. On the other side, Illán and Viedma [133] observed that the Nusselt number decreased with the ice fraction at the same Reynolds number, as shown in Fig. 27(d), and same conclusions were reached when using corrugated tube.

The results given by Yamagishi et al. [9] showed h_{local} of MPCS flowing through heated tube was higher than that of pure water and increased with the slurry fraction, however, the comparison should be conducted at the same Reynolds number. The flow turbulence of slurry would be damped as increasing particle fraction, which caused the reduction of heat transfer coefficient, therefore h_{local} of MPCS decreased as increasing particle fraction under the condition of same flow velocity. Ma et al. [28] noticed the same phenomena when studying TBAB CHS flowing through the heated tubes. However, other researchers reported different results about the heat transfer of MPCS in the heated tubes: Wang et al. [12,13] found the Nusselt number of 5 wt% MPCS was higher than that of 10 wt% MPCS even at the same Reynolds number (2100–3452); Rao et al. [152] reported the mean heat transfer coefficients of MPCS in a minichannel, which increased as slurry fraction at low flow velocity (0.05 kg min^{-1}) but decreased in the case of high flow velocity (0.15–0.35 kg min^{-1}); Tumuluri et al. [15] measured the heat transfer coefficient of 7 wt% and 11 wt% MPCS in heated tube, showing h_{local} of 11 wt% MPCS was nearly the same as that of 7 wt% MPCS if the Reynolds number was the same. However, h_{local} decreased distinctly with slurry fraction at the same flow velocity.

Song et al. [27] obtained quite similar variation of heat transfer coefficient of type A TBAB CHS flowing in heated tube to that of ice slurry reported by Niezgoda-Żelasko [145], as comparing Fig. 28(a) to 27(b). At a certain flow velocity and as the increase of slurry fraction, the flow of TBAB CHS was gradually damped from turbulent state to laminar state, therefore the heat transfer coefficient changed little with low slurry fraction ($x_s < 10$ wt%) since the flow velocity dominated the heat transfer performance in the turbulent flow region. The re-laminarization occurred at 10 wt% $< x_s <$ 15 wt% which caused large reduction of heat transfer coefficient, thereafter the heat transfer coefficient increased in the laminar flow region. Kumano et al. [31] also reported the similar results of TBAB CHS, as shown in Fig. 28(b1) and (b2), however, the re-laminarization occurred at the slurry fraction of about 15–17 wt%.

3.4.3. Influence of flow passage geometry on heat transfer

Niezgoda-Żelasko and Żelasko [148] discussed the impacts of tube diameter on the heat transfer coefficients based on the test results of ice slurry flowing through circular tubes and rectangular channels. Smaller hydraulic diameter enhanced the micro-convection effect of ice particles and therefore improved the heat transfer coefficient. However, other factors bring disadvantages for the heat transfer in the case of smaller tube: Reynolds number at the same flow velocity was lower than that in the case of larger tube, and the melted near-wall layer was thicker which hindered the heat transfer between tube wall and the fluid core. Thus, the authors believed that the smaller hydraulic diameter the smaller increase of heat transfer coefficients compared to the single-phase carrier fluid. Results reported by Kumano et al. [150] about ice slurry also supported this conclusion.

The application of corrugated tube by Bédécarrats et al. [123] enhanced the heat transfer of the flowing ice slurry, about

Table 7
Heat transfer of CHS.

Authors	Initial solution concentration	Slurries	Geometries	Flow rates	Correlations	Comments
Takao et al. [21]		TBAB CHS with cold carry capacity of 64–95 kJ kg^{-1}	Plate-fin heat exchanger, Copper tube, D_i=10 mm	1–11 kg min^{-1}		h_m generally increased with v_s; h_m was larger than that of water at 1–6 kg min^{-1} flow rate, however, was smaller at higher flow rate; h_m was little smaller when the cold carry capacity was higher
Song et al. [27]	30 wt%	Type A TBAB CHS, x_s=0–18.4 wt%	Stainless steel tube, D_i=14 mm, L=2.8 m	0.35–6.8 m s^{-1}	*Laminar flow*: $Nu_m = 1.231 \times 10^{-5} Re^{1.6606}\,Pr^{0.7073}$, *Turbulent flow*: $Nu_m = 5.254 \times 10^{-4} Re^{0.9097}\,Pr^{1.1202}$	h_m generally increased with v_s; h_m increases slightly or was near constant in the turbulent flow region; as x_s increasing to a certain value, h_m dropped largely, and the flow was re-laminarized; h_m increased with x_s in laminar flow region
	17.3 wt%	Type B TBAB CHS, x_s=0–26.2 wt%			*Laminar flow*: $Nu_m = 1.798 \times 10^{-3} Re^{0.6648}\,Pr^{1.3309}$, *Turbulent flow*: $Nu_m = 6.085 \times 10^{-4} Re^{0.9130}\,Pr^{1.2061}$	Variation of h_m was similar to type A CHS, except that h_m in turbulent region increased rapidly with x_s
Ma et al. [28]	10 wt%	Type B TBAB CHS, φ_s=0–20 vol%	Copper tube, D_i=6, 14 mm, L=1.1 m	0–2.5 m s^{-1} in 6 mm pipe, 0–1.2 m s^{-1} in 14 mm tube	*Laminar flow*: $Nu(x) = 0.2368(Re_{MR}\,Pr)^{0.5873} Ste^{-0.0795} \left(\frac{D_i}{x}\right)^{0.2645} \left(\frac{d_p}{D_i}\right)^{-0.0182}$ *Transitional and turbulent flow*: $Nu(x) = 0.0219(Re_{MR}\,Pr)^{0.7093} Ste^{-0.0498} \left(\frac{D_i}{x}\right)^{0.2009} \left(\frac{d_p}{D_i}\right)^{-0.2441}$	h was enhanced compared to water at the same Reynolds number; h decreased at the melting region and increased at the following solution region; h increased with φ_s and Reynolds number, while φ_s was more important for laminar flow and Reynolds number dominated the heat transfer in turbulent flow; the influence of heating power was distinct in the case of 6 mm tube
Ma and Zhang [33]	10 wt%	Type B TBAB CHS: φ_s=0–17.5 vol%	Plate heat exchanger, 10 plates, D_h=4 mm, W=72 mm, H=310 mm	2.5–13 L min^{-1}	$Nu_{local} = 0.338 Re_{MR}^{0.667} Pr^{1/3} \left(1 + \frac{\Delta\omega \Delta H}{C_p \Delta T}\right)^{0.037}$	h_{local} fluctuated before the transition from slurry to aqueous solution, and increased sharply when turning into solution; $h_{overall}$ basically increased with the inlet water temperature, however, it dropped as the increase of φ_s until an un-fully melting happened
Kumano et al. [31]	22.5 wt%	Type A TBAB CHS, 0–20 wt%	Stainless steel pipe, D_i=7.5, 10.2 mm, L=1 m	$1000 < Re < 7500$	Type A TBAB CHS: $Nu = 3.33 Gz_M^{0.18} x_s^{0.42} (D/l)^{0.55}$,	In laminar flow region, h increased with x_s, but decreased along the heating tube, especially at the tube inlet, and the effect of Re was not significant, the ratio of measured Nu to the calculated single-phase Nu was about 1–2.5 and increased with x_s; in turbulent flow region, h was almost constant with x_s, but dropped at about 15 wt%, then increased slightly at high x_s, h changed little along the heating tube and increased with Re distinctly, the ratio of Nu was almost 1 with all x_s
	8.5 wt%	Type B TBAB CHS, 0–20 wt%			Type B TBAB CHS: $Nu = 6.35 Gz_M^{0.22} x_s^{0.52} (D/l)^{0.32}$	
Suziki et al. [157]	35 wt% ammonium alum	12 wt% ammonium alum hydrate slurry	Copper tube, D_i=13 mm, L=2 m	0.5–1.5 m s^{-1}		With the same Re, Nu of slurry was higher than that of solution and water; Nu decreased as the addition of surfactant caused by the laminarization

1.5–2.5 times heat transfer coefficient was achieved in comparison with smooth tube. The same conclusion was reached by Alvarado et al. [11] about MPCS. They compared the heat transfer coefficient of MPCS flowing through both regular and enhanced 8 mm tubes at the same flow velocity, and found that the average heat transfer enhancement was about 30% with 7 wt% slurry. However, the enhancement reduced when the slurry fraction increased due to the turbulence damping.

3.4.4. Heat transfer characteristics of PCS in heat exchangers

In addition to in the heated tubes, heat transfer performances of PCS in the heat exchangers have also been investigated. Fig. 29(a)–(d) shows the typical heat transfer coefficients of ice slurry in the plate heat exchangers and double-tube heat exchangers, all with hot water in the other side of heat exchangers. As the increase of ice fraction from 5 to 22 wt%, Bellas et al. [135] obtained nearly constant values of the overall heat transfer coefficient in a plate heat exchanger, as shown in Fig. 29(a). Moreover, the overall heat transfer coefficient reasonably increased with the flow rate. The authors believed that the overall heat transfer coefficient was the function of ice crystal size, Reynolds number and the flow passage geometry. Different from the results reported by Bellas et al. [135], the overall heat transfer coefficient in plate heat exchanger measured by Nørgaard et al. [136] increased with the inlet ice fraction, as shown in Fig. 29(b). As shown in Fig. 29(c), Lee et al. [146] found that the heat transfer coefficient of ice slurry flowing through double-tube heat exchanger showed weak dependence on ice fraction when the flow rate was low, and there was a sharp increase when the ice fraction was higher than about 10%. However, when the flow rate was high, the heat transfer coefficient increased gradually as the ice fraction

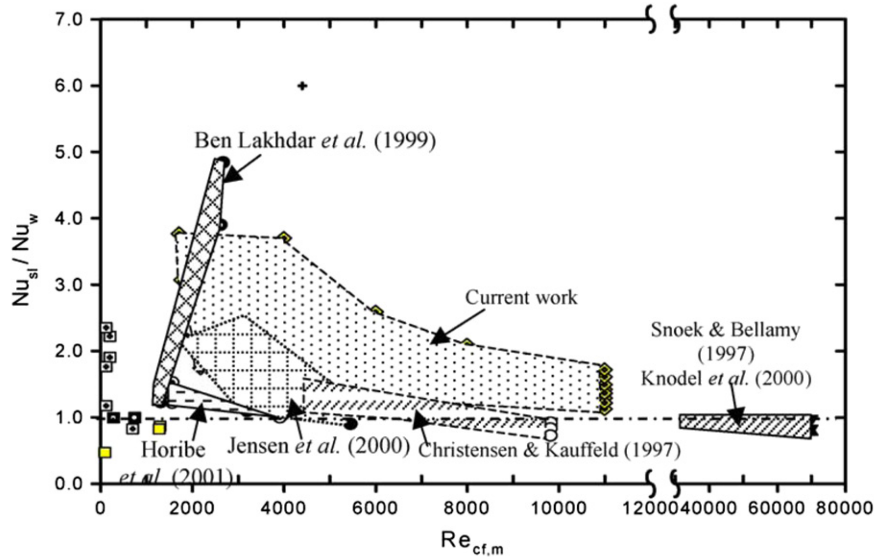


Fig. 23. Ratio of Nusselt number of ice slurry to that of the chilled water [112]. The references in the figure are those in [112].

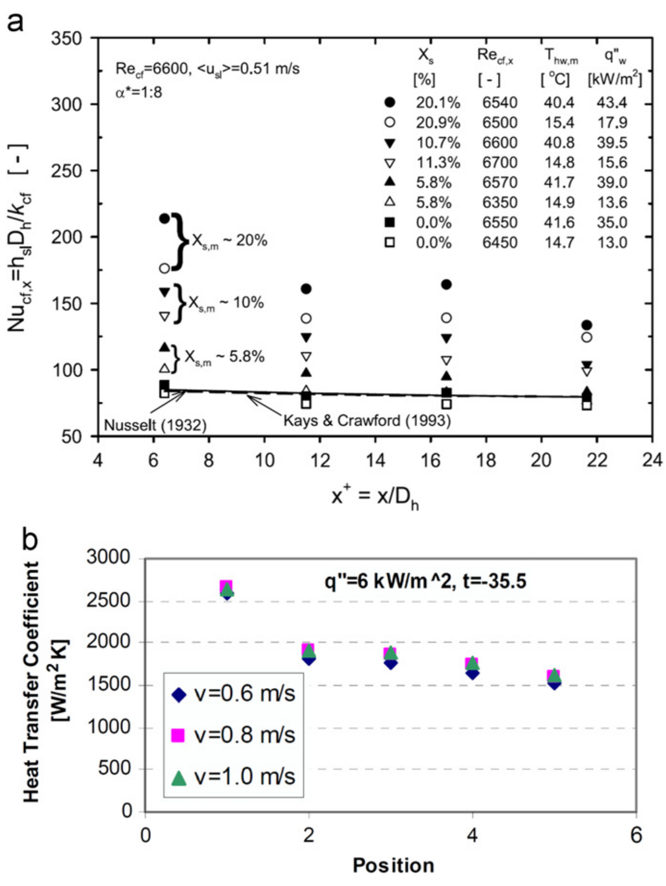


Fig. 24. Local heat transfer coefficients and Nusselt numbers of ice slurry flowing through heated tubes under constant heat flux, (a) rectangular channel, 533 mm × 100 mm × 13 mm, heated at one side by hot water [112] and (b) generated within HYCOOL fluid, −35.5 °C, 21 mm stainless steel pipe [137].

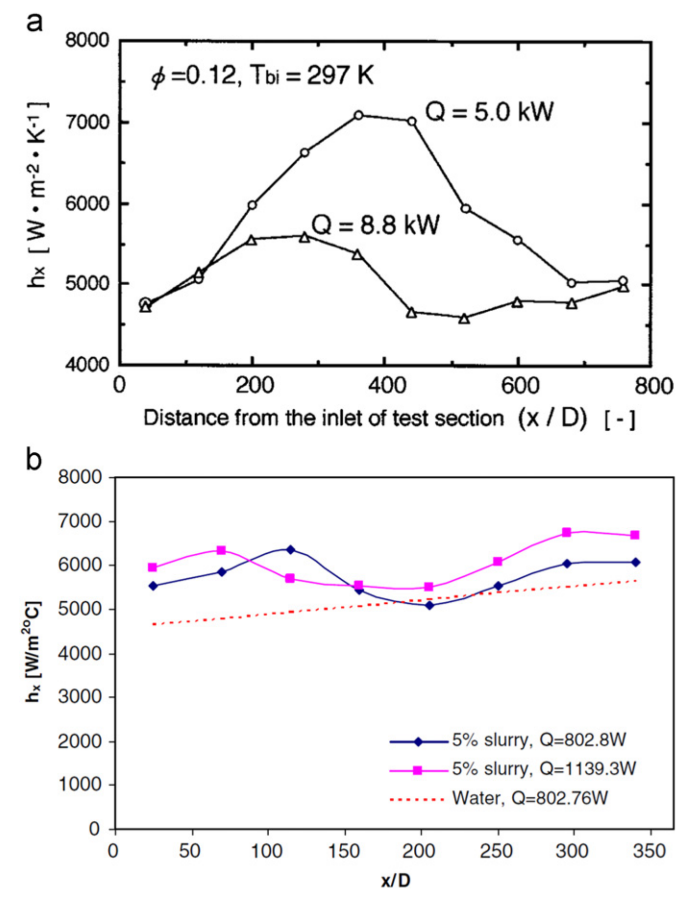


Fig. 25. Local heat transfer coefficients of MPCS flowing turbulently through heated tubes under constant heat flux, (a) Yamagishi et al. [9], 10.1 mm tube and (b) Wang et al. [12], 4 mm tube.

increasing from 0% to 26%. The authors also pointed that the impact of hot water temperature on the heat transfer coefficient could be neglected in spite of the increase of heat transfer rate with hot water temperature. Bédécarrats et al. [123] presented the variation of heat transfer coefficients of ice slurry flowing through double-tube heat exchanger with smooth and corrugated inner tubes, and the typical results in smooth tube is shown in Fig. 29(d). It was noticed that the variation of heat transfer

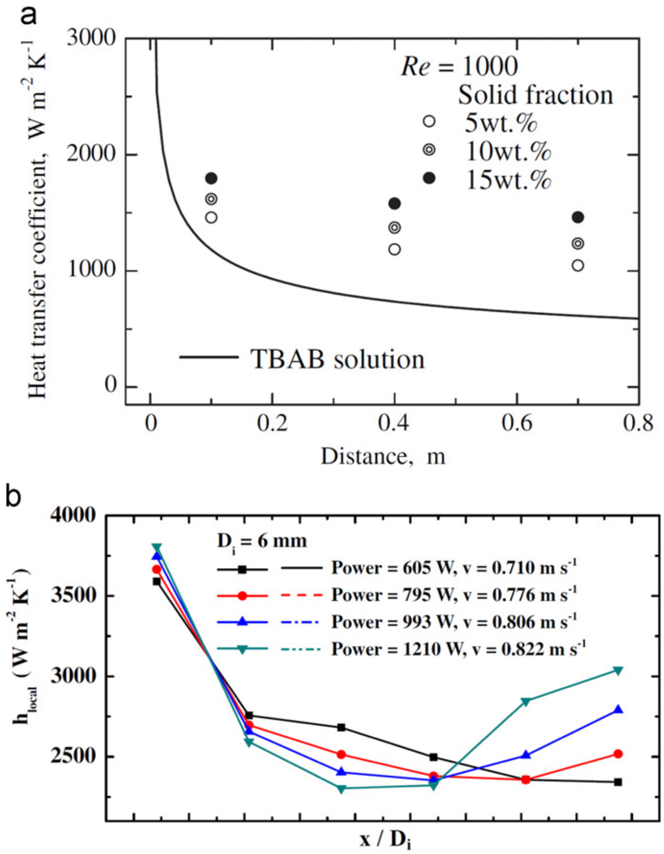


Fig. 26. Local heat transfer coefficients of CHS flowing through heated tubes under constant heat flux, (a) Kumano et al. [31], 7.5 mm tube and (b) Ma et al. [28], 6 mm tube.

coefficient was similar to that of the pressure drop shown in Fig. 20(b). At lower flow rate range, the flow of ice slurry with 0% ice fraction was in the laminar region, therefore the increase of ice fraction led to more ice particles melting near the heat transfer wall and hence the heat transfer coefficient increased; at higher flow rate range, the flow of ice slurry with 0% ice fraction was in the turbulent region, and the turbulence decreased with ice fraction until the flow changed to laminar flow, therefore it was noticed that the heat transfer coefficient increased with ice fraction in the turbulent region and followed by a reduction in the transition region, and then a more rapid increase in the laminar region, as shown in the figure. The authors attributed the rapid increase of heat transfer coefficient in laminar region to the thinner ice-free thermal boundary layer which was caused by the enhanced particle–wall interactions with higher ice fraction. Higher hot water temperature was found to result in higher heat transfer coefficient both in laminar and turbulent regions except in the transitional region. Fernández-Seara et al. [118] investigated the heat transfer performance of ice slurry in a terminal fan-coil unit. Results showed the heat transfer was enhanced as using ice slurry instead of chilled water by the factor of 3.7–4.6, which depended on the fan rotation rate as well as the ice fraction. The dominated thermal resistance of the overall heat transfer was on the air side, where the ratio was in the range of 80–88%. However, Illán and Viedma [158] did not recommend the direct application of ice slurry in fan-coil unit, since the frost formation, the partial blockage of fan coil inlet collector and the excessive diameter ratio (d_p/D_i) displayed the disadvantages of ice slurry compared to the single-phase flow.

Ma and Zhang [33] investigated the heat transfer of TBAB CHS in a plate heat exchanger, and concluded that the local heat transfer coefficient was highly dependent on the flow velocity but slightly dependent on the slurry fraction, and h_{local} would increased drastically after the slurry turning to solution due to the low viscosity and high *Re* of solution. Meanwhile, the overall heat transfer coefficient decreased with the slurry fraction both at a certain flow velocity and inlet hot water temperature.

3.4.5. Heat transfer correlations

Except Knodel et al. [132] who developed the heat transfer correlation of ice slurry flowing through heated tube simply by multiplying a factor on Petukhov correlation of single-phase fluid, other researchers considered the heat transfer coefficient or Nusselt number of ice slurry flowing through heated tube or heat exchanger as the complicated function of Reynolds number, Prandtl number, ice fraction, ratio of the particle diameter to the size of flow passage and the ratio of the viscosity of bulk fluid to that of the fluid at the wall and so on. For the correlation of local Nusselt number, Graetz number ($Gz=RePrD_h/x$) is widely utilized [112,147–149]. The index of *Gz* in the correlation is positive, which indicates the increment of Nusselt number with Reynolds number, Prandtl number as well as the entrance distance. The index of ice fraction is also positive to reflect the impact of ice particles on heat transfer. As aforementioned, the influence of tube diameter on heat transfer lies in both the micro-convection effect of ice particles and the near-wall thermal layer, therefore the index of diameter ratio (d_p/D_i) might be positive and negative [133,145,148,150] under different situations. Niezgoda-Żelasko [145] and Niezgoda-Żelasko and Żelasko [148] recommended a term of $((\Delta H/C_p\Delta T)(\Delta x_s/100))$ to reflect the influence of ice melting on the heat transfer when developing the heat transfer correlation, which showed good agreement with experimental results.

Similar to $((\Delta H/C_p\Delta T)(\Delta x_s/100))$, Charunyakorn et al. [159] proposed the utilization of Stefan number, ($Ste= (Cpq_wD_i/(2\lambda_s))/(x_s\Delta H)$), to reflect the influences of latent heat and heating power on the heat transfer in developing the heat transfer correlation of MPCS flowing through heated tube, and Goel et al. [151] validated the importance of *Ste* on the heat transfer of MPCS experimentally, therefore Wang et al. [13] used this parameter to develop the heat transfer correlation of MPCS in heated tube and the relative error was shown to be within $\pm 10\%$. Ma et al. [28] also utilized this term for TBAB CHS flowing through heated tube and the similar term of $(1+\Delta x_s\Delta H/(C_p\Delta T))$ for TBAB CHS flowing through plate heat exchanger [33]. Good results were achieved using these latent heat terms.

4. Application of PCS to refrigeration and air conditioning and performance evaluation

4.1. Ice slurry

Because of the numerous advantages, ice slurry is undoubtedly promising and can be used in various applications, including air conditioning, refrigeration, process cooling and so on. Many ice slurry systems were installed in Japan, which mainly concentrated in air conditioning system with thermal energy storage, while the applications in Europe and USA cover all the fields. The typical utilization of ice slurry can be divided into the following ways: direct contact cooling application, typically represented by fish cooling system; direct application, ice slurry flows directly to the load side and exchanges the thermal energy with the high temperature air or water; direct carrier liquid application, only liquid phase in the slurry is pumped to the load side to avoid the blockage in the narrow flow passages; indirect application, ice slurry is only employed as the thermal storage material while the

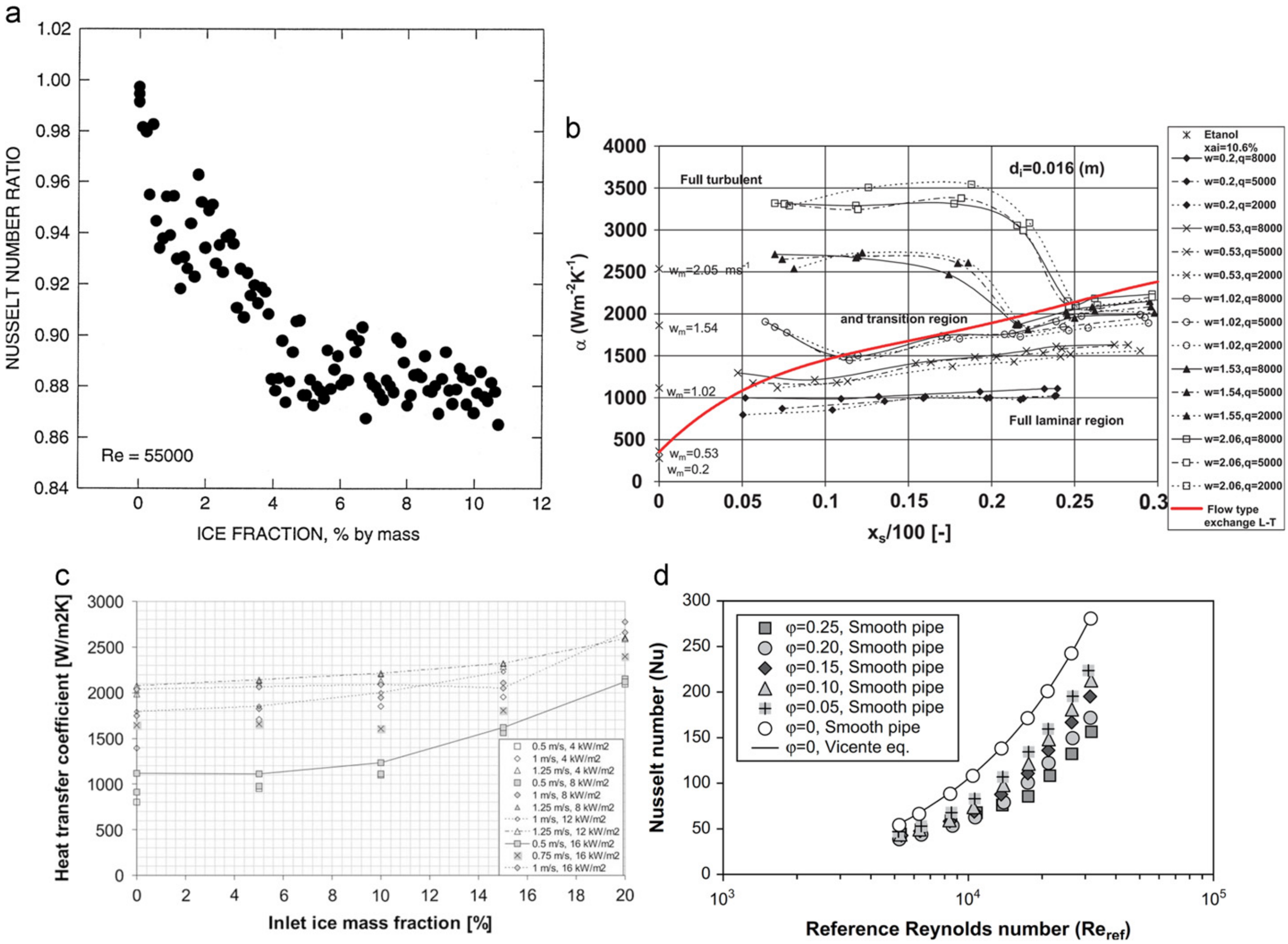


Fig. 27. Mean heat transfer coefficients and Nusselt numbers of ice slurry flowing through heated tubes under constant heat flux, (a) 24 mm stainless steel tube, $q=15$ kW m^{-2} [132]; (b) 16 mm cooper tube, w is flow rate (m s^{-1}) and q is heat flux (W m^{-2}) [145]; (c) 21 mm stainless steel tube [149] and (d) smooth stainless steel tube, φ is the inlet ice fraction [133].

cold energy is first exchanged and delivered to the load side by another coolant, such as chilled water.

A typical application of direct ice slurry application system in large-scale building is the CAPCOM building in Osaka, Japan [3,160]. The building is 20 stores and totally has 16,784 m^2 floor area, where the 2nd to 16th floor are cooled by ice slurry. The ice slurry is generated and stored at the 17th floor, as shown in Fig. 30. There are two ice slurry units driven by gas driven absorption refrigeration system with 272 kW cooling capacity each. The ice slurry is generated by a shell-and-tube ice generator, and ice is formed inside the tube and is then stored in 96 m^3 storage tank. Each unit has three alternating operated heat exchangers, and two for freezing and one for defrosting. 8 mixers, which are totally 55 kW, are installed in the tank to agitate the mixture of ice and water, then 40 wt% ice slurry at the temperature range of −2.4 to −2.6 °C is obtained. The ice slurry is pumped from the tank first through an ice slurry separator to adjust the slurry fraction to 20 wt%, and then reaches the air handing units on the floors of 2–16. Due to the low temperature and large cooling capacity of ice slurry, the air distribution temperature in the handing unit is designed to 12 °C which is lower than the normally-used temperature at 15 °C, therefore the air flow rate is reduced by about 22% which leads to capital and operation cost reduction. Compared to the predicted performance of an equivalent conventional ice thermal storage system which has higher air distribution temperature, the total energy consumption of ice slurry system during the summer of 1996 achieved 4% reduction resulted from the energy saving in hydraulic and air distribution.

An indirect ice slurry system was built for a 190,000-square-foot basketball arena and athletic complex cooling usage at Virginia Commonwealth University in USA [161], which has a seating capacity of 7500 people. The system schematic is shown in Fig. 31. The base aqueous solution used for ice slurry generation is 7% glycol solution, of which the freezing temperature is −2.2 °C. As shown in the figure, the solution is pumped to the ice slurry generator which has the capacity of 380 t (about 1336 kW), and −8.3 °C primary refrigerant is utilized for ice generation. The ice slurry is generated and stored at −3.3 °C. However, the ice slurry is not pumped to the load side directly, only the chilled solution at 1.1 °C is extracted from the tank to the building heat exchanger to cool water, which is located about 100 yards from the ice slurry system. After heat exchanging, warm solution at 11.6 °C returns. Thereafter, 2.2 °C water is supplied to the air handing unit to satisfy the proper fresh air in the 7500 seat arena. Compared to the conventional 5–7 °C coolant, the supply of 2.2 °C water causes the scale reduction of many devices, such as air coil, fan motor, water pump, duct

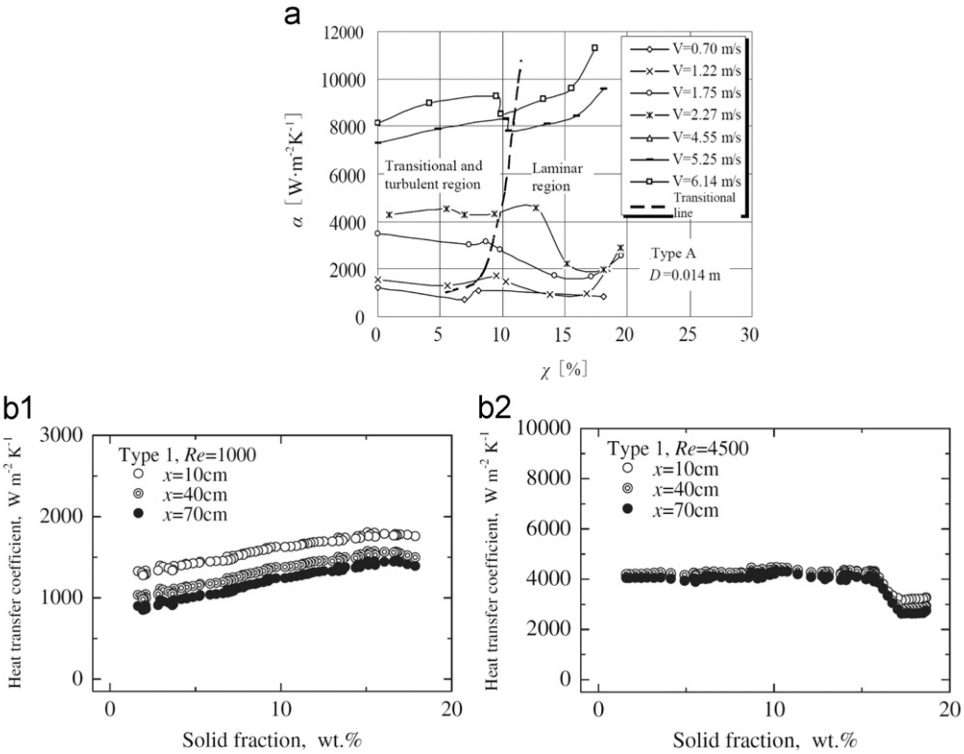


Fig. 28. Mean heat transfer coefficients of type A TBAB CHS flowing through heated tubes under constant heat flux, (a) 14 mm tube, Song et al. [27] and (b1), (b2) 7.5 mm tube, Kumano et al. [31].

and pipe etc. The annual operation cost is reduced by approximately $75,000.

Sunwell Technologies Inc. [162] has supplied a number of direct contact ice slurry systems for fish processing and preservation as well as for supermarket display usage. The named Deepchill Variable-State Ice System can provide 0–100 wt% ice slurry with 0.25–0.5 mm round crystals at the temperature range of −30 to 0 °C, which is easily pumpable. All components that employed in the ice slurry generation, storage and delivery are constructed by medical grade stainless steel or food grade plastic composites, while the slurry is always sealed and never exposed to outside contaminants. Hence, the slurry is considered as clean and reliable enough for direct contact with food. 25–40 wt% ice slurry is usually utilized and can cool the target goods to −2 to 0 °C in several minutes.

Ice slurry system constructed in a large European institutional kitchen in France [4,163] provides a complete cooling chain in this kitchen, including refrigerated room, refrigeration system, refrigerators, recooling vessels, the food service conveyor belts, plate dispensers and cooling tray transport trolleys. This system employs 16 scraped surface ice slurry generator of 185 kW total cooling capacity and 3 cylindrical storage tank of 22 m^3 to generate and store ethanol/water ice slurry. It was found that the usage of ice slurry could provide a constant low temperature for food processing and satisfy all the cooling requirements in the large kitchen

4.2. MPCS

An MPCS thermal energy storage system was constructed for cooling in Narita Airport in Japan [18] without replacing the existed 2500 RT (about 8792.5 kW) electrical turbo chiller. This project aimed to improve the decrease in capacity and performance caused by refrigerant substituting for environmental conservation. Non-toxic and phase change temperature controllable material, *n*-Paraffin waxes, was selected as the PCM. The slurry is the mixture of water and 2 μm microcapsules, and the melting temperature and the corresponding latent heat of which are 8 °C and 75.9 kJ kg^{-1}, respectively. The storage tank is 24.7 m in height and 7.4 m in diameter. Cold energy is stored during night time. MPCS at 11.5 °C is pumped by ordinary centrifugal pumps from the top of the storage tank, and is cooled in a plate-fin type heat exchanger by 3.5 °C coolant, as shown in Fig. 32(a). Phase change process occurs, the slurry is then cooled to 4 °C and stored at the bottom of the tank. The stored cold energy is released during day time as shown in Fig. 32(b). By the heat exchange with cold MPCS, the coolant of 5.1 °C is obtained and pumped to the load side. COP of the chiller and the system during the cold storage process is about 5.4 and 3.2, respectively, which is lower than the COP of 5.9 and 4.4 when there is no energy storage. Compared to the old storage system using external melting ice, though the thermal storage density of the used MPCS system is about 60% smaller, the operation cost is 32% lower.

Griffiths and Eames [16] investigated the performance of MPCS as the heat transfer medium in a test chamber containing a chilled ceiling panel, and the schematic diagram of which is shown in Fig. 33. The authors employed the MPCS with a melting temperature of 18 °C and 2–8 μm microcapsules produced by BASF, and the phase change temperature is close to the working temperature of chilled ceiling at 16–18 °C. The authors compared the performance of chilled water and MPCS with 40% concentration. To maintain the test chamber at a constant temperature of 19 °C, flow rate of 0.7 L s^{-1} was required when water was utilized as the heat transfer medium, while only 0.25 L s^{-1} was required for 40% MPCS to maintain the space temperature at 20–21 °C, since the average specific heat of the slurry in the temperature of 16–17.5 °C was as high as 9 kJ kg^{-1} K^{-1}, with sometimes a value of 11–12 kJ kg^{-1} K^{-1}. Through the continuous operation for over four months, the MPCS with 40% concentration was validated as heat transfer medium on chilled ceiling panel instead of water,

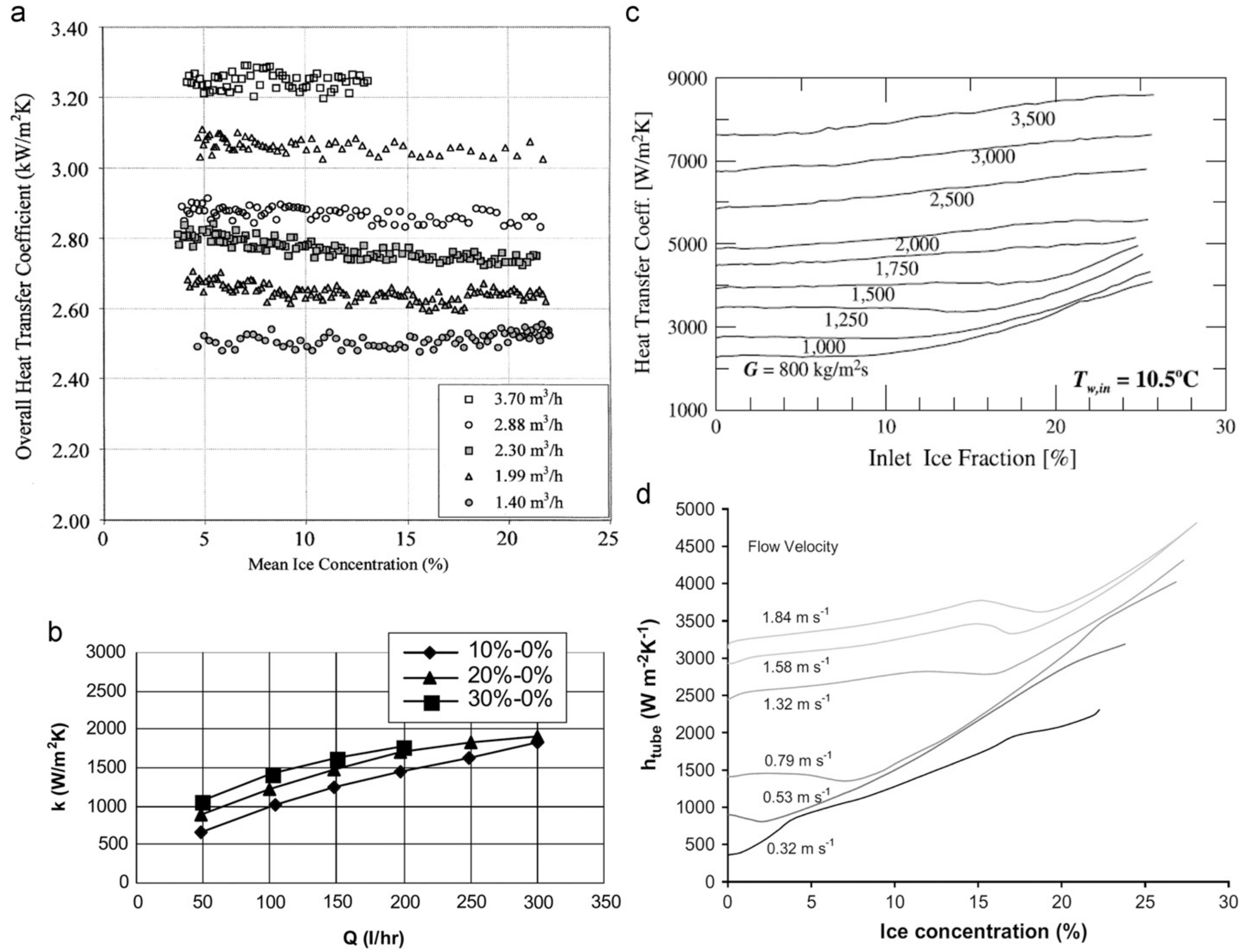


Fig. 29. Overall heat transfer coefficients of ice slurry through heat exchangers, (a) plate heat exchanger, 24 plates, D_h=4 mm, W=112 mm, H=310 mm [135]; (b) plate heat exchanger, 10 plates, D_h=4 mm, W=70 mm, H=300 mm [136]; (c) double-tube heat exchanger, inner tube D_i=13.84 mm, outer tube D_i=25 mm, L=1.5 m [146] and (d) double-tube heat exchanger, inner tube D_i=22 mm, outer tube D_i=33 mm, L=2 m [123].

and there was neither deposition of microcapsules in pipe nor the degradation of the slurry, and the system pumping power was reduced due to small flow rate. However, the authors noticed that the control procedure for cooling the slurry should be optimized.

4.3. TBAB CHS

Takao et al. [21] introduced the operation results of the TBAB CHS air conditioning system in the office building of NKK Keihin Works, which was constructed by the JFE Engineering Corporation. Total area of the two floors building is about 4000 m^2, where 1700 m^2 is the cooling object of TBAB CHS. As shown in the system sketch in Fig. 34, an absorption refrigerator is utilized. The cold carry capacity of the employed TBAB CHS is approximate 2 times of that of chilled water, which is about 59 MJ m^{-3}, therefore the coolant flow rate was reduced by 50%. The heat exchange between TBAB CHS and air inside the room was undertaken by plate fin heat exchanger, and the diameter of the cooper tube for TBAB CHS was reduced to 10 mm because of the low flow rate. The overall heat transfer coefficient in the heat exchanger was about 250–300 W m^{-2} K^{-1} as the CHS flow rate varying from 1 to 10 kg min^{-1}, which was higher than that of water when the flow rate was smaller than about 6.0 kg min^{-1}. However, the overall heat transfer coefficient was lower at higher flow rate range. Compared to the utilization of chilled water, though there was a 20% increase of the pressure drop of TBAB CHS, the operation pumping power measured in the representative day of August of 2000 was reduced by 47% due to the lower flow rate, while the total energy consumption had a reduction by 21%.

Ogi [164] reported the thermal energy storage air conditioning system using TBAB CHS in Kawasaki Underground Azalea which has a total area of about 56,000 m^2. The project was also conducted by JFE Engineering Corporation and was finished in 2008. The system schematic diagram is shown in Fig. 35. The system was modified based on an existing air conditioning system, which consisted an air handling unit (AHU) system using 3 heat pump of 550 Rt (about 1934 kW) each, and a fan coil unit (FCU) system with a centrifugal chiller of 500 Rt (about 1758 kW). Thermal energy storage by water was employed by the FCU system using a storage tank of 700 m^3. When TBAB CHS was introduced to the FCU system instead of water, the centrifugal chiller was substituted by a screw chiller with 500 Rt cooling capacity and the COP was improved from 4.19 to 4.44. Since the cold carry capacity of TBAB CHS was about 2 times as large as that of the chilled water, the stored cold energy was improved from

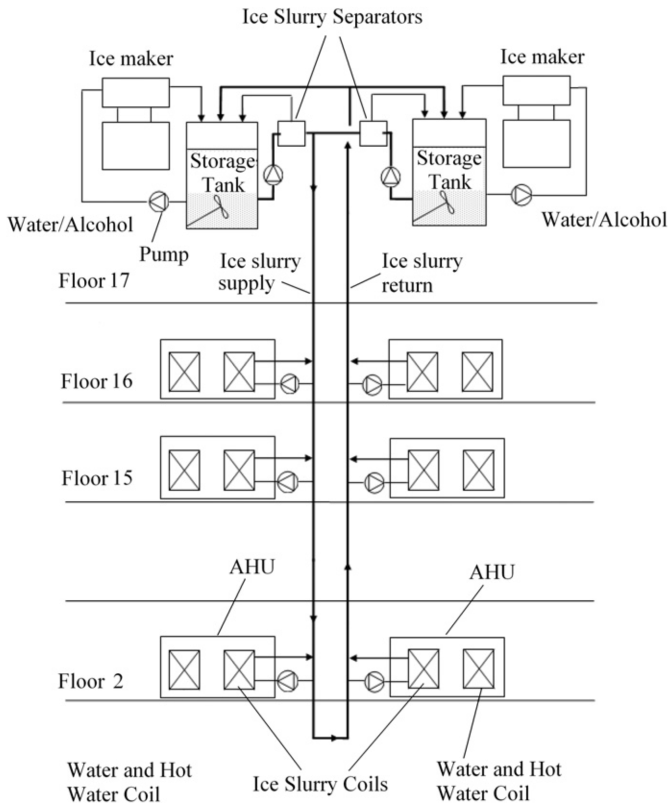


Fig. 30. Schematic diagram of direct ice slurry application CAPCOM building [160].

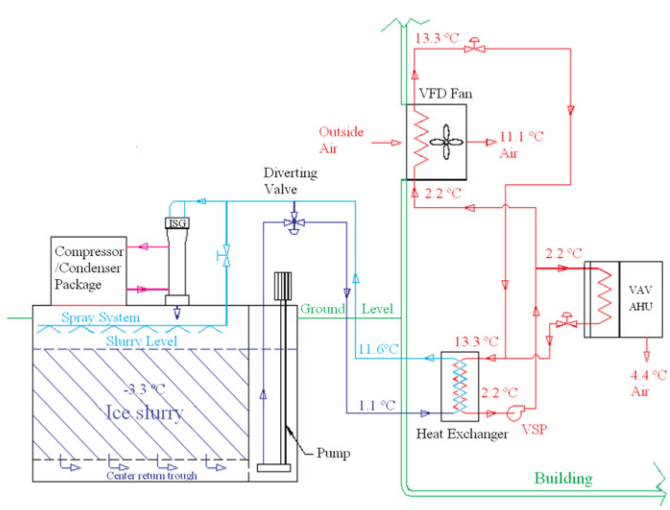


Fig. 31. Schematic diagram of indirect ice slurry application in university arena [161].

840 Rth (about 2954 kWh) by water to 1650 Rth (about 5803 kWh) by TBAB CHS without changing the storage tank. Compared to the original water storage system, the new TBAB CHS storage system led to a 40.17% reduction of electricity consumption and a 40.28% reduction of CO_2 emission.

Moreover, all the other TBAB CHS projects conducted by JFE Engineering Corporation, including the systems of Takenaka Corporation (2004), Tsurumi office building of JFE Engineering Corporation (2005), Kuraray Kurashiki Office Production Technology Center (2007), NTN Okayama Plants (2009), achieved more than 20% energy saving [165,166].

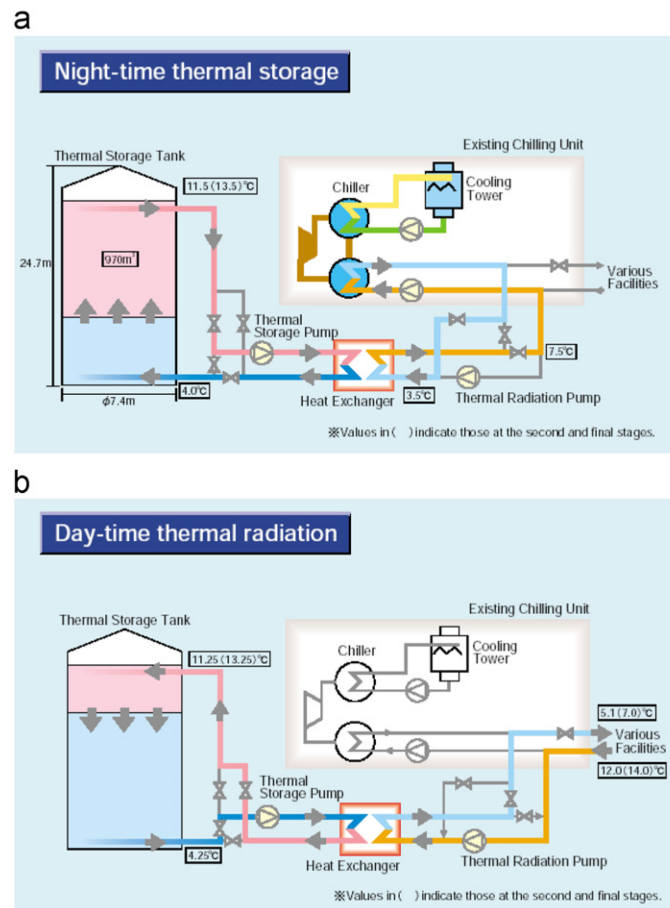


Fig. 32. Operation strategies of the MPCS system during (a) night time and (b) day time [18].

5. Conclusions

In this paper, the application of phase change material slurries, i.e., ice slurry, MPCS as well as CHS in the secondary loop refrigeration and air conditioning system have been reviewed, and the utilizations of PCS are expected to facilitate the energy saving and environmental conservation. The paper mainly focuses on the generation method and storage strategies, the flow and heat transfer characteristics and the applications of these slurries in real projects. There are many common generation methods of ice slurry in which the necessary technologies are used to prevent the generated solid crystals from adhering to the heat transfer surface to deteriorate the heat transfer, e.g., using scraper or rod or fluidized solid particles to detach the adherence, using the supercooling method to avoid the crystals forming on heat transfer surface, using direct contact heat exchange to improve the heat transfer, and so on. The producing process for MPCS is relatively complicated and higher cost, which may limit its application. The homogeneous storage of ice slurry and CHS benefits the extraction but has limitation on storage density, while the heterogeneous storage can achieve high storage density but requires additional power for extraction and the crystals size may become larger. Though PCS has been widely investigated and utilized, the fundamental investigations on flow and heat transfer characteristics are still divergent because of the complex influences by many factors, therefore further studies are still required. Moreover, the application of these slurries show quite positive significance on energy saving and environment conservation.

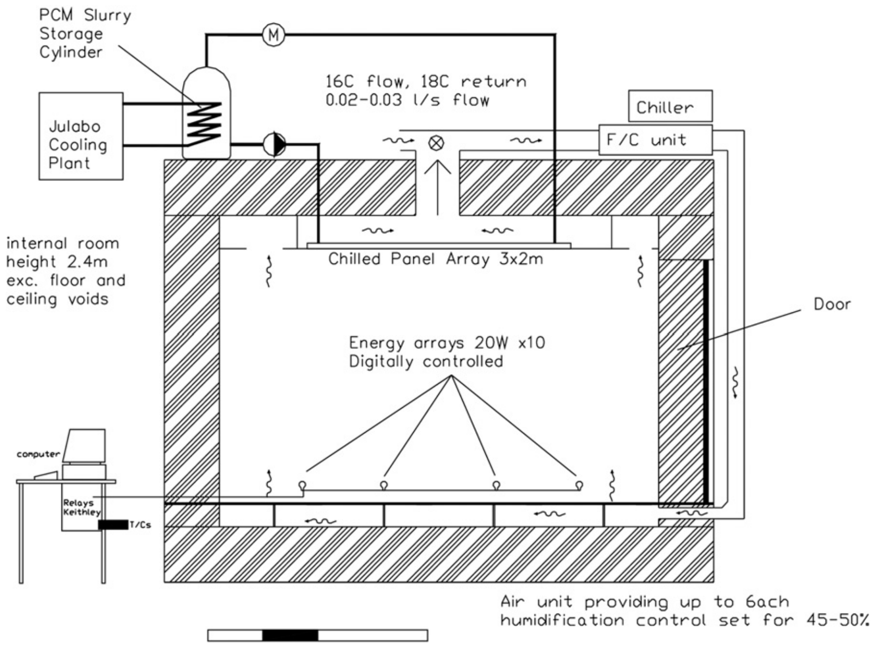


Fig. 33. Schematic diagram of chilled ceiling in the testing chamber [16].

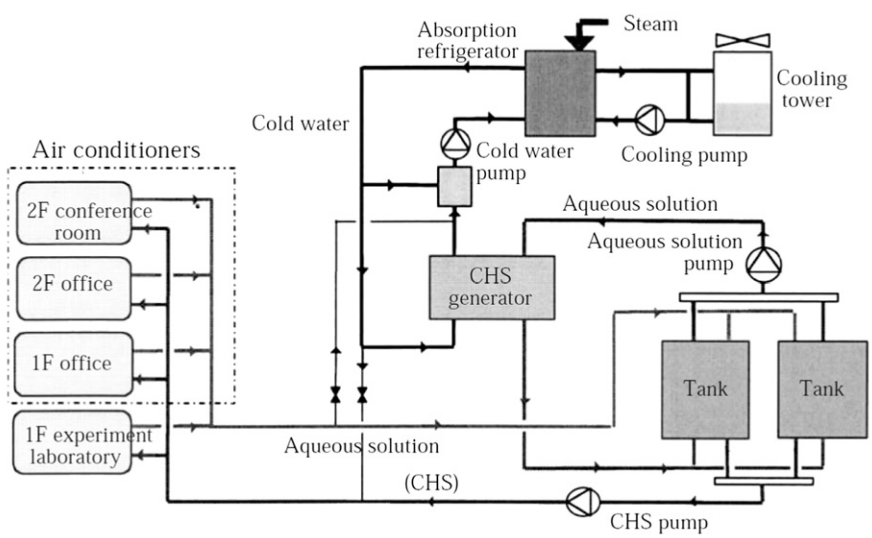


Fig. 34. Schematic diagram of air conditioning system using TBAB CHS in the office building of NKK Keihin Works [21].

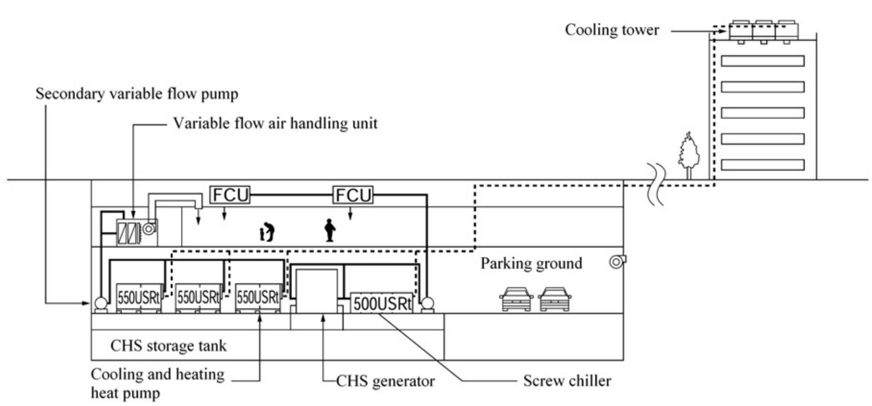


Fig. 35. Schematic diagram of air conditioning system using TBAB CHS in Kawasaki Underground Azalea [164].

However, MPCS and CHS are still not thoroughly investigated and applied, which suggests that more fundamental researches are still necessary for MPCS and CHS.

Acknowledgment

This research is jointly supported by the National Natural Science Foundation of China under the Contract no. 51176109, the "Shu Guang" training project under the Contract no. 09SG11 and the Science and Technology Commission of Shanghai Municipality under the Contract no. 10160710700. This research is also partially supported by the Specialized Research Fund for the Doctoral Program of Higher Education of China under the Contract no. 20100073110039.

References

[1] Inaba H. New challenge in advanced thermal energy transportation using functionally thermal fluids. International Journal of Thermal Sciences 2000;39:991–1003.
[2] Egolf PW, Kauffeld M. From physical properties of ice slurries to industrial ice slurry applications. International Journal of Refrigeration 2005;28:4–12.
[3] Bellas I, Tassou SA. Present and future application of ice slurries. International Journal of Refrigeration 2005;28:115–21.
[4] Kauffeld M, Wang MJ, Goldstein V, Kasza KE. Ice slurry applications. International Journal of Refrigeration 2010;33:1491–505.
[5] Wang MJ, Kusumoto N. Ice slurry based thermal storage in multifunctional buildings. Heat and Mass Transfer 2001;37:597–604.
[6] Fang Y, Kuang S, Gao X, Zhang Z. Preparation and characterization of novel nanoencapsulated phase change materials. Energy Conversion and Management 2008;49:3704–7.
[7] Zhang P, Ma ZW, Wang RZ. An overview of phase change material slurries: MPCS and CHS. Renewable and Sustainable Energy Reviews 2010;14:598–614.
[8] Delgado M, Lazaro A, Mazo J, Zalba B. Review on phase change material emulsions and microencapsulated phase change material slurries: materials, heat transfer studies and applications. Renewable and Sustainable Energy Review 2012;16:253–73.
[9] Yamagishi Y, Takeuchi H, Pyatenko AT, Kayukawa N. Characteristics of microencapsulated PCM slurry as a heat-transfer fluid. AIChE Journal 1999;45(4):696–707.
[10] Inaba H, Kim MJ, Horibe A. Melting heat transfer characteristics of microencapsulated phase change material slurries with plural microcapsules having different diameters. Journal of Heat Transfer 2004;126:558–65.
[11] Alvarado JL, Marsh C, Sohn C, Phetteplace G, Newell T. Thermal performance of microencapsulated phase change material slurry in turbulent flow under constant heat flux. International Journal of Heat and Mass Transfer 2007;50:1938–52.
[12] Wang X, Niu J, Li Y, Wang X, Chen B, Zeng R, et al. Flow and heat transfer behaviors of phase change material slurries in a horizontal circular tube. International Journal of Heat and Mass Transfer 2007;50:2480–91.
[13] Wang X, Niu J, Li Y, Zhang Y, Wang X, Chen B, et al. Heat transfer of microencapsulatd PCM slurry flow in a circular tube. AIChE Journal 2008;54:1110–20.
[14] Chen B, Wang X, Zeng R, Zhang Y, Wang X, Niu J, et al. An experimental study of convective heat transfer with microencapsulated phase change material suspension: laminar flow in a circular tube under constant heat flux. Experimental Thermal and Fluid Science 2008;32:1638–46.
[15] Tumuluri K, Alvarado JL, Taherian H, Marsh C. Thermal performance of a novel heat transfer fluid containing multiwalled carbon nanotubes and microencapsulated phase change materials. International Journal of Heat and Mass Transfer 2011;54:5554–67.
[16] Griffiths PW, Eames PC. Performance of chilled ceiling panels using phase change material slurries as the heat transport medium. Applied Thermal Engineering 2007;27:1756–60.
[17] Wang XH, Niu JL. Performance of cooled-ceiling operating with MPCM slurry. Energy Conversion and Management 2009;50:583–91.
[18] Shibutani S. PCM micro-capsule slurry thermal storage system for cooling in Narita airport. In: Proceedings of the 3rd workshop of the IEA ECES IA Annex 17; 2002.
[19] Fowler DL, Loebenstein WV, Pall DB, Kraus CA. Some unusual hydrates of quaternary ammonium salts. Journal of the American Chemical Society 1940;62(5):1140–2.
[20] Fukushima S, Takao S, Ogoshi H, Ida H, Matsumoto S, Akiyama T, et al. Development of high-density cold latent heat with clathrate hydrate. NKK Technical Report 1999;166:65–70.
[21] Takao S, Ogoshi H, Matsumoto S, Takashi K, Sugiyama M, Akiyama T, et al. New air conditioning systems using hydrate slurry. NKK Technical Report 2001;174:6–11 [in Japanese].
[22] JFE Engineering Corporation. ⟨http://www.nedo.go.jp/⟩; 2008.
[23] Oyama H, Shimada W, Ebinuma T, Kamata Y, Takeya S, Uchida T, et al. Phase diagram, latent heat, and specific heat of TBAB semiclathrate hydrate crystals. Fluid Phase Equilibria 2005;234:131–5.
[24] Hayashi K, Takao S, Ogoshi H, Matsumoto S. Research and development on high-density cold latent-heat medium transportation technology. In: Proceedings of the IEA Annex-10-PCMs and chemical reactions for thermal energy storage 4th workshop, Japan; 2000.
[25] Darbouret M, Cournil M, Herri JM. Rheological study of TBAB hydrate slurries as secondary two-phase refrigerants. International Journal of Refrigeration 2005;28:663–71.
[26] Xiao R, Wu SS, Tang LG, Huang C, Feng ZP. Experimental investigation of the pressure-drop of clathrate hydrate slurry (CHS) flow of tetrabutylammonium bromide (TBAB) in straight pipe. In: Proceedings of 10th international conference on thermal energy storage. NJ, USA; 2006.
[27] Song WJ, Xiao R, Huang C, He SH, Dong KJ, Feng ZP. Experimental investigation on TBAB clathrate hydrate slurry flows in a horizontal tube: forced convective heat transfer behaviors. International Journal of Refrigeration 2009;32(7):1801–7.
[28] Ma ZW, Zhang P, Wang RZ, Furui S, Xi GN. Forced flow and convective melting heat transfer of clathrate hydrate slurry in tubes. International Journal of Heat and Mass Transfer 2010;53:3745–57.
[29] Ma ZW, Zhang P. Pressure drops and loss coefficients of a phase change material slurry in pipe fittings. International Journal of Refrigeration 2012;35:992–1002.
[30] Kumano H, Hirata T, Kudoh T. Experimental study on the flow and heat transfer characteristics of a tetra-n-butyl ammonium bromide hydrate slurry (first report: flow characteristics). International Journal of Refrigeration 2011;34:1953–62.
[31] Kumano H, Hirata T, Kudoh T. Experimental study on the flow and heat transfer characteristics of a tetra-n-butyl ammonium bromide hydrate slurry (second report: heat transfer characteristics). International Journal of Refrigeration 2011;34:1963–71.
[32] Zhang P, Ma ZW, Wang RZ. Experimental investigation of the hydraulic and thermal performance of a phase change material slurry in the heat exchangers. Journal of Thermal Science and Engineering Applications 2011;3:011004.
[33] Ma ZW, Zhang P. Pressure drop and heat transfer characteristics of clathrate hydrate slurry in a plate heat exchanger. International Journal of Refrigeration 2011;34:796–806.
[34] Yamazaki M, Sasaki C, Kakiuchi H, Osano YT, Suga H. Thermal and structural characterization of trimethylolethane trihydrate. Thermochimica Acta 2002;387:39–45.
[35] Kakiuchi H, Yabe M, Yamazaki M. A study of trimethylolethane hydrate as a phase change material. Journal of Chemical Engineering of Japan 2003;36:788–93.
[36] Suzuki H, Itotagawa T, Indartono YS, Usui H, Wada N. Rheological characteristics of trimethylolethane hydrate slurry treated with drag-reducing surfactants. Rheologica Acta 2006;46:287–95.
[37] Suzuki H, Wada N, Komoda Y, Usui H, Ujiie S. Drag reduction characteristics of trimethylolethane hydrate slurries treated with surfactants. International Journal of Refrigeration 2009;32:931–7.
[38] Mizushima T, Inada T, Takemura F, Yabe A, Kawamura H. Melting characteristics of tetra *n*-butyl ammonium fluoride clathrate hydrate. Thermal Science & Engineering 2008;16:41–8.
[39] Stamatiou E, Meewisse JW, Kawaji M. Ice slurry generation involving moving parts. International Journal of Refrigeration 2005;28:60–72.
[40] Hayashi K, Kasza KE. Ice slurry cooling research: microscale study of ice particles characteristics, role of freezing point depressant, and influence on slurry fluidity. In: Proceedings of the ASHRAE meeting. Atlanta, Georgia; 2001.
[41] Stamatiou E. Experimental study of the ice slurry thermal–hydraulic characteristics in compact plate heat exchangers. PhD thesis. Canada: University of Toronto; 2003.
[42] Stamatiou E, Kawaji M. Heat transfer characteristics in compact scraped surface ice slurry generators. In: Proceedings of 21st IIR international congress of refrigeration. Washington, DC, USA; 2003.
[43] Rodriguez Pascual M, Derksen JJ, Van Rosmalen GM, Witkamp GJ. Flow and particle motion in scraped heat exchanger crystallizers. Chemical Engineering Science 2009;64:5153–61.
[44] Ben Lakhdar M, Cerecero R, Alvarez G, Guilpart J, Flick D, Lallemand A. Heat transfer with freezing in a scraped surface heat exchanger. Applied Thermal Engineering 2005;25:45–60.
[45] Nariyuki T, Nobuyuki Y, Masahiro K. Auger type ice machine. JP 5918363; 1984.
[46] Sugie H, Hamajima M, Sato A. Auger type ice-making machine. US 2003/0079489 A1; 2003.
[47] Lim HY. Ice slurry generator. WO 2004/046624 A1; 2004.
[48] Douzet J, Herri JM, Brantuas P, Flick D. Building of a life size testing unit for air conditioning by using TBAB hydrate slurry as a secondary two-phase refrigerant. In: Proceedings of the 9th international conference on phase-change materials and slurries for refrigeration and air-conditioning. Sofia, Bulgaria; 2010.
[49] Daitoku T, Utaka Y. An effect of scraper shapes on detachment of solid adhered to cooling surface for formation of clathrate hydrate slurry. Heat Transfer—Asian Research 2007;36(8):489–500.

[50] Gladis SP, Marciniak MJ, O'Hanlon JE Joseph-B, Yundt B. Ice crystal slurry TES system using the orbital rod evaporator. In: Conference proceedings of the EPRI international conference on sustainable thermal energy storage. Bloomington, USA; 1996.

[51] Paul Mueller Company. Ice slurry applications, 〈http://www.genemco.com/〉.

[52] Klaren DG. Development of a vertical flash evaporator. PhD thesis. The Netherlands: Delft University of Technology; 1975.

[53] Pronk P, Meewisse JW, Infante Ferreira CA. Heat transfer model for a fluidised bed ice slurry generator. In: Proceedings of the 4th workshop on ice slurries of the IIR. Osaka, Japan; 2001.

[54] Klaren DG, van der Meer JS. A fluidized bed chiller: a new approach in making slush-ice. In: Proceedings from the 13th national industrial energy technology conference. Houston, USA; 1991.

[55] Meewisse JW, Infante Ferreira CA. Fluidized bed ice slurry generator: operating range. In: Proceedings of the fifth workshop on ice slurries of the IIR. Stockholm, Sweden; 2002.

[56] Meewisse JW, Infante Ferreira CA. Validation of the use of heat transfer models in liquid/solid fluidized beds for ice slurry generation. International Journal of Heat and Mass Transfer 2003;46:3683–95.

[57] Pronk P, Meewisse JW, Infante Ferreira CA, Witkamp GJ. Ice slurry production with a circulating fluidized bed heat exchanger. In: Proceedings of the international congress of refrigeration. Washington, DC; 2003.

[58] Pronk P, Infante Ferreira CA, Witkamp GJ. Circulating fluidized bed heat exchanger for ice slurry production. In: Proceedings of the IIR conference on thermophysical properties and transfer processes of refrigerants. Vicenza, Italy; 2005.

[59] Pronk P, Infante Ferreira CA, Witkamp GJ. Measuring particle–wall impacts in a fluidized bed heat exchanger. In: Proceedings of the IIR conference on thermophysical properties and transfer processes of refrigerants. Vicenza, Italy; 2005.

[60] Bédécarrats JP, David T, Castaing-Lasvignottes J. Ice slurry production using supercooling phenomenon. International Journal of Refrigeration 2010; 33:196–204.

[61] Faucheux M, Muller G, Havet M, LeBail A. Influence of surface roughness on the supercooling degree: case of selected water/ethanol solutions frozen on aluminium surface. International Journal of Refrigeration 2006;29: 1218–1224.

[62] Takao O, Tokio O, Toshio H, Sakae K. Ice machine for accumulating heat. JP 63217171; 1988.

[63] Satoko Y. Ice-based regeneratice device. JP7019540; 1995.

[64] Yasutoshi S, Yasuhiro K. Supercooling releasing device for supercooled water type icemaker. JP7139770; 1995.

[65] Masayuki I, Gakuo F. Method for discharging supercooled water in supercooling ice making system. JP8285418; 1996.

[66] Okawa S, Saito A. Experimental study on controlling the initiation of freezing of supercooled water. In: Proceedings of the 11th international heat transfer conference. Kyongju, Korea; 1998.

[67] Inada T, Zhang X, Yabe A, Kozawa Y. Active control of phase change from supercooled water to ice by ultrasonic vibration 1. Control of freezing temperature. International Journal of Heat and Mass Transfer 2001; 44(23):4523–31.

[68] Zhang X, Inada T, Yabe A, Lu S, Kozawa Y. Active control of phase change from supercooled water to ice by ultrasonic vibration 2. Generation of ice slurries and effect of bubble nuclei. International Journal of Heat and Mass Transfer 2001;44(23):4533–9.

[69] Petersen A, Schneider H, Rau G, Glasmacher B. A new approach for freezing of aqueous solution under active control of the nucleation temperature. Cryobiology 2006;53:248–57.

[70] Tanino M, Kozawa Y. Ice-water two-phase flow behavior in ice heat storage systems. International Journal of Refrigeration 2001;24:639–51.

[71] Kozawa Y, Aizawa N, Tanino M. Study on ice storing characteristics in dynamic-type ice storage system by using supercooled water. Effects of the supplying conditions of ice-slurry at deployment to district heating and cooling system. International Journal of Refrigeration 2005;28:73–82.

[72] Ise H, Tanino M, Kozawa Y. Ice storage system in Kyoto station building. Information booklet for the technical tour of the fourth workshop of IIR Ice Slurry Working Party; 2001.

[73] JFE Engineering Corporation. 〈http://www.meti.go.jp/〉; 2006.

[74] JFE Engineering Corporation. The clathrate hydrate slurry thermal storage system for air-conditioning of large-scale buildings. JFE Technical Report 2008;21:56–8 [in Japanese].

[75] Ogoshi H, Furumoto N, Ida H. Method and apparatus for producing clathrate hydrate slurry, and method for operating the same apparatus. US 2009/0266106 A1; 2009.

[76] Song WJ, Xiao R, Huang C, He SH, Dong KJ, Feng ZP. Study on sonocrystallisation of TBAB aqueous solution. In: Proceedings of the 8th IIR conference on phase change materials and slurries for refrigeration and air conditioning. Karlsruhe; 2009.

[77] Kiatsiriroat T, Siriplubpla P, Nuntaphan A. Performance analysis of a refrigeration cycle using a direct contact evaporator. International Journal of Energy Research 1998;22:1179–90.

[78] Kiatsiriroat T, Vithayasai S, Vorayos N, Nuntaphan A, Vorayos N. Heat transfer prediction for a direct contact ice thermal energy storage. Energy Conversion and Management 2003;44:497–508.

[79] Thitipatanapong R, Limmeechokchai B, Chungpaibulpatana S. Investigation of direct-contact heat exchanger for ice slurry production. In: Proceedings of the 2nd regional conference on energy technology toward a clean environment. Thailand: KMUTT; 2003.

[80] Thongwik S, Vorayos N, Kiatsiriroat T, Nuntaphan A. Thermal analysis of slurry ice production system using direct contact heat transfer of carbon dioxide and water mixture. International Communications in Heat and Mass Transfer 2008;35:756–61.

[81] Wijeysundera NE, Hawlader MNA, Chan WBA, Kamal Hossain M. Ice-slurry production using direct contact heat transfer. International Journal of Refrigeration 2004;27:511–9.

[82] Hawlader MNA, Wahed MA. Analyses of ice slurry formation using direct contact heat transfer. Applied Energy 2009;86:1170–8.

[83] Wahed MA, Hawlader MNA. An analysis of a direct contact ice slurry generator. In: Proceedings of the 2008 ASME summer heat transfer conference. Jacksonville, Florida, USA; 2008.

[84] Ophir A, Rojanskiy H, Siluk R, Kanievski A, Kanievski L. Compact heat pump using water as refrigerant. US 2009/0100857 A1; 2009.

[85] I.D.E. Technologies Ltd. Vacuum Ice Maker (VIM) for Thermal Energy Storage (TES), 〈http://www.ide-tech.com/〉; 2010.

[86] Ophir A. Energy efficient vacuum ice-maker using water as refrigerant for thermal energy storage and heat pumps, 〈http://www.slidefinder.net/O/OphirIDEACampus07/17712969〉.

[87] Bapat DW, Kulkarni SV. Method and apparatus for generating ice slurry. WO 2008/062438 A2; 2008.

[88] Shin HT, Lee YP, Jurng J. Spherical-shaped ice particle production by spraying water in a vacuum chamber. Applied Thermal Engineering 2000; 20:439–54.

[89] Kim BS, Shin HT, Lee YP, Jurng J. Study on ice slurry production by water spray. International Journal of Refrigeration 2001;24:176–84.

[90] Egolf PW, Kitanovski A, Ata-Caesar D, Vuarnoz D, Meili F. Cold storage with ice slurries. International Journal of Energy Research 2008;32:187–203.

[91] Hansen TM, Radosevic M, Kauffeld M. Behavior of ice slurry in thermal storage systems. ASHRAE Research Project 1166; 2002.

[92] Meili F, Sari O, Vuarnoz D, Egolf PW. Storage and mixing of ice slurries in tanks. In: Proceedings of the third workshop on ice slurries of the International Institute of Refrigeration IIF/IIR. Lucerne, Switzerland; 2001.

[93] Grandum S, Nakagomi K. Characteristics of ice slurry containing antifreeze protein for ice storage application. Journal of Thermophysics and Heat Transfer 1997;11(3):461–6.

[94] Inaba H, Inada T, Horibe A, Suzuki H, Usui H. Preventing agglomeration and growth of ice particles in water with suitable additives. International Journal of Refrigeration 2005;28:20–6.

[95] Gibbs BF, Kermasha S, Alli I, Mulligan CN. Encapsulation in the food industry: a review. International Journal of Food Sciences and Nutrition 1999;50:213–24.

[96] Green KB. Carbonless paper production. Ohio NCR Corporation; 1953.

[97] Gouin S. Microencapsulation: industrial appraisal of existing technologies and trends. Trends in Food Science & Technology 2004;15:330–47.

[98] Hawlader MNA, Uddin MS, Khin MM. Microencapsulated PCM thermal-energy storage system. Applied Energy 2003;74:195–202.

[99] Özonur Y, Mazman M, Paksoy HÖ, Evliya H. Microencapsulation of coco fatty acid mixture for thermal energy storage with phase change material. International Journal of Energy Research 2006;30:741–9.

[100] Yang R, Xu H, Zhang YP. Preparation, physical property and thermal physical property of phase change microcapsule slurry and phase change emulsion. Solar Energy Materials & Solar Cells 2003;80:405–16.

[101] Brown EN, Kessler MR, Sottos NR, White SR. In situ poly(urea-formaldehyde) microencapsulation of dicyclopentadiene. Journal of Microencapsulation 2003;20(6):719–30.

[102] Alkan C, Sari A, Karaipekli A, Uzun O. Preparation, characterization, and thermal properties of microencapsulated phase change material for thermal energy storage. Solar Energy Materials & Solar Cells 2009;93:143–7.

[103] Cho JS, Kwon A, Cho CG. Microencapsulation of octadecane as a phase-change material by interfacial polymerization in an emulsion system. Colloid & Polymer Science 2002;280:260–6.

[104] Siddhan P, Jassal M, Agrawal AK. Core content and stability of *n*-octadecane-containing polyurea microencapsules produced by interfacial polymerization. Journal of Applied Polymer Science 2007;106:786–92.

[105] Ai YF, Jin Y, Sun J, Wei DQ. Microencapsulation of *n*-hexadecane as phase change material by suspension polymerization. e-Polymers 2007;98:1–9.

[106] Sánchez L, Sánchez P, Lucas A, Carmona M, Rodríguez JF. Microencapsulation of PCMs with a polystyrene shell. Colloid Polymer Science 2007;285:1377–85.

[107] Gharsallaoui A, Roudaut G, Chambin O, Voilley A, Saurel R. Application of spray-drying in microencapsulation of food ingredients: an overview. Food Research International 2007;40:1107–21.

[108] Ayel V, Lottin O, Peerhossaini H. Rheology, flow behaviour and heat transfer of ice slurries: a review of the state of the art. International Journal of Refrigeration 2003;26:95–107.

[109] Kitanovski A, Vuarnoz D, Ata-Caesar D, Egolf PW, Hansen TM, Doetsch C. The fluid dynamics of ice slurry. International Journal of Refrigeration 2005;28:37–50.

[110] Vuarnoz D, Sari O, Egolf PW, Liardon H. Ultrasonic velocity profiler UVP-XW for ice-slurry flow characterisation. In: Proceedings of the third international symposium on ultrasonic Doppler method for fluid mechanics and fluid engineering, Lausanne, Switzerland; 2002.

[111] Stamatiou E, Kawaji M. Thermal and flow behaviour of ice slurries in a vertical rectangular channel, Part I: local distribution measurements in

adiabatic flow. International Journal of Heat and Mass Transfer 2005; 48:3527–43.
[112] Stamatiou E, Kawaji M. Thermal and flow behaviour of ice slurries in a vertical rectangular channel, Part II: forced convective melting heat transfer. International Journal of Heat and Mass Transfer 2005;48:3544–59.
[113] Kitanovski A, Poredoš A. Concentration distribution and viscosity of ice-slurry in heterogeneous flow. International Journal of Refrigeration 2002;25:827–35.
[114] Kitanovski A. PhD thesis. Slovenia: University of Ljubljana, Faculty of Mechanical Engineering; 2003.
[115] Rached W, Sicard F, Lafargue A, Thorel D. Ice slurry: pressure drop and deposition velocity. International Journal of Refrigeration 2007;30: 1393–400.
[116] Hirochi T, Maeda Y, Yamada S, Shirakashi M, Hattori M, Saito A. Flow patterns of ice/water slurry in horizontal pipes. Journal of Fluids Engineering 2004;126:436–41.
[117] Grozdek M, Khodabandeh R, Lundqvist P. Experimental investigation of ice slurry flow pressure drop in horizontal tubes. Experimental Thermal and Fluid Science 2009;33:357–70.
[118] Fernández-Seara J, Diz R, Uhía FJ, Alberto Dopazo J. Experimental analysis on pressure drop and heat transfer of a terminal fan-coil unit with ice slurry as cooling medium. International Journal of Refrigeration 2010;33:1095–104.
[119] Niezgoda-Żelasko B, Zalewski W. Momentum transfer of ice slurry flows in tubes, experimental investigations. International Journal of Refrigeration 2006;29:418–28.
[120] Kumano H, Hirata T, Shirakawa M, Shouji R. Flow characteristics of ice slurry in narrow tubes. International Journal of Refrigeration 2010;33: 1513–22.
[121] Stokes JR, Telford JH, Williamson AM. The flowability of ice suspensions. Journal of Rheology 2005;49:139–48.
[122] Niezgoda-Żelasko B, Żelasko J. Generalized non-Newtonian flow of ice-slurry. Chemical Engineering and Processing 2007;46:895–904.
[123] Bédécarrats JP, Strub F, Peuvrel C. Thermal and hydrodynamic considerations of ice slurry in heat exchangers. International Journal of Refrigeration 2009;32(7):1791–800.
[124] Monteiro ACS, Bansal P. Pressure drop characteristics and rheological modelling of ice slurry flow in pipes. International Journal of Refrigeration 2010;33:1523–32.
[125] Dammel F, Stephan P. Heat transfer to suspensions of microencapsulated phase change material flowing through minichannels. Journal of Heat Transfer 2012;134 020907-1–8.
[126] Ho CJ, Huang JB, Chen CP, Tsai PS, Yang YM. Forced convection performance of a MEPCM suspension through an iso-flux heated circular tube: an experimental study. Heat and Mass Transfer 2012;48:487–96.
[127] Wang L, Lin G. Experimental study on the convective heat transfer behavior of microencapsulated phase change material suspensions in rectangular tube of small aspect ratio. Heat and Mass Transfer 2012;48:83–91.
[128] Zeng R, Wang X, Chen B, Zhang Y, Niu J, Wang X, et al. Heat transfer characteristics of microencapsulated phase change material slurry in laminar flow under constant heat flux. Applied Energy 2009;86:2661–70.
[129] Zhang Y, Rao Z, Wang S, Zhang H, Li L, Zhang M. Characterization and thermal properties of the microencapsulated PCM slurry. Advanced Materials Research 2011;284–286:940–4.
[130] Yamagishi Y, Sugeno T, Ishige T, Takeuci H, Pyatenko AT. An evaluation of microencapsulated PCM for use in cold energy transportation medium. In: Proceedings of the 31st intersociety energy conversion engineering conference, IECEC 96; 1996. p. 2077–83.
[131] Hashimoto S, Kawamura K, Ito H, Nobeoka M, Ohgaki K, Inoue Y. Rheological study on tetra-n-butyl ammonium salt semi-clathrate hydrate slurries. In: Proceedings of the 7th international conference on gas hydrate. Edinburgh, UK; 2011.
[132] Knodel BD, France DM, Choi US, Wambsganss MW. Heat transfer and pressure drop in ice-water slurries. Applied Thermal Engineering 2000;20: 671–85.
[133] Illán F, Viedma A. Experimental study on pressure drop and heat transfer in pipelines for brine based ice slurry. Part I: operational parameters correlations. International Journal of Refrigeration 2009;32:1015–23.
[134] Meewisse JW, Infante Ferreira CA. Freezing point depression of various ice slurries. In: IIF/IIR, Commission B1. Paderborn, Germany; 2001.
[135] Bellas J, Chaer I, Tassou SA. Heat transfer and pressure drop of ice slurries in plate heat exchangers. Applied Thermal Engineering 2002;22:721–32.
[136] Nørgaard E, Sørensen TA, Hansen TM, Kauffeld M. Performance of components of ice slurry systems: pumps, plate heat exchangers, and fittings. International Journal of Refrigeration 2005;28:83–91.
[137] Hägg C. Ice slurry as secondary fluid in refrigeration systems—fundamentals and applications in supermarkets. Licentiate thesis. Stockholm: School of Industrial Engineering and Management; 2005.
[138] Shire GSF, Quarini GL, Rhys TDL, Evans TS. The anomalous pressure drop behaviour of ice slurries flowing through constrictions. International Journal of Multiphase Flow 2008;34:510–5.
[139] Illán F, Viedma A. Prediction of ice slurry performance in a corrugated tube heat exchanger. International Journal of Refrigeration 2009;32:1302–9.
[140] Shire GSF, Quarini GL, Evans TS. Pressure drop of flowing ice slurries in industrial heat exchangers. Applied Thermal Engineering 2009;29:1500–6.
[141] Rao Y, Dammel F, Stephan P, Lin G. Flow frictional characteristics of microencapsulated phase change material suspensions flowing through rectangular minichannels. Science in China Series E: Technological Sciences 2006;49:445–56.
[142] Xiao R, Song WJ, Huang C, He SH, Dong KJ, Feng ZP. Re-laminarization of TBAB hydrate slurry flow in tube. Journal of Engineering Thermophysics 2009;30(6):971–3 [in Chinese].
[143] Suzuki H, Konaka T, Komoda Y, Ishigami T, Fudaba T. Flow and heat transfer characteristics of ammonium alum hydrate slurry treated with surfactant. Journal of Chemical Engineering of Japan 2012;45(2):136–41.
[144] Matousek V. Pressure drops and flow patterns in sand-mixture pipes. Experimental Thermal and Fluid Science 2002;26:693–702.
[145] Niezgoda-Żelasko B. Heat transfer of ice slurry flows in tubes. International Journal of Refrigeration 2006;29:437–50.
[146] Lee DW, Yoon ES, Joo MC, Sharma A. Heat transfer characteristics of the ice slurry at melting process in a tube flow. International Journal of Refrigeration 2006;29:451–5.
[147] Ionescu C, Haberschill P, Kiss I, Lallemand A. Local and global heat transfer coefficient of a stabilised ice slurry in laminar and transitional flows. International Journal of Refrigeration 2007;30:970–7.
[148] Niezgoda-Żelasko B, Żelasko J. Melting of ice slurry under forced convection conditions in tubes. Experimental Thermal and Fluid Science 2008;32: 1597–608.
[149] Grozdek M, Khodabandeh R, Lundqvist P, Palm B, Melinder Å. Experimental investigation of ice slurry heat transfer in horizontal tube. International Journal of Refrigeration 2009;32:1310–22.
[150] Kumano H, Hirata T, Shouji R, Shirakawa M. Experimental study on heat transfer characteristics of ice slurry. International Journal of Refrigeration 2010;33:1540–9.
[151] Goel M, Roy SK, Sengupta S. Laminar forced convection heat transfer in microencapsulated phase change material suspensions. International Journal of Heat and Mass Transfer 1994;37:593–604.
[152] Rao Y, Dammel F, Stephan P, Lin G. Convective heat transfer characteristics of microencapsulated phase change material suspensions in minichannels. Heat and Mass Transfer 2007;44:175–86.
[153] Diaconu BM, Varga S, Oliveira AC. Experimental assessment of heat storage properties and heat transfer characteristics of a phase change material slurry for air conditioning applications. Applied Energy 2010;87:620–8.
[154] Diaconu BM, Varga S, Oliveira AC. Experimental study of natural convection heat transfer in a microencapsulated phase change material slurry. Energy 2010;35:2688–93.
[155] Wang L, Lin GP, Ding YL. Heat transfer and rheological behavior of nanoparticle compound microencapsulated phase change material suspensions. AIP Conference Proceedings 2010.
[156] Delgado M, Lázaro A, Mazo J, Marín J, Zalba B. Experimental analysis of a microencapsulated PCM slurry as thermal storage system and as heat transfer fluid in laminar flow. Applied Thermal Engineering 2012;36:370–7.
[157] Suzuki H, Konaka T, Komoda Y, Ishigami T, Fudaba T. Flow and heat transfer characteristics of ammonium alum hydrate slurry treated with surfactant. Journal of Chemical Engineerign of Japan 2012;45(2):136–41.
[158] Illán F, Viedma A. Experimental study of ice slurry performance in a standard fan coil. International Journal of Refrigeration 2009;32:1808–14.
[159] Charunyakorn P, Sengupta S, Roy SK. Forced convection heat transfer in microencapsulated phase change material slurries: flow in circular ducts. International Journal of Heat and Mass Transfer 1991;34(3):819–33.
[160] Kauffeld M. Ice slurry. In: Proceedings of the managing challenges in thermal energy transportation with advanced thermal energy storage technology, IEA/ECES annex 5th workshop. Freiburg, Germany; 1998.
[161] Nelson P, Pippin J, Dunlap J. University ice slurry system. In: Proceedings of the IDEA College/University conference. New Orleans, USA; 1999.
[162] Sunwell Technologies Inc. 〈http://www.sunwell.com/suntech1.htm〉.
[163] Compingt A, Blanc P, Quidort A. Slurry for refrigeration industrial kitchen application. In: Proceedings of the 8th conference on phase-change materials and slurries for refrigeration and air conditioning. Karlsruhe; 2009.
[164] Ogi Y. Cases study of thermal energy storage air conditioning system using CHS in Kawasaki underground Azalea. Pump and Its Applications 2007; 74:35–8 [in Japanese].
[165] JFE Engineering Corporation. 〈http://www.meti.go.jp/〉; 2006.
[166] Hasegawa M. Cases study of thermal energy storage air conditioning system using CHS. Pump and Its Applications 2009;78:26–9 [in Japanese].